

MICROCOPY RESOLUTION TEST CHART
NATIONAL BUREAU OF STANDARDS-1963-A

AD-A190 616

DTIC FILE COPY

1



Spectral Analysis
of Short Data Records

THESIS

Thorlough E. Carter Jr.
First Lieutenant, USAF

AFIT/GE/ENG/87D-9

DTIC
ELECTE
MAR 25 1988
S E D

DEPARTMENT OF THE AIR FORCE
AIR UNIVERSITY

AIR FORCE INSTITUTE OF TECHNOLOGY

Wright-Patterson Air Force Base, Ohio

This document has been approved
for public release and since its
distribution is unlimited.

88 3 24 478

①

AFIT/GE/ENG/87D-9

Spectral Analysis
of Short Data Records

THESIS

Thorlough E. Carter Jr.
First Lieutenant, USAF

AFIT/GE/ENG/87D-9

SELECTED
9

Approved for public release; distribution unlimited

AFIT/GE/ENG/87D-9

Spectral Analysis
of Short Data Records

THESIS

Presented to the Faculty of the School of Engineering
of the Air Force Institute of Technology

Air University

In Partial Fulfillment of the
Requirements for the Degree of
Master of Science in Electrical Engineering

Thorlough E. Carter, B.S.E.E.

First Lieutenant, USAF

December 1987

Approved for public release; distribution unlimited

Preface

The purpose of this research is to investigate two methods of spectral estimation for typical radar type signals. The two methods investigated are Blackman-Tukey and Burg. A comparison of the two methods is made based on their statistical properties and computational efficiency.

Valuable guidance was provided by Maj Glenn Prescott of the Air Force Institute of Technology (AFIT) during the course of this work. His help is gratefully appreciated. My deepest gratitude is expressed to my dear wife, Alfreda, for her constant support and encouragement. Her help in preparing the manuscript has enable me to accomplish a major goal in my life. Another major goal that we both accomplished during my stay at AFIT was the birth of our beautiful daughter Ashlee. A special thanks is given to our divine creator.



Accession For	
NTIS GRA&I	<input checked="" type="checkbox"/>
DTIC TAB	<input type="checkbox"/>
Unannounced	<input type="checkbox"/>
Justification	
By _____	
Distribution/	
Availability Codes	
Dist	Avail and/or Special
A-1	

Table of Contents

	Page
Preface	ii
List of Figures	v
Absrtact	viii
I. Overview	1
Introduction	1
Background	2
Problem Statement	7
Scope	7
Assumptions	7
Presentation	8
II. ISPX Software Package and Previous Research . .	9
Introduction	9
ISPX Software Package	10
Previous Research	13
III. Detailed Theory	16
Introduction	16
Conventional Spectral Estimation - Via the BT Method	18
Modern Spectral Estimation - Via the AR/Burg Method	30
Comparison of the BT and Burg Methods . . .	42
IV. Analysis	44
Introduction	44
Problem One	46
Problem Two	55
Problem Three	63
Problem Four	66
Threshold Detection Routine	73
V. Conclusions and Recommendations	78
Conclusions	78
Recommendations	79

Appendix A: Subroutine Used for Spectral Estimation	81
Appendix B: Threshold Detection Routine	88
Bibliography	97
Vita	100

List of Figures

figure	page
1.1 Generic Receiver Block Diagram	2
3.1 Continuous and Discrete Random Processes and their Respective PSD's	19
3.2 Plots for both Autocorrelation Estimators . . .	22
3.3 The Ideal PSD of a Strong and a Weak Signal Embedded in WGN	24
3.4 The Simple PSD of a Weak and Strong Signal Example for Various Values of N	25
3.5 A Functional Description of the BT Method . . .	26
3.6 The BT PSD of the Weak and Strong Signal Example	28
3.7 Transform Interpolation by Zero Padding	31
3.8 An All-Pole Filter for Generating an AR Process	33
4.1 Sixty-Four Samples of a Single Sinusoid in WGN, SNR = 10 dB	47
4.2 Sixty-Four Samples of a Single Sinusoid in WGN, SNR = 15 dB	48
4.3 Sixty-Four Samples of a Single Sinusoid in WGN, SNR = 20 dB	49
4.4a BT Estimator of the Single Sinusoid in WGN, SNR = 10 dB	50
4.4b BT Estimator of the Single Sinusoid in WGN, SNR = 15 dB	51
4.4c BT Estimator of the Single Sinusoid in WGN, SNR = 21 dB	52
4.5 Superposition of the BT Estimator for SNR's 10, 15, and 20 dB	53
4.6 Superposition of the Burg Estimator for SNR's 10, 15, and 20 dB with $P = 2$	54

4.7	Sixty-Four Samples of a Single Sinusoid in WGN, SNR = 15 dB	57
4.8	BT Estimator of Two Sinusoids in WGN, SNR = 15 dB	58
4.9a	Burg Estimator of Two Sinusoids in WGN, SNR = 15 dB with P = 4	60
4.9b	Burg Estimator of Two Sinusoids in WGN, SNR = 15 dB with P = 6	61
4.9c	Burg Estimator of Two Sinusoids in WGN, SNR = 15 dB with P = 10	62
4.10	Sixty-Four Samples of a Single Sinusoid in WGN, SNR = 15 dB	64
4.11	BT Estimator of Two Sinusoids in WGN, SNR = 15 dB	65
4.12a	Burg Estimator of Two Sinusoids in WGN, SNR = 15 dB with P = 4	67
4.12b	Burg Estimator of Two Sinusoids in WGN, SNR = 15 dB with P = 14	68
4.12c	Burg Estimator of Two Sinusoids in WGN, SNR = 15 dB with P = 20	69
4.13	Sixty-Four Samples of a Single Sinusoid in WGN, SNR = 15 dB	70
4.14	BT Estimator of Four Sinusoids in WGN, SNR = 15 dB	71
4.15	Burg Estimator of Four Sinusoids in WGN, SNR = 15 dB with P = 24	72
4.16	Burg Estimator of Two Sinusoids in WGN, SNR = 15 dB with P = 24	77
B.1	Burg Estimator of a Single Sinusoid in WGN, SNR = 15 dB with P = 24	90
B.2	Burg Estimator of Two Sinusoids in WGN, SNR = 15 dB with P = 24	91
B.3	Burg Estimator of Three Sinusoids in WGN, SNR = 15 dB with P = 24	92

B.4	Burg Estimator of Four Sinusoids in WGN, SNR = 15 dB with P = 24	93
B.5	Burg Estimator of Five Sinusoids in WGN, SNR = 15 dB with P = 24	94
B.6	Burg Estimator of Two Sinusoids in WGN, SNR = 15 dB with P = 24	95
B.7	Burg Estimator of Three Sinusoids in WGN, SNR = 15 dB with P = 24	96

Abstract

The purpose of this study was to examine the Blackman-Tukey (BT) and Burg methods of spectral estimation for typical electronic warfare received signals. Such signals are generally short in duration, resulting in short data records. The BT method is a conventional spectral estimation scheme and is based on computing the discrete Fourier transform of the autocorrelation sequence (ASC) derived from the data record. An inherent problem of this approach is that of data windowing. Data windowing may result in poor frequency resolution, particularly for short data records.

The Burg method of spectral estimation, a modern approach, is capable of providing relatively good frequency resolution for short data records. However, this method requires sufficient input signal-to-noise ratio (SNR). The idea here is to extend the ACS by extrapolation (or prediction) rather than windowing the data.

The Burg method was found to yield far superior performance for data records consisting of 64 data samples. Note, however, that a minimum SNR of 15 dB was assumed. Using this method a "smart" routine was developed that automatically determines the actual frequency components of the data record.

SPECTRAL ANALYSIS
OF SHORT DATA RECORDS

I. Overview

Introduction

The motivation for this study is the need for improved detection of hostile signals (i.e., signals that are radiated by hostile emitters). An emitter is any signal source (i.e., a radar, a jammer, etc). The signal radiated by the emitter is made up of many measurable characteristics. Wiley (33:8-12) provides a summary of the measurable signal characteristics and the emitter capabilities inferred from these characteristics. The most common measurable signal characteristics are:

1. Pulse repetition frequency (PRF)
2. Transmitted signal power
3. Transmitted beamwidth
4. Operating frequency

The carrier (or operating) frequency of the hostile signal is the signal characteristic of interest in this study. The intent of this study is to examine two methods (Blackman-Tukey and Burg) for determining the operating frequency of one or more emitters, via the power spectral density (PSD).

Background

The basic scenario is an electronic warfare (EW) receiver detecting signals from hostile emitters. Figure 1.1 shows a generic block diagram of a receiver. No distinction is made between the receiver and the digital processor. However, note that all blocks to the right of the dashed line represent digital hardware.

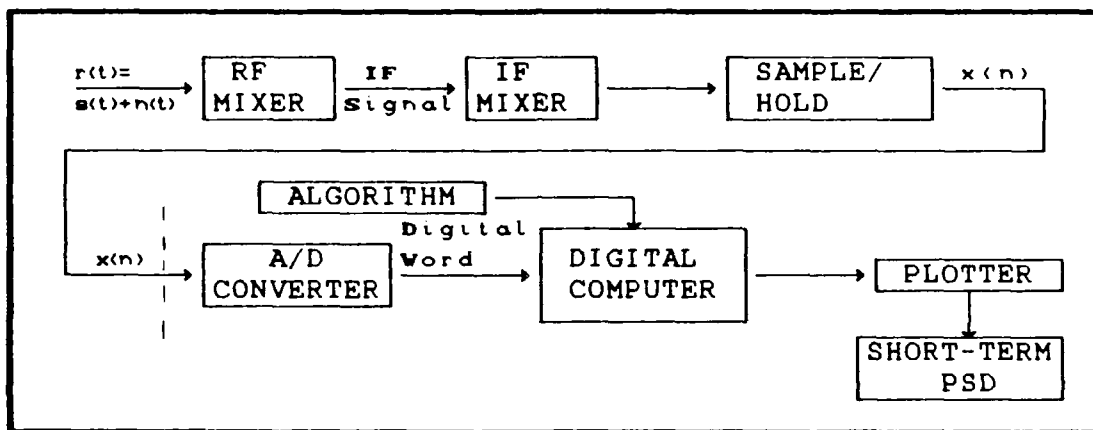


Figure 1.1. Generic Receiver Block Diagram

The receiver input signal $r(t)$ operates within the radio frequency (RF) band, 300 MHz to 30 GHz. Hence, the signal is termed the RF signal. For the purpose of this study, the RF signal is assumed to operate at the high end of the RF band (greater than say 1GHz). The RF signal is down-converted (or translated) to an appropriate baseband frequency and then sampled, as indicated in Figure 1.1. The purpose of sampling the baseband representation of $r(t)$ is to allow for digital processing. Generally, digital

processing is more efficient and less costly than analog (28:119). However, quantization error (or noise) is an inherent problem of digital processing. This error results from the roundoff effect that occurs when converting a continuous signal into a set of finite discrete levels. Tong (31:512-521) provides a detailed discussion of quantization error and methods for reducing this error.

The sampling theorem states that a baseband signal is completely reconstructed (no information loss) if the sampling rate is at least twice the highest frequency component of the baseband signal (9:230). Ideally, sampling is desirable at the RF bandpass signal - allowing for an all digital EW receiver. Unfortunately, digital technology is not capable of providing reasonable results when the RF signal is above 1 GHz. The bandpass sampling theorem requires that the sampling rate lie between $2B$ and $4B$, inclusively. The variable B is the bandwidth of the RF signal which can be on the order of 1000's of MHz. Current digital circuitry is unable to sample at such fast rates (27:55). Once the baseband signal is sampled and converted into a digital word, the digital computer is used to determine the PSD of the signal.

The above discussion did not consider the statistical nature of the bandpass signal $r(t)$. The signal $r(t)$ consists of the transmitted hostile signal $s(t)$ plus noise $n(t)$. The noise is induced onto the hostile signal by the

channel (medium of propagation). Thus, $r(t)$ is actually a random signal (or random process).

A random process is completely described statistically if all its N -th order joint density functions are known (i.e., N approaches infinity), a practical impossibility (9:482). For many practical applications, only the first and second order statistics are used to describe a random process (24:208). The autocorrelation function, a second order statistic, for a continuous time random process is defined as

$$R_x(t, t+\tau) = E\{x(t)x(t+\tau)\} \quad (1.1)$$

where $E\{\cdot\}$ denotes the expected value (or statistical average) of the product $x(t)x(t+\tau)$. If a random process $x(t)$ is wide sense stationary (WSS), then

$$R_x(t, t+\tau) = R_x(\tau) \quad (1.2)$$

This implies that the autocorrelation function is independent of time shifts. The variable τ is called the lag variable, the amount of time by which t lags behind $t+\tau$. If $x(t)$ is also ergodic, then

$$E\{x(t)x(t+\tau)\} = \langle x(t)x(t+\tau) \rangle \quad (1.3)$$

where $\langle \cdot \rangle$ denote the time average (13:250). Thus, ergodicity requires that the result of the statistical (or ensemble) average and the time average be identical. The receiver input signal $r(t)$ is assumed to be both WSS and ergodic.

The above considers the case of a continuous time

random process. However, as eluded to earlier the continuous process $r(t)$ is down-converted to a baseband frequency and sampled. Therefore, a discrete implementation of the autocorrelation function is desired. A sampled continuous time random process is a discrete time random process. Papoulis (24:290) shows that if a continuous time random process $x(t)$ is WSS with autocorrelation $R_x(\tau)$, then $x(n)$, a sampled version of $x(t)$, has an autocorrelation given by

$$R_x(k) = E\{x(n)x(n+k)\} \quad (1.4)$$

This is called the discrete autocorrelation function (or autocorrelation sequence) and is a sampled version of $R_x(\tau)$.

The ground work has been developed and it is now time to define the PSD. According to the Wiener-Khintchine theorem (14:181), the PSD of an ergodic discrete time random process is given by

$$P_x(f) = \text{DTFT} [R_x(k)] \quad (1.5)$$

This says that the PSD is the discrete-time Fourier transform (DTFT) of $R_x(k)$ and, conversely,

$$R_x(k) = \text{DTFT}^{-1}[P_x(f)] \quad (1.6)$$

The discrete autocorrelation function is the inverse discrete-time Fourier transform of the PSD. A more definitive explanation and expression of $R_x(k)$ and $P_x(f)$ are presented in Chapter III. It is important to understand the motivation for stating the discrete autocorrelation

function. The random signal processed by the digital computer for computation of its PSD is not continuous but discrete. This is the signal $x(n)$ that appears as the output of the sampler in Figure 1.1. Several methods have been developed for implementation on digital computers, that determine the PSD of a discrete random signal based on its discrete autocorrelation function (18:1382). In order to be consistent with current literature, the discrete random signal $x(n)$ is hence forth referred to as a data record (or discrete time series).

The two methods considered in this study are Blackman-Tukey (BT) and Burg. The BT method is a fast Fourier transform (FFT) technique employed to determine the PSD of a data record. This method, commonly referred to as a conventional approach, is computationally efficient and generally produces reasonable results. However, degrading frequency resolution problems arise when the data record being considered is short.

The Burg method, referred to as a modern approach, attempts to overcome the frequency resolution problems of the BT method, particularly for short data records. The idea here is to construct a parametric linear discrete model that approximates the data record. The PSD is computed based on this model. The motivation for using the Burg method is its promise for better frequency resolution.

The BT and Burg methods are discussed in detail in Chapter III.

Problem Statement

Several approaches are available to determine the PSD of a random process. There are pros and cons associated with the selection of any one of the approaches. Two candidate approaches are examined in this study. The two approaches are applied to several known data records. A comparison of the two approaches is made based on their statistical properties and computational efficiency.

Scope

This study proposes to examine the merits of the BT and Burg methods of spectral estimation for typical hostile emitter signals. The evaluation of the two methods is based solely on manual calculations and computer simulations. No hardware prototypes are attempted. Also, a "smart routine" is introduced that attempts to automatically determine the spectral peaks corresponding to emitter frequencies.

Assumptions

The emitters are assumed to transmit at a single operating frequency per pulse. Of course, each emitter transmits at its own respective frequency. The reason for the restriction of a single frequency per pulse is because of software limitations. That is, the software package used, Interactive Signal Processing Executive (ISPX), to

simulate the emitter signals does not allow the user to vary the frequency per pulse. Thus, $r(t)$ is assumed to consist of distinct frequencies corresponding to each emitter.

The random process $r(t)$ is assumed WSS. Practically, many random processes are not strictly WSS. Hence, the PSD cannot be defined as given by (1.5). However, if the duration of the observation interval (the number of data points) is small, the process may be considered locally WSS (24:125). A locally WSS process is one for which the variations of the autocorrelation function is small over the duration of the observation interval. Most real world random processes are considered locally WSS.

Presentation

Chapter II provides a brief discussion of the ISPX software package used and a discussion of previous research. Chapter III provides the development of the theory for both the BT and the Burg methods of spectral estimation. Chapter IV discusses findings as they relate to several known input data records for both methods. Chapter V provides conclusions and recommendations for further study.

II. ISPX Software Package and Previous Research

Introduction

The purpose of this chapter is twofold - to briefly discuss the ISPX software package and to present previous research on the BT and Burg methods of spectral estimation. The ISPX software package currently resides on the Air Force Wright Aeronautical Laboratories (AFWAL) VAX computer in the directory of Dr. James Tsui. The package allows the user to generate a variety of "real world" data records. A number of different spectral estimation methods can be applied to each data record, and the results viewed graphically. However, as mentioned in the previous chapter only the BT and Burg methods are considered in this study. The ISPX package is a tool which very nicely allows for studying the characteristics of the BT and Burg methods. The findings presented in Chapter IV are a result of applying the appropriate routines of ISPX to several known data records. The appropriate routines are provided in Appendix A. Reference to each routine is made in the next chapter.

The data record is traditionally processed by using FFT based (or conventional) methods of spectral estimation. There are inherent limitations associated with conventional methods. The most prominent limitations are poor frequency resolution and leakage. As will be discussed in the following two chapters, these limitations become more pronounced for short data records. Short data records are a

common occurrence for receiver systems like that outlined in Chapter I. In an attempt to alleviate the inherent limitations of conventional methods, researchers have devised other methods of spectral estimation. The other methods are referred to in the literature as modern spectral estimation methods. The modern methods, however, are not a "fix-all" solution to spectral estimation for all data records. They also have their limitations. The BT and Burg methods are respectively considered conventional and modern spectral estimation methods. Both methods are discussed in detailed in the next chapter.

ISPX Software Package

This section is intended to provide a brief overview of the ISPX software package. The interested reader is referred to reference (2:1-20) for a more complete discussion of ISPX. The ISPX package provides a number of signal processing operations. However, only the operations required to analyze the previous two mentioned spectral estimation methods are discussed. The operations are:

1. Generate data arrays
2. Choose PSD method and execute
3. Plot an array

The generate data operation allows the user to generate a wide variety of "real world" data records. Each data record generated can consists of up to five independent sinusoids. The variable parameters of each sinusoid are

frequency, amplitude, delay, and duration. The values of these parameters are specified by the user; however, default values are provided. This multiple sinusoid feature allows the user to simulate a data record corresponding to a received signal consisting of sinusoids from different emitters. A pseudo random WGN process can be embedded on the data record to emulate the effects of the noisy channel. The noise amplitude is the parameter the user changes to vary the input signal-to-noise ratio (SNR) of the data record. That is, for a desired input SNR, the noise amplitude required may be calculated by the following

$$NA = \frac{1}{\sqrt{2}} \left[\frac{SA}{10^{SNR/20}} \right] \quad (2.1)$$

where NA and SA represent noise and signal amplitudes, respectively.

Once the data record is established, the PSD operation is performed. The newly generated data record is sampled, and the appropriate PSD choice is made. The user specifies the sampling frequency, such that the Nyquist baseband sampling theorem is obeyed. A unity sampling frequency allows the user to deal in normalized (or fractional) frequency. Of course, the frequencies contained in the data record must be chosen accordingly. For simplicity, the examples presented in Chapter IV are all based on a unity sampling frequency. ISPX allows the user to select one of several spectral estimation schemes, both conventional and

modern. However, as eluded to earlier only the conventional BT and the modern Burg methods are considered in this study. In selecting the BT method, the user must specify the number of frequency samples, the largest lag, and the lag window. Each of these parameters are discussed fully in the next chapter. However, it is worth noting the different lag windows provided by ISPX. They are:

1. Cosine
2. Hamming
3. Kaiser-Bessel

As will be discussed in the following chapters, the hamming lag window provides the overall best performance for the examples considered in this study. In selecting the Burg method, the user must specify the number of frequency samples, and the model order number. Again, these parameters are discussed in the next chapter.

The plotting operation is invoked after the user specifies the appropriate PSD method. The plotting operation allows the user to graphically illustrate the spectral estimation schemes. The user is provided the option of plotting the results of up to four spectral estimation schemes on a single graph. This feature is particularly useful for making visual comparisons between different spectral estimation methods, or comparisons of the same method with differing parameters.

Previous Research

This section provides a brief summary of current research in the area of spectral estimation. Specifically, research done over the past decade pertaining to the BT and Burg methods of spectral estimation is presented.

Cooper and Kaveh (7:313-323) considers the effects of noise on the spectral estimate provided by the Burg method. They note that as the noise increases the resolution of the spectral estimation becomes progressively worse. In an attempt to mitigate the effects of the noise, they increased the model order number of the estimate. Noting that the resolution improved; however, spurious (or unwanted) peaks began to appear. They also compared the spectral estimates produced by both the BT and Burg methods for a given data record. The data record consisted of two sinusoids corresponding to doppler shifts from two radar targets. They note that the number of lags required by the BT method are generally greater than the model order number required by the Burg method to achieve a given frequency resolution.

Haykin (12:258-262) applies the Burg method to solve the problem of estimating the angle(s) of arrival of plane wave(s) impinging on a linear array antenna from unknown direction(s). The location of the spectral peaks indicates the directions of the incident plane waves. For an input SNR of 18dB, he notes that for a single source (one target) illuminating a linear vertical array composed of eight

equally spaced horn antennas: (1) the location of the spectral peak coincides very closely with the actual direction of the source; (2) the resolution increases with increasing model order number; and (3) spurious spectral peaks appear as the model order number is increased. In fact, there may be as many as P peaks in the spectrum. The variable P is called the model order number and will be discussed in the next chapter.

Kunt (19:326-339) provides several examples illustrating the performance of the BT spectral estimator. He notes that as the data samples of a given data record are decreased, the frequency resolution of the estimator also decreases. He investigates the resolution-leakage phenomenon of several lag windows. Substantiating the well-known fact, that for a sinusoidal process the frequency resolution of the estimator is largely determined by the main lobe and sidelobe characteristics of the lag window chosen. These characteristics tend to become less favorable as the number of data samples decreases. For this reason, the BT spectral estimator typically provides poor results for short data records. Particularly, when the data record consists of two or more closely spaced sinusoids.

Bishop and Ulrych (4:189-192) investigate the Akaike criterion (briefly discussed in the next chapter) for determining the model order number of the Burg spectral estimator. Ideally, the correct model number is that number

which results in a minimum value of the Akaike criterion. They note that the Akaike criterion typically results in model order numbers that are too low. They emphasize that model order number selection is in general a difficult problem, and that the Akaike criterion and other proposed criteria serve only as guidelines. However, they state that for sinusoidal processes the Akaike criterion yields the "best" results.

III. Detailed Theory

Introduction

The power spectral density (PSD) and its estimation are receiving much attention by researchers in many disciplines. The PSD is considered an effective medium that allows for characterizing a stationary random process (6:27). Two common but distinctly different schemes are usually considered when attempting to estimate the true PSD. They are:

1. The conventional method of PSD estimation
2. The modern method of PSD estimation

The most notable conventional method is the method proposed by Blackman and Tukey (BT) - the BT method (5:187-282). This method is based on computing the DFT of a finite windowed (or tapered) autocorrelation sequence (ACS). Thus, the BT method produces a PSD estimate which is the transform of the window function convolved with the simple PSD estimator. The window function plays a very important role in determining the resolution and the sidelobe phenomena associated with the estimate of the BT method, particularly for sinusoidal processes embedded in additive WGN. Often, the selection of the window function that provides the "optimal" compromise between high resolution and low sidelobes is determined empirically (23:84-86). The BT method generally provides unacceptable results for short data records - a smeared spectral estimate with very poor

resolution (1:450). Short data records occur frequently in practice, particularly for radar systems in which only a few data samples are available for each received pulse (18:1381). A common error is that of appending a sequence of zeroes to the data record in hope for improved resolution. This technique, commonly referred to as zero padding, merely reduces the spacing between adjacent spectral lines by interpolation (21:43).

The motivation for modern methods is their promise for better frequency resolution, particularly for short data records. The most notable modern method is the autoregressive (AR) method (11:56). The idea here is to model the data record by an all-pole rational transfer function. This allows for extrapolation of data samples beyond the observation interval, not implicitly assuming the samples are zero as with conventional methods (7:321). Theoretically, the data samples can be extended indefinitely. More data samples allow for computation of more autocorrelation lags, and therefore in general an improvement in resolution. Also, for all practical purposes, the window function is removed; therefore, the degrading effects of sidelobes are alleviated. Of course, the accuracy of the PSD estimate provided by the AR method depends directly on the accuracy of the rational transfer function used to model the data record. The approach for estimating the PSD, using the AR method, is drastically

different from that of the BT method. The parameters of the assumed model are estimated from the available autocorrelation lags, and then the theoretical PSD implied by the model is calculated using the estimated parameters. There are several known techniques for estimating the parameters of the assumed model (20:562). In this chapter, only the Burg approach is considered.

The following sections provide a detailed discussion of the BT and Burg methods.

Conventional Spectral Estimation - Via the BT Method

The PSD simply represents the power distribution of the random process along the frequency axis (26:137). For a WSS continuous random process $x(t)$, the true PSD is given by the Fourier transform

$$P_x(f) = \int_{-\infty}^{\infty} R_x(\tau) \exp(-j2\pi f\tau) d\tau \quad (3.1)$$

of the autocorrelation function $R_x(\tau)$. Therefore, the PSD of the WSS discrete random process $x(n)$ is given by the discrete-time Fourier transform (DTFT)

$$P_x(f) = \sum_{k=-\infty}^{\infty} R_x(kT) \exp(-j2\pi f kT) \quad (3.2)$$

of the ACS $R_x(kT)$, which corresponds to equal distant shifted versions of $P_x(f)$ (see Figure 3.1) (6:291). The

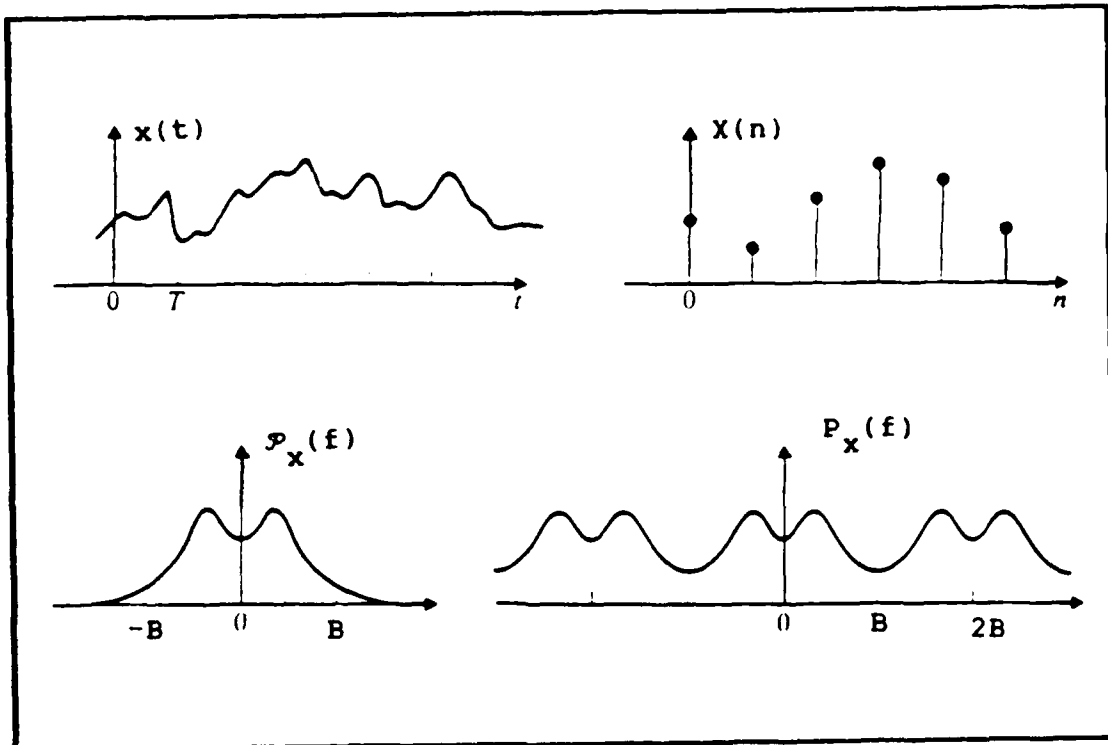


Figure 3.1. Continuous and Discrete Random Processes and their Respective PSD's (6:291)

ACS (10:54), assuming a real and ergodic $x(n)$, as defined by Eq (1.4) is given as

$$R_x(k) = \lim_{M \rightarrow \infty} \frac{1}{2M+1} \sum_{n=-M}^M x(n)x(n+k) \quad (3.3)$$

For simplicity in notation, the sampling interval T is implied (i.e., $k = kT$ and $n = nT$). Properties of the ACS are

$$\begin{aligned} R_x(k) &= R_x(-k) \\ R_x(0) &\geq |R_x(k)| \end{aligned} \quad (3.4)$$

These properties indicate that the ACS is a real even

sequence (for real $x(n)$) with a maximum at the zero lag.

The computation of the ACS is practically impossible, requiring an infinite number of data samples. An estimate of the ACS is the only alternative. Hence, the PSD as given by Eq (3.2) can at best be approximated. Two commonly used autocorrelation estimates (17:73-74) are

$$\tilde{R}_x(k) = \frac{1}{N} \sum_{n=0}^{N-|k|-1} x(n)x(n+k) \quad (3.5a)$$

and

$$\hat{R}_x(k) = \frac{1}{N-|k|} \sum_{n=0}^{N-|k|-1} x(n)x(n+k) \quad (3.5b)$$

where N is the total number of data samples (i.e., $x(n)$ for $n = 0$ to $n = N-1$). Thus, a total of $2N-1$ lags of the autocorrelation estimates are possible. The symbol $\tilde{}$ denotes the biased estimator and symbol $\hat{}$ the unbiased estimator. A biased estimator is one in which its expected value (or mean) deviates from the actual value being estimated. The expected value of an unbiased estimator is the actual value (30:9). The expected values of the biased and unbiased autocorrelation estimators are, respectively,

$$E\{\tilde{R}_x(k)\} = \left[1 - \frac{|k|}{N}\right]R_x(k) \quad (3.6a)$$

and

$$E\{\hat{R}_x(k)\} = R_x(k) \quad (3.6b)$$

Observe that the expected value of the biased autocorrelation estimator is equal to the actual value $R_x(k)$ weighted by the Bartlett (or triangular) window. The expected value of the unbiased autocorrelation estimator is the actual value. Intuitively, it might be thought that the unbiased autocorrelation estimator is the best choice for use in Eq (3.2). However, Chen (6:27-28), Kunt (19:293-295), and Marple (21:146-149) show that as the lag value k approaches its limit (i.e., k approaches $N-1$), the variance (or fluctuation) of the unbiased autocorrelation estimator increases dramatically as compared with that of the biased autocorrelation estimator. This increased variance causes the unbiased autocorrelation estimator to yield results not always satisfying the properties of Eq. (3.4). Figure 3.2 presents plots of both estimators for a data record generated by a first-order digital filter, with a psuedo WGN input process (19: 296-297). The plots are for different values of k and N . A comparison of the plots indicates the variance of the unbiased estimator is greater for $k \approx N$. However, the variance of both estimators appears identical for $k \ll N$. The latter occurs most often in typical radar type problems. Therefore, some researchers argue that the unbiased autocorrelation estimator is in fact the best choice based solely on Eq (3.6).

A more valid comparison, suggested by Jenkins and Watt (15:179-181), is to consider the mean square error (mse) of

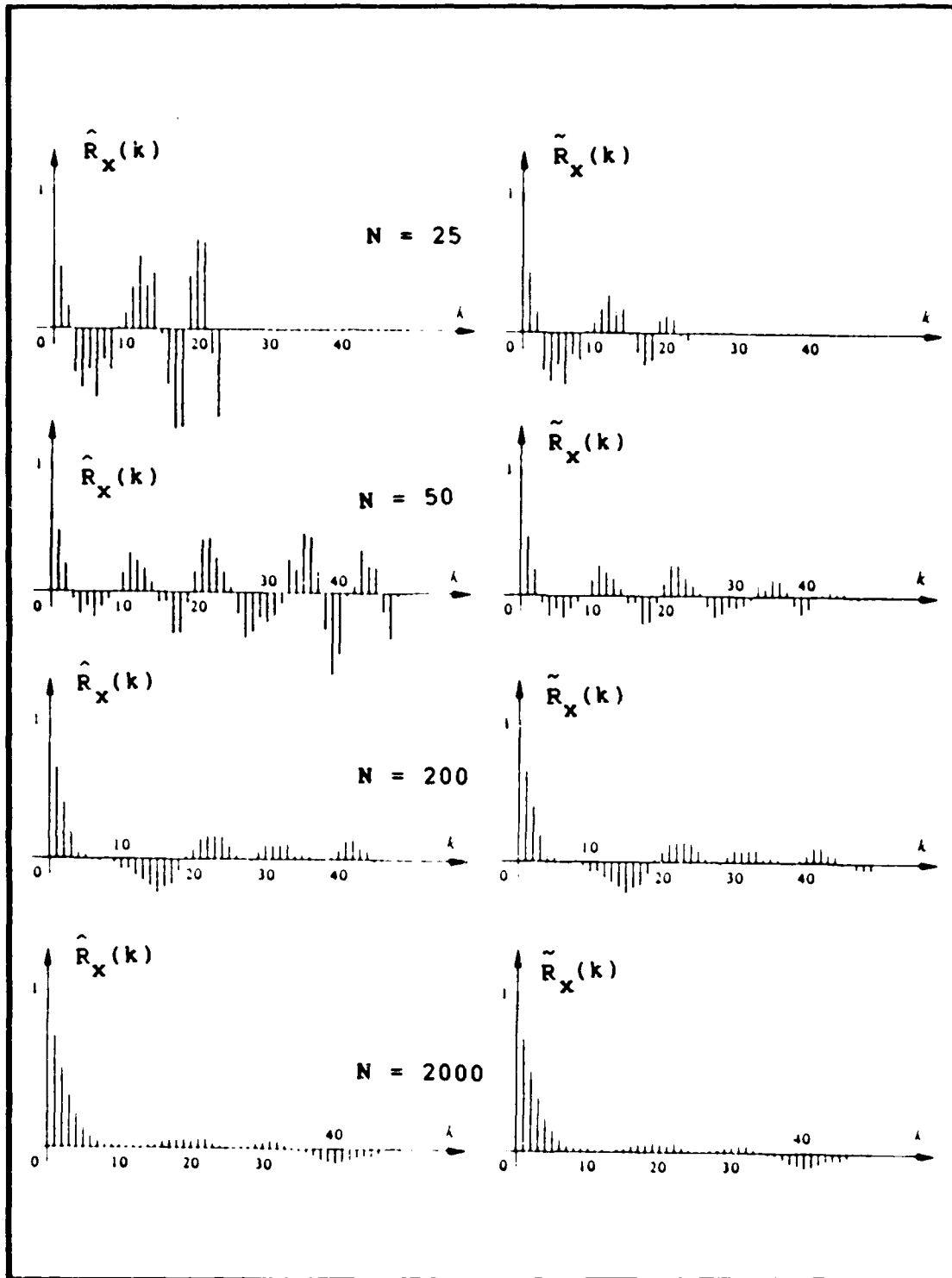


Figure 3.2. Plots for both Autocorrelation Estimators (19:296-297)

the two autocorrelation estimators. Jenkins and Watt concluded that the mse of the biased autocorrelation estimator $\tilde{R}_x(k)$ is typically smaller for all values of k . Therefore, in this study the PSD is estimated using the biased autocorrelation estimator, namely

$$\tilde{P}_x(f) = \sum_{k=-(N-1)}^{N-1} \tilde{R}_x(k) \exp(-j2\pi fk) \quad (3.7)$$

defined for $-1/2T \leq f \leq 1/2T$. This equation represents a low-pass filtered approximation of $P_x(f)$ and hence an approximation of $\mathcal{P}_x(f)$ (see Figure 3.1). The use of $\tilde{R}_x(k)$ in Eq (3.7) is not to suggest that the biased autocorrelation estimator always yields a superior estimate of the PSD. Jenkins and Watt only suggested that the PSD determined from the biased autocorrelation estimator is better on average, particularly for large k .

The PSD estimator given in Eq (3.7) is called the simple (or periodogram) PSD estimator (29:238). This estimator, at first glance, might appear to approach that of Eq (3.2) for large N . If this happened, then the simple PSD estimator is said to be consistent. A consistent estimator is one in which its bias and variance both tend to zero as the number of data samples increases (32:71). Kay (17:80-82) and Kunt (19:302-304) show that the simple PSD estimator is not consistent, as a consequence of the autocorrelation estimator. Although the bias of the simple PSD estimator asymptotically approaches zero as the data

samples increases, the variance

$$\text{Var}\{\tilde{P}_x(f)\} \cong P_x^2(f) \quad (3.8)$$

remains essentially constant - the square of the desired PSD. Figure 3.3 shows the true PSD of a random signal consisting of a weak and strong sinusoid embedded in WGN.

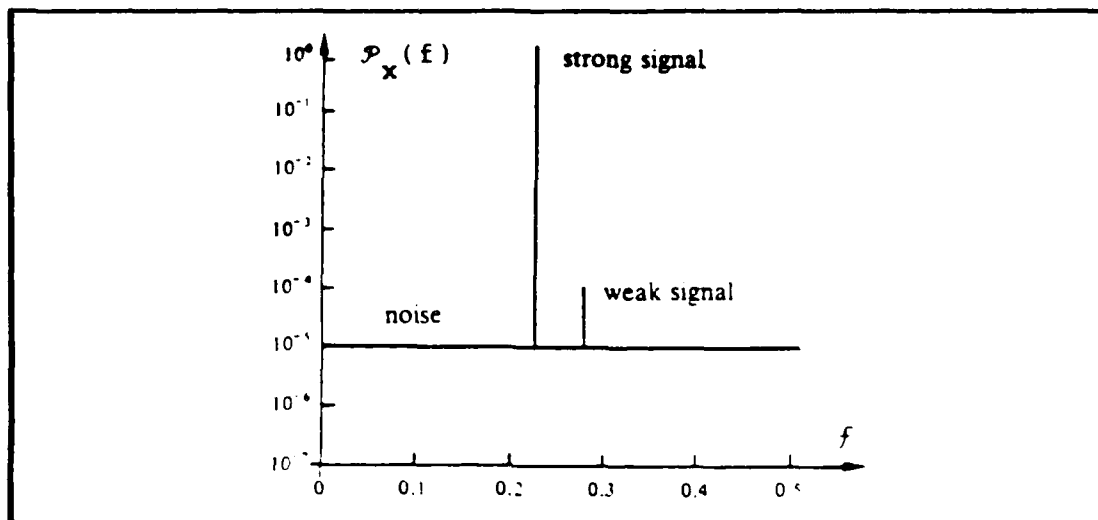


Figure 3.3. The Ideal PSD of a Strong and a Weak Signal Embedded in WGN (19:328)

Note that the frequency axis represents a fractional (or normalized) frequency - the actual frequency divided by the sampling frequency $f_s = 1/T$. Figure 3.4 depicts the results of the simple PSD estimator for several data record lengths. As expected, the variance appears to remain essentially constant for different values of N . Many researchers agree that the simple PSD estimator generally provides unreliable results, particularly if there is no a priori knowledge of the true PSD (1:448).

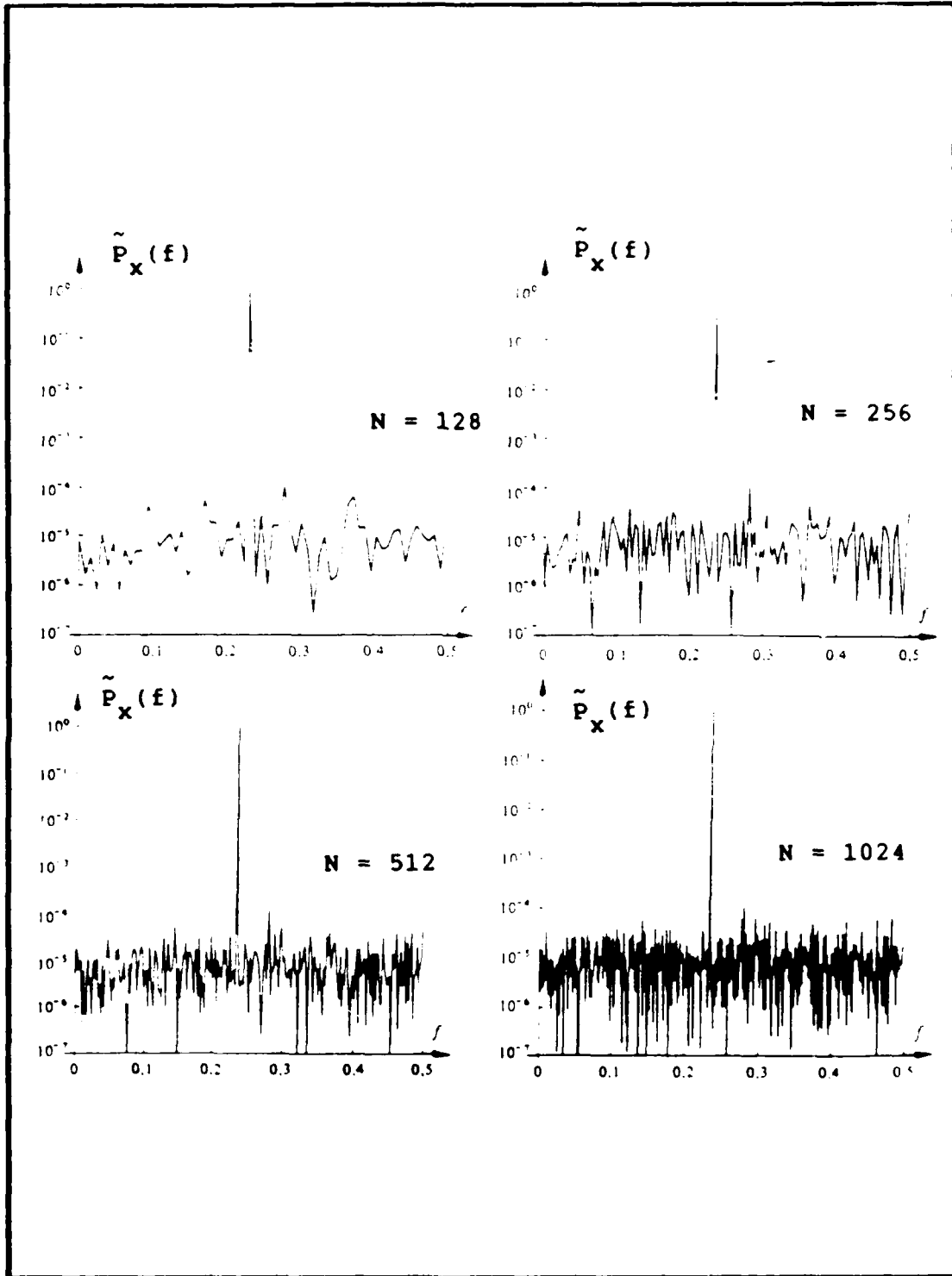


Figure 3.4. The Simple PSD of Weak and Strong Signal Example for Various Values of N (19:328)

A method to reduce the variance of the simple PSD estimator is functionally described in Figure 3.5. The biased autocorrelation estimator is computed from a given data record, windowed, and then transformed.

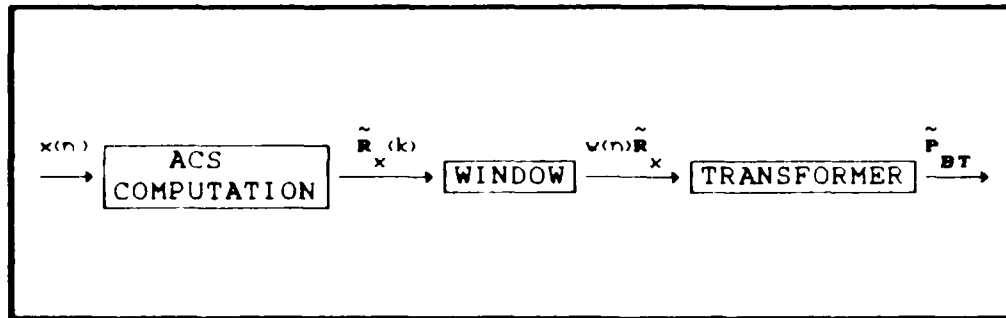


Figure 3.5. A Functional Description of the BT Method

This method is mathematically expressed as

$$\tilde{P}_{BT}(f) = \sum_{k=-M}^M w(k) \tilde{R}_x(k) \exp(-j2\pi fk) \quad (3.9)$$

where $M \leq N-1$ and $w(k)$ is called the lag window with the following properties

$$\begin{aligned} 0 \leq w(k) \leq w(0) &= 1 \\ w(k) &= w(-k) \\ w(k) &= 0 \quad \text{for } |k| > M \end{aligned} \quad (3.10)$$

The subscript BT is used to designate this as the Blackman and Tukey PSD estimator - Blackman and Tukey pioneered the development of this estimator. The BT PSD estimator can also be represented as

$$\begin{aligned}\tilde{P}_{BT}(f) &= \text{DTFT}\left\{w(k)\tilde{R}_x(k)\right\} \\ &= \int_{-1/2T}^{1/2T} W(f-\xi)P_x(\xi)d\xi\end{aligned}\quad (3.11)$$

where $W(f)$, the spectral window, is the discrete-time Fourier transform of the lag window. Thus, the BT PSD estimator is commonly considered a smoothed (or filtered) version of the simple PSD estimator. All is not gain, however, when using the BT PSD estimator. The BT PSD estimator allows for a reduction of variance at the expense of increasing the bias, or equivalently a reduction of sidelobes at the expense of deteriorating the frequency resolution. Kay (82-84) shows that the mean and variance of the BT PSD estimator are, respectively,

$$E\left\{\tilde{P}_{BT}(f)\right\} \cong \int_{-1/2T}^{1/2T} W(f-\xi)P_x(\xi)d\xi\quad (3.12)$$

and

$$\text{Var}\left\{\tilde{P}_{BT}(f)\right\} \cong \frac{1}{N} P_x^2(f) \sum_{k=-M}^M w^2(k)\quad (3.13)$$

If a small bias is desired, then M is chosen large such that the spectral window acts as a dirac delta function. On the other hand, for small variance M is chosen small as indicated by Eq (3.13). Clearly, a compromise of acceptable bias and variance has to be determined. In most cases, this

compromise depends on the particular application of the estimator. Figure 3.6 shows the BT PSD estimator of the spectrum given in Figure 3.4, assuming a Blackman lag window. A comparison of Figures 3.5 and 3.6 indicates that although the weak sinusoid is not detected, the BT PSD estimator is much smoother (less variance). Therefore, the BT PSD estimator is considered more reliable (19:334).

The selection of the lag window is considered an "art" in conventional PSD estimation. The lag window is not to be

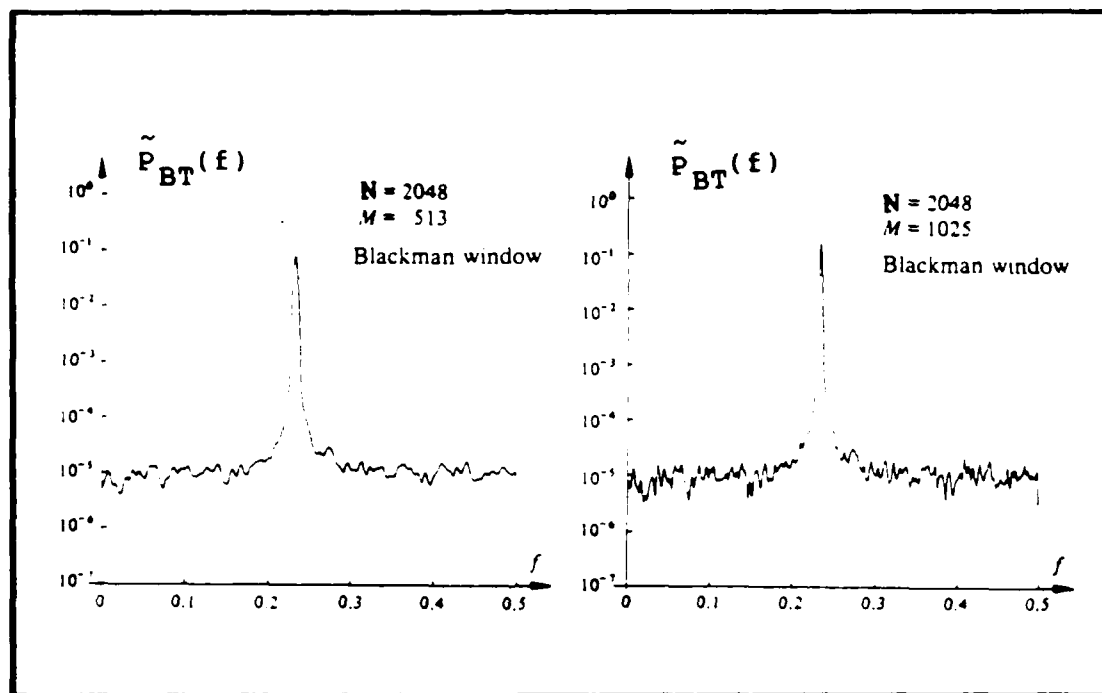


Figure 3.6. The BT PSD of the Weak and Strong Signal Example (19:334).

confused with the data window. The data window is unavoidable as implied by Eq (3.5). That is, the autocorrelation estimator is computed based on a finite

number of data samples (the data record). The Blackman-Tukey approach as defined by Eq (3.9) assumes that the data window is rectangular. The lag window, however, is optional and is used primarily to reduce the variance (11:63). Unfortunately, there is no algorithm that precisely defines the approach for selecting the most appropriate lag window. For this reason, many discrete-time lag windows have been proposed for use in PSD estimation. An empirical approach of window selection is usually done, especially if there is no a priori knowledge of the random process. It is beyond the scope of this study to consider the detailed characteristics of the many proposed lag windows (see any of the above mentioned references). However, it suffices to say that the spectral resolution of the BT PSD estimator depends largely on the main lobe of the spectral window. Also, the sidelobes of the spectral window greatly influences the variance of the BT PSD estimator.

The implementation of the BT PSD estimator on digital computers requires

$$\begin{aligned} \tilde{P}_{BT}(f_i) &= \sum_{k=-M}^M w(k) \tilde{R}_x(k) \exp(-j2\pi f_i k) \\ &= \text{DFT} \left\{ w(k) \tilde{R}_x(k) \right\} \end{aligned} \quad (3.14)$$

where $f_i = i/KT$ for $0 \leq i \leq K-1$. The discrete Fourier transform (DFT) differs from the DTFT in that both the time and frequency representation of the process are discrete.

Generally, a fast Fourier transform (FFT) algorithm is used to compute Eq (3.14) (see Appendix A). The value of K is arbitrary, but usually $K \gg M$, so that sharp details in the PSD estimate will not be missed (21:152). If $K \gg M$, then the argument of Eq (3.14) is zero padded from $M+1$ to K . Zero padding decreases the spacing between spectral line components in the DFT and does not really improve the resolution between two closely spaced spectral components of the signal (see Figure 3.7). The spectral resolution is improved, particularly for short data records, by considering modern techniques of spectral estimation. These techniques extend the ACS by extrapolation (or prediction) rather than appending zeroes. The following section considers the modern technique of autoregressive (AR) spectral estimation.

Modern Spectral Estimation - Via the AR/Burg Method

The autoregressive (AR) spectral estimation technique is a parametric method which attempts to model the data record with an all-pole rational transfer function. Ulrych and Bishop (4:185) argue that many discrete-time random processes encountered in practice may be described by

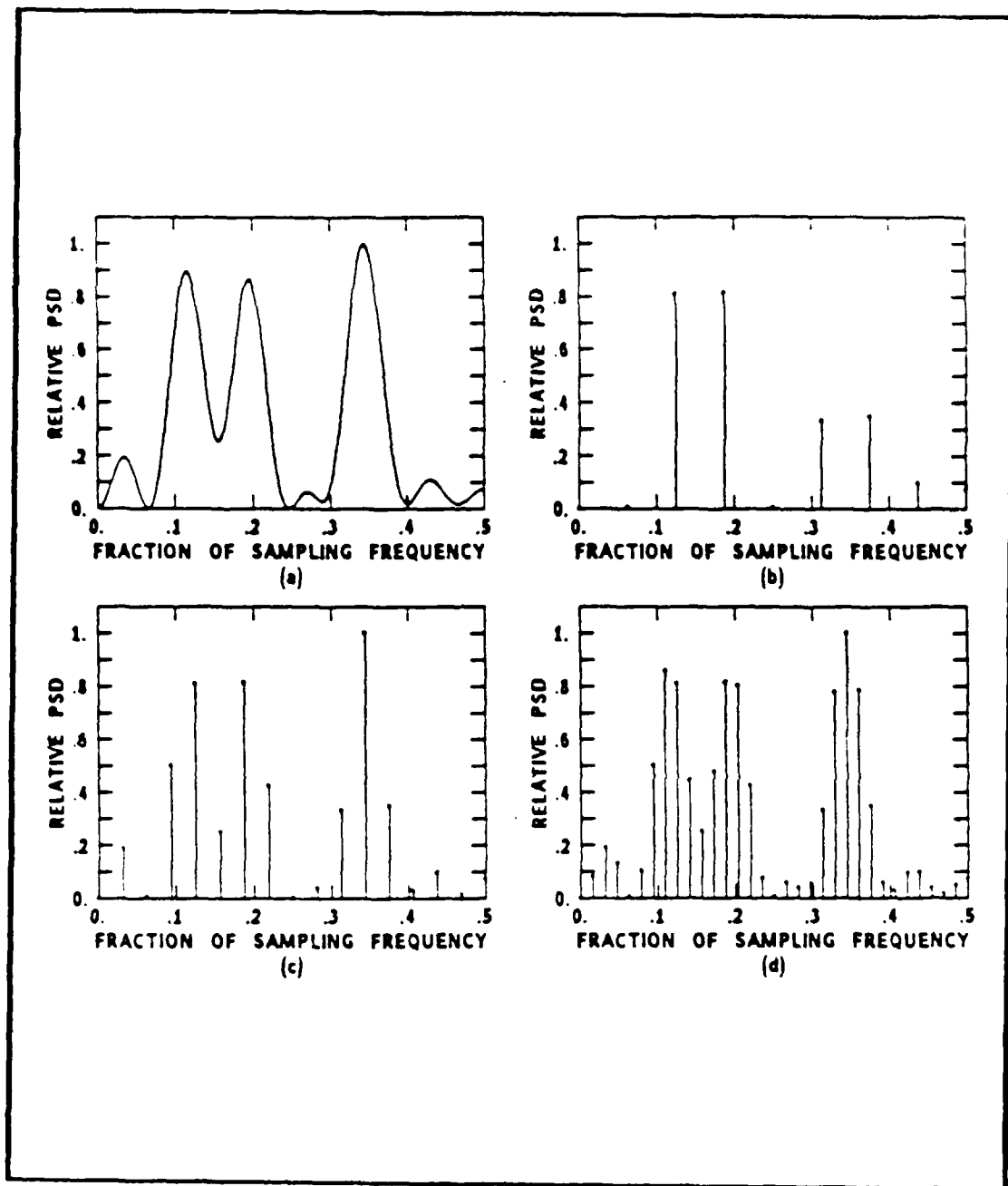


Figure 3.7. Transform Interpolation by Zero Padding (21:24)
 (a) Magnitude of DTFT for a 16-point data record
 (b) Magnitude of DFT with no zero padding
 (c) Magnitude of DFT with two times zero padding
 (d) Magnitude of DFT with eight times zero padding

$$x(n) = - \sum_{k=1}^P a_p(k)x(n-k) + \eta(n) \quad (3.15)$$

where $a_p(1), a_p(2), \dots, a_p(P)$ are the P-th AR coefficients, and $\eta(n)$ is the sample of a zero-mean WGN random process with variance σ_p^2 . The above difference equation is referred to as an AR-process because $x(n)$ is a linear regression on itself with $\eta(n)$ representing the error. The variable P represents the order of the AR-process and plays a very significant role in determining the spectral density. More is said about the significance of P shortly. Taking the z-transform on both sides of Eq (3.15) and combining terms yields the system function

$$H(z) = \frac{1}{1 + \sum_{k=1}^P a_p(k)z^{-k}} \quad (3.16)$$

Thus, the AR-process is viewed as being generated by applying a zero-mean WGN process to an all-pole digital filter (see Figure 3.8). The system function is assumed to be both stable and causal (i.e., all poles lie inside the unit circle). This condition is necessary to insure that $x(n)$ is WSS (17:179), an assumption made throughout this study. The evaluation of $H(z)$ along the unit circle, $z = \exp(j2\pi f)$, yields the all-pole transfer function

$$H(f) = \frac{1}{1 + \sum_{k=1}^P a_p(k)\exp(-j2\pi fk)} \quad (3.17)$$

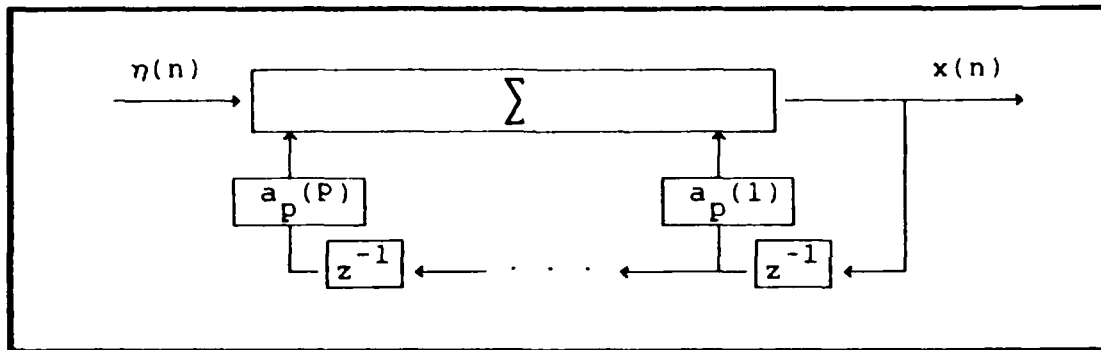


Figure 3.8. An All-Pole Filter for Generating and AR Process (12:250)

Therefore, the PSD of the random process, that implied by the linear discrete model, is

$$P_{AR}(f) = \frac{\sigma_p^2}{\left| 1 + \sum_{k=1}^P a_p(k) \exp(-j2\pi f k) \right|^2} \quad (3.18)$$

for $-1/2T \leq f \leq 1/2T$. This indicates that the problem of PSD estimation, via the AR method, is actually a problem of parameter estimation. The AR PSD is defined once the parameters $\{a_p(1), a_p(2), \dots, a_p(P), \sigma_p^2\}$ and P are determined. A myriad of methods are available for estimating these parameters. The interested reader is referred to Kay (17:243-261), Marple (21:206-230), Akaike (3:716-723), and Parzen (25:723-730). This study only examines the Burg method of estimating the parameters $\{a_p(1), a_p(2), \dots, a_p(P), \sigma_p^2\}$. Also, the procedure proposed by Akaike for estimating the model order P is briefly

discussed. However, before proceeding to discuss these two methods, the basis for the high frequency resolution attributed to the AR PSD method needs to be made clear. DuBroff (31:1622-1623) shows that an equivalent representation of the AR PSD is given by

$$P_{AR}(f) = \sum_{k=-\infty}^{\infty} \mathcal{R}_x(k) \exp(-j2\pi fk) \quad (3.19)$$

where

$$\mathcal{R}_x(k) = \begin{cases} R_x(k) & \text{for } 0 \leq k \leq P \\ \sum_{\ell=1}^P a(\ell) \mathcal{R}_x(k-\ell) & \text{for } k > P \end{cases} \quad (3.20)$$

Thus, assuming that the first $P+1$ true autocorrelation lags are known, via Eq (3.3). Eq (3.20) implies that autocorrelation lags may be recursively extended indefinitely. Although, computing the AR PSD with Eq (3.19) is not very practical. The usefulness of this equivalent form is to readily illustrate the basis for the high frequency resolution. That is, in contrast to the BT PSD estimator no windowing and no zero padding occurs. Hence, the AR PSD does not possess the sidelobe phenomena of the BT PSD estimator and generally has much better frequency resolution.

The problem of estimating the parameters $\{a_p(1), a_p(2), \dots, a_p(P), \sigma_p^2\}$ is now considered. Burg is credited

for developing the maximum entropy spectral density. Considering how best to estimate the extended autocorrelation lags, Burg argued that the time series (or data record) characterized by the known and extrapolated ACS should have maximum entropy. This implies that the time series is the most random. The rationale for this choice is that it provides for the flattest and the most minimum bias spectral estimate (17:199). Ulrych and Bishop (4:183-200) and a host of other researchers show that the maximum entropy spectral density is identical to the AR PSD for linear Gaussian random processes. Hence, the terms AR PSD and Burg PSD are used synonymously in this study.

Burg also suggested that in estimating the parameters $\{a_p(1), a_p(2), \dots, a_p(p), \sigma_p^2\}$, the Levinson-Durbin recursive algorithm be used. A detailed discussion of this algorithm is found in Kay (17:181-191). In summary, the Levinson-Durbin recursive algorithm provides estimates of the AR parameters by the following procedure

$$\tilde{\sigma}_0^2 = \tilde{R}_x(0) = \frac{1}{N} \sum_{N=0}^{N-1} |x(n)|^2 \quad (3.21)$$

For $k = 1, 2, \dots, p$

$$\tilde{a}_k(i) = \begin{cases} \tilde{a}_{k-1}(i) + \Gamma_k \tilde{a}_{k-1}(k-i), & i=1, \dots, k-1 \\ \Gamma_k, & i=k \end{cases} \quad (3.22)$$

and

$$\tilde{\sigma}_k^2 = (1 - |\Gamma_k|^2) \tilde{\sigma}_{k-1}^2 \quad (3.23)$$

The mathematical form of Eq (3.23) is analogous to the transmission of power through a terminated two-port device. Hence, Γ_k is known in the literature as the reflection coefficient (12:254). The estimate AR parameters $\{\tilde{a}_p(1), \tilde{a}_p(2), \dots, \tilde{a}_p(p), \tilde{\sigma}_p^2\}$ are known once the reflection coefficient is determined. Burg proposed to estimate the reflection coefficient by minimizing the sum of the forward and backward prediction error powers. The forward and backward prediction errors are defined, respectively, as

$$F_k(n) \equiv x(n) + \sum_{k=1}^P a_p(k)x(n-k) \quad (3.24a)$$

and

$$B_k(n) \equiv x(n-P) + \sum_{k=1}^P a_p(k)x(n-P+k) \quad (3.24b)$$

These two equations represent prediction-error filters operating in the forward and backward direction, respectively. The Burg method of determining Γ_k insures that if operating in the forward direction, then the prediction of $x(n)$ given $\{x(n-1), x(n-2), \dots, x(n-P)\}$ is the "best" possible prediction (i.e., the mean square error or forward prediction error power is minimized). Similarly, if operating in the backward direction, then the prediction of $x(n-P)$ given $\{x(n-P+1), x(n-P+2), \dots, x(n-1), x(n)\}$ is the "best" possible prediction (i.e., the backward prediction error power is minimized). Haykin (12:243-251) shows that

when the forward and backward prediction error powers are minimized, the resultant errors, Eq (3.24), take on the form of WGN processes. If this happens, then Eq (3.24) is equivalent to the AR process described by Eq (3.15). The sum of the forward and backward prediction error powers is given by

$$\rho_k = E \left\{ |F_k(n)|^2 + |B_k(n)|^2 \right\} \quad (3.25)$$

The reflection coefficient Γ_k is obtained by minimizing the above expression. Before doing so, it is convenient to make the following substitution for the forward and backward error

$$F_k(n) = F_{k-1}(n) + \Gamma_k B_{k-1}(n-1) \quad (3.26a)$$

and

$$B_k(n) = B_{k-1}(n-1) + \Gamma_k F_{k-1}(n) \quad (3.26b)$$

These two relations provide a recursive method for determining the errors and are obtained by simply substituting Eq (3.22) into Eq (3.24). After the substitution of Eq (3.26) into (3.25), ρ_k is differentiated with respect to Γ_k and set equal to zero. Applying some simple algebraic manipulations, it is easy to show that Γ_k is given by

$$\Gamma_k = -2 \frac{\sum_{n=k}^{N-1} F_{k-1}(n) B_{k-1}(n-1)}{\sum_{n=k}^{N-1} \left[|F_{k-1}(n)|^2 + |B_{k-1}(n-1)|^2 \right]} \quad (3.27)$$

where the expectations are approximated by spatial averages. Kay (17:255-256) shows Eq (3.27) guaranties that $\Gamma_k \leq 1$. Hence, the Burg method for determining the reflection coefficient provides poles which are on or inside the unit circle, resulting in a stable or marginally stable filter.

In an attempt to try and put the above method into some perspective, the computations are to proceed as follows:

1. The initial conditions are:

$$\tilde{\sigma}_0^2 = \tilde{R}_x(0) = \frac{1}{N} \sum_{n=0}^{N-1} |x(n)|^2 \quad (3.28a)$$

and

$$F_0(n) = B_0(n) = x(n), \quad n = 0, 1, 2, \dots, N-1 \quad (3.28b)$$

2. Compute the reflection coefficient, Eq (3.27), for $k = 1$
3. Compute the variance, Eq (3.23), for $K = 1$
4. Compute the AR coefficients, Eq (3.22), for $k = 1$
5. Compute the prediction error updates, Eq (3.26), for $K = 1$
6. Increment K by one, go back to step 2, and repeat.
7. Stop computation after the desired order P is reached.

To illustrate these steps consider the simple first-order AR process given by

$$x(n) = -a_1(1)x(n-1) + \eta(n) \quad (3.29)$$

Multiplying both sides of this equation by $x(n-k)$ and taking the expected values for $k=0$ to $k=1$ yields

$$\begin{bmatrix} \tilde{R}_x(0) & \tilde{R}_x(1) \\ \tilde{R}_x(1) & \tilde{R}_x(0) \end{bmatrix} \begin{bmatrix} 1 \\ a_1(1) \end{bmatrix} = \begin{bmatrix} \sigma_1^2 \\ 0 \end{bmatrix} \quad (3.30)$$

This matrix notation is commonly referred to as the set of first-order Yule-Walker equations (4:190). The unknown parameters are obviously $\{a_1(1), \Gamma_1^2\}$. The procedure outlined in the above seven steps yields the following relations

$$\Gamma_1 = -2 \frac{\sum_{n=1}^{N-1} x(n)x(n-1)}{\sum_{n=1}^{N-1} [|x(n)|^2 + |x(n-1)|^2]} \quad (3.31)$$

$$\tilde{\sigma}_1^2 = (1 - |\Gamma_1|^2) \tilde{\sigma}_0^2 \quad (3.32)$$

$$\tilde{a}_1(1) = \Gamma_1 \quad (3.33)$$

$$F_1(n) = x(n) + \Gamma_1 x(n-1) \quad (3.34)$$

and

$$B_1(n) = x(n-1) + \Gamma_1 x(n) \quad (3.35)$$

Thus, given $x(n)$ for $n = 0$ to $n = N-1$, the estimate parameters $\{\tilde{a}_1(1), \tilde{\Gamma}_1^2\}$ are easily obtainable. Note that for higher orders of P , steps two through six are repeated until the desired AR parameter estimates $\{\tilde{a}_p(1), \tilde{a}_p^2, \tilde{a}_p(P), \tilde{\Gamma}_p^2\}$ are obtained. These estimates are substituted into Eq (3.18) in order to obtain the AR (or Burg) PSD estimator, namely

$$\tilde{P}_{AR}(f) = \frac{\tilde{\sigma}_P^2}{\left| 1 + \sum_{k=1}^P \tilde{a}_P(k) \exp(-j2\pi fk) \right|^2} \quad (3.36)$$

Unfortunately, the recursive algorithm outlined above does not provide any constraint on the order P . That is, the AR parameter estimates may be recursively determined for any order P . However, if the value of P is too low, then the AR PSD estimator results in a smooth spectral estimate with poor frequency resolution. On the other hand, if the value of P is too high, then the estimator results in a spectral estimate with spurious peaks. This phenomenon is illustrated in the next chapter.

A number of researchers, such as Akaike (3:716-723), Parzen (25:723-730), and Kashyap (32:996-998), have proposed different schemes to determine the "correct" model order P . The word correct is in quotes, because model order determination is generally a non-trivial problem and in most cases the schemes suggested serve only as guidelines (22:2-11). Ulrych and Bishop (4:189-192) empirically found that the procedure suggested by Akaike provides the best estimate of P for AR linear Gaussian random processes. This procedure simply requires that P be selected such that the final prediction error (FPE) given by

$$FPE_P = \begin{cases} \left(\frac{N+P}{N-P} \right) \tilde{\sigma}_P^2, & 0 \leq P \leq N/2 \\ \left(\frac{N+P}{N-P} \right) \left(\frac{N}{1.5-P} \right) \tilde{\sigma}_P^2, & N/2 < P \leq N-1 \end{cases} \quad (3.37)$$

is minimized. The idea here is to select some maximum model order $L \leq N - 1$. Then successively compute the FPE for integer values of $P = 1$ to $P = L$. The value of P resulting in the minimum FPE is the "correct" model order. This approach is desirable if there is no a priori knowledge of the random processes. For this study, however, model orders are determined empirically since there is such a "wealth" of knowledge about the simulated random processes (see Chapter IV).

Observe that the denominator of Eq (3.36) is simply the squared magnitude of the DFT of the sequence $\{\tilde{a}_P(1), \dots, \tilde{a}_P(P)\}$, where $\tilde{a}_P(0) = 1$. Thus, once the AR parameter estimates $\{\tilde{a}_P(1), \tilde{a}_P(2), \dots, \tilde{a}_P(P), \tilde{\sigma}_P^2\}$ are recursively determined as discussed above, the AR PSD estimator, Eq (3.36), is determined by using a FFT algorithm (see Appendix A).

The statistics of the AR PSD estimator are generally impossible to obtain (17:211). However, Makhoul (20:568-569) shows that for large data records (i.e. N approaches infinity) the mean and variance of the AR PSD estimator are, respectively

$$E\left\{ \tilde{P}_{AR}(f) \right\} \cong P_{AR}(f) \quad (3.38a)$$

and

$$\text{Var} \left\{ \tilde{P}_{AR}(f) \right\} \cong \frac{2P}{N} P_{AR}^2(f) \quad (3.38b)$$

Although these results may be of very little practical importance. That is, they may not provide good approximations for practical problems. Nonetheless, it is instructive to note the variance dependence on the model order P . Observe that the model order selection represents for AR spectral estimation the classical trade-off between resolution and variance.

Comparison of the BT and Burg Methods

A comparison of the BT and Burg methods seems the logical progression for the final development of this chapter. Also, the discussion in this section leads rather nicely to the analysis presented in the next chapter.

Several areas are worth considering when comparing the BT and Burg methods. The most prominent are: computational complexity, resolution, and variance. The Burg method is generally more computationally burdensome. This is evident by considering Eq (3.36). As eluded to earlier the denominator in Eq (3.36) can be efficiently evaluated by an FFT routine. The additional computation results from having to recursively determine the appropriate AR parameter estimates before invoking the FFT routine; however, if resolution is the only concern. Cooper and Kaveh (7:320) show that the model order required by the Burg method is

generally much less than the number of lags required by the BT method. Under this condition, the computation time of the Burg method is comparable to that of the BT method.

As discussed previously, the frequency resolution of the BT method is determined largely by the lag window (or spectral window). A simple exercise in Fourier transforming readily shows that the frequency resolution is inversely proportional to M , where $M \leq N - 1$ (see Eq (3.9)). Marple (21:664) shows that the frequency resolution of the Burg method for sinusoidal processes is approximately given by

$$\Delta f_{AR} \cong \frac{1.03}{P[\text{SNR}(P+1)]^{0.31}} \quad (3.39)$$

Thus, the frequency resolution, via the Burg method, decreases with decreasing SNR but also increases with increasing model order number P . The frequency resolution of the BT method is totally independent of input SNR. More is said about frequency resolution for both methods in the next chapter.

A comparison of Eqs (3.13) and (3.38b) shows that for a given data record length N the model order number P is analogous to the lag window length M . That is, the variance of both methods tends to increase as their respective parameter increases.

The following chapter provides a qualitative comparison of the two methods for several data records.

IV. Analysis

Introduction

The purpose of this chapter is to graphically examine the two spectral analysis techniques presented in the previous chapter. The two techniques are applied to several known data records and comparisons made. Also, a "smart routine" is introduced that attempts to automatically determine peaks corresponding to actual frequencies of given PSD plots.

A major "limitation" of the receiver system described in Chapter I is that of pulse duration. That is, the pulse received by the receiver is relatively short in duration, resulting in only a few data samples available for processing. The data record resulting from the received pulse is, therefore, considered a short data record. As mentioned in Chapter III, computing the PSD of short data records may provide less than desirable results.

The Avionics Lab suggested that the number 64 is a good average representative number of data samples available for each received pulse. Hence, each data record considered in this chapter consists of only 64 data samples. Recall, that the received pulse may be composed of a number of sinusoids. That is, two or more hostile emitters may be operating simultaneously. As stated in Chapter I, each emitter is assumed to transmit at a single operating frequency. The received pulse, and therefore the data record are composed

of sinusoids corresponding to the operating frequency of each emitter. For example, if two emitters are operating simultaneously at different frequencies, then the data record consists of two equivalent baseband sinusoids corresponding to the two emitter frequencies.

The data records evaluated are intended to represent "real world" type hostile emitter signals. A psuedo random WGN process is added to each data record and represents the noise corruption caused by the medium of propagation. Again, the BT and Burg methods of spectral estimation are applied to each data record and comparisons made. Of the available lag windows provided by the ISPX software package, the hamming window yields the best compromise between frequency resolution and leakage. This window is used in determining the BT PSD estimator for all cases considered with $M = N/2$ (or $M = 32$), see Eq (3.9). As mentioned earlier, determining the model order number P of an AR process is a non-trivial task, and therefore will be determined empirically. However, data records that are exclusively sinusoidal (i.e., no embedded noise) require a model order number $P = 2m$ for m number of sinusoids (17:213). This criterion will serve as a basis for empirically determining the correct model order P .

Problem One

The first problem considered is a data record consisting of a single sinusoid embedded in WGN. This input data record is given by

$$x(n) = \sin[2\pi(0.2)n] + g(n) \quad (4.1)$$

where $g(n)$ is a psuedo random WGN process. Figures 4.1 through 4.3 show this input process for signal-to-noise ratios (SNR's) of 10, 15, and 20 dB, respectively. Figure 4.4 shows the BT PSD estimator of Eq (4.1) for each specified SNR. Observe that the frequency resolution defined by the main lobe centered about the fractional frequency 0.2 is independent of SNR. This point is further illustrated by superimposing these three results as indicated in Figure 4.5. Figure 4.6 depicts the result of overlapping the Burg PSD estimator for each specified SNR. The model order selected is two. Observe that as the SNR decreases the respective spectral peaks are broadened and displaced from the true position (indicated by the vertical dashed line). This illustration clearly shows that the frequency resolution of the Burg PSD estimator is directly proportional to the input SNR. Furthermore, it is noted that only the spectral peak corresponding to the 20 dB SNR correctly resolves the true fractional frequency of 0.2. The broadening and displacement of the other two spectral peaks are due to the increased noise (or lower SNR). A quantitative relationship that explains this phenomenon is a

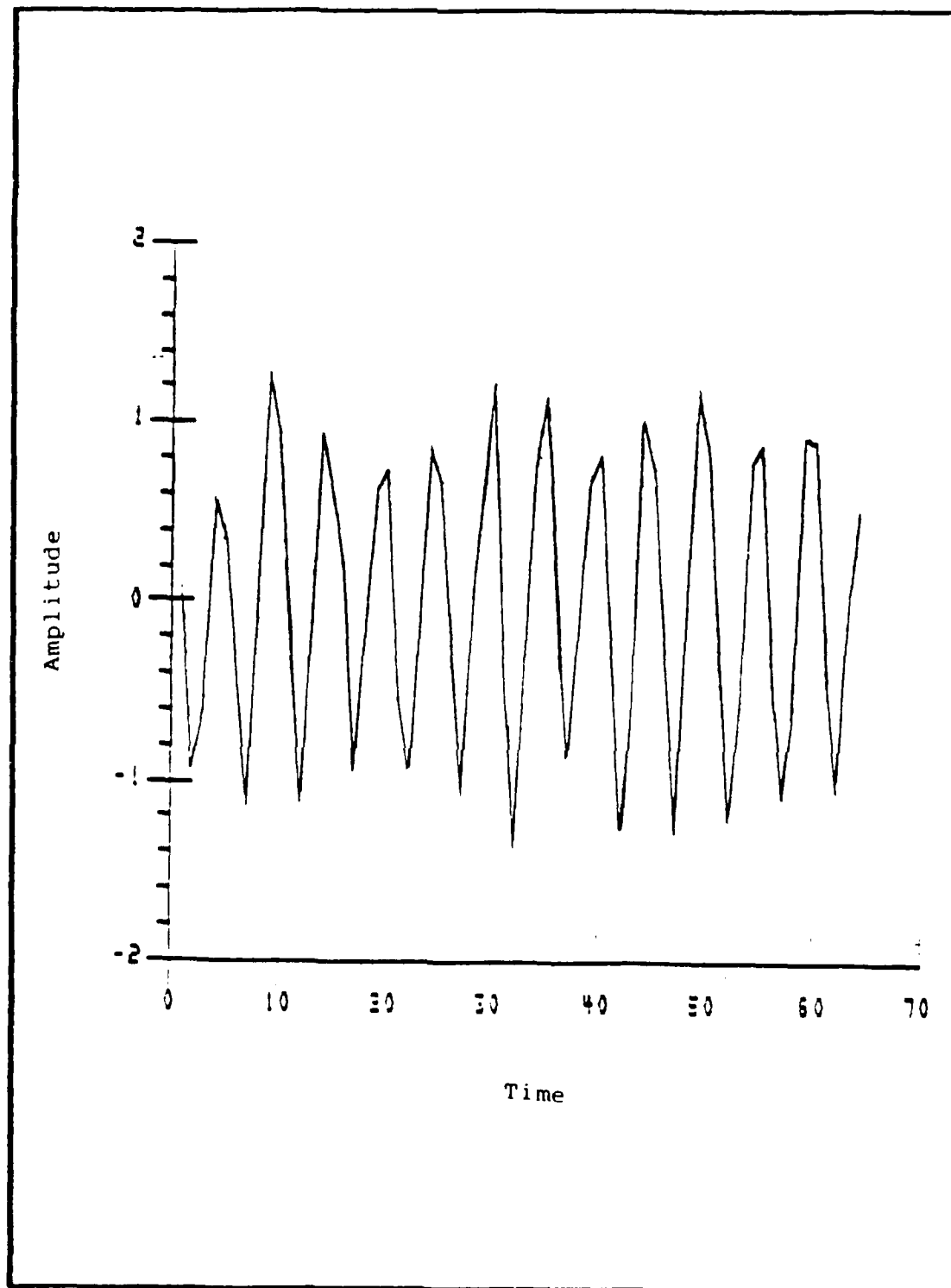


Figure 4.1. Sixty-Four Samples of a Single Sinusoid in WGN, SNR = 10 dB

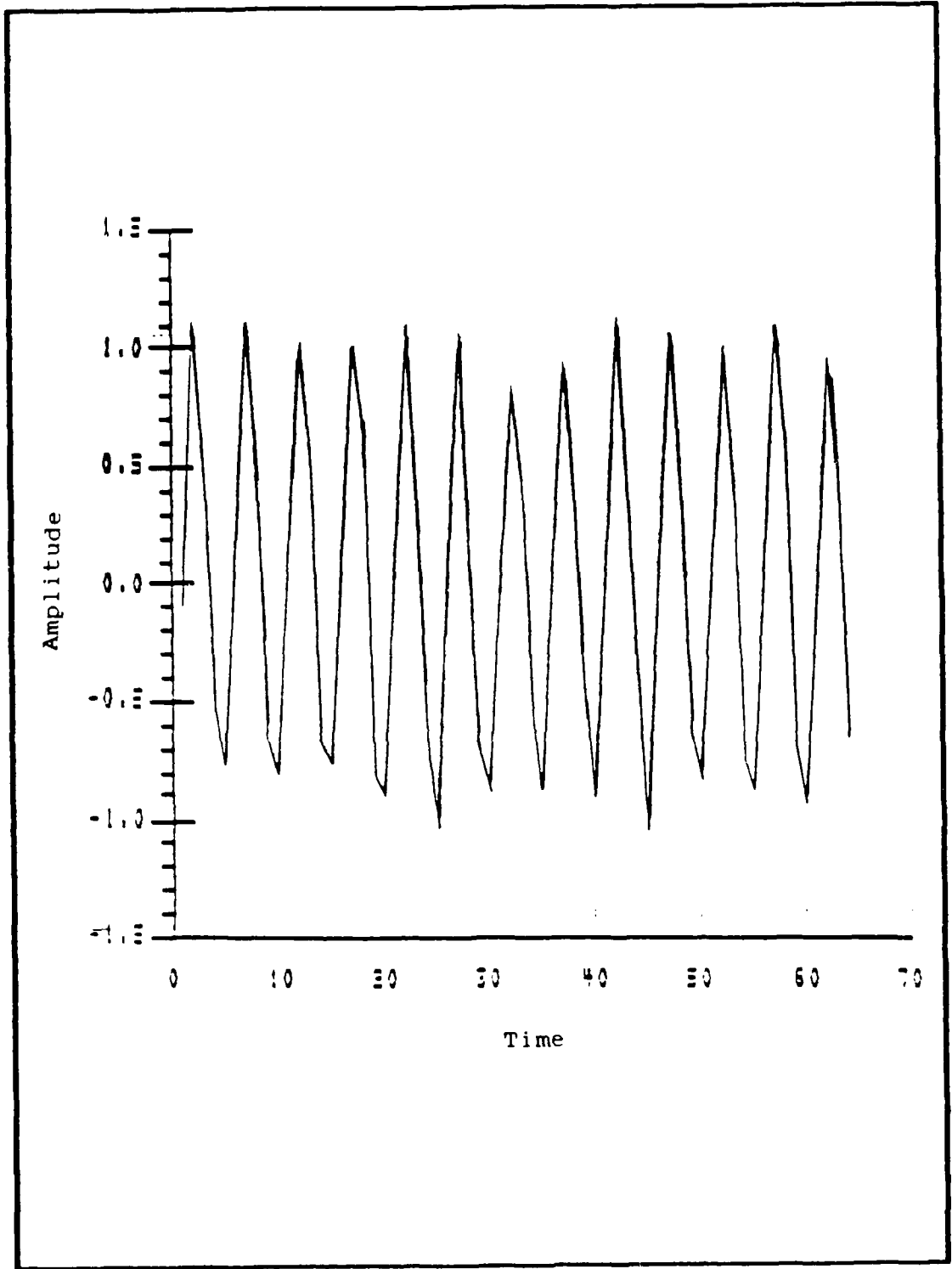


Figure 4.2. Sixty-Four Samples of a Single Sinusoid in WGN, SNR = 15 dB

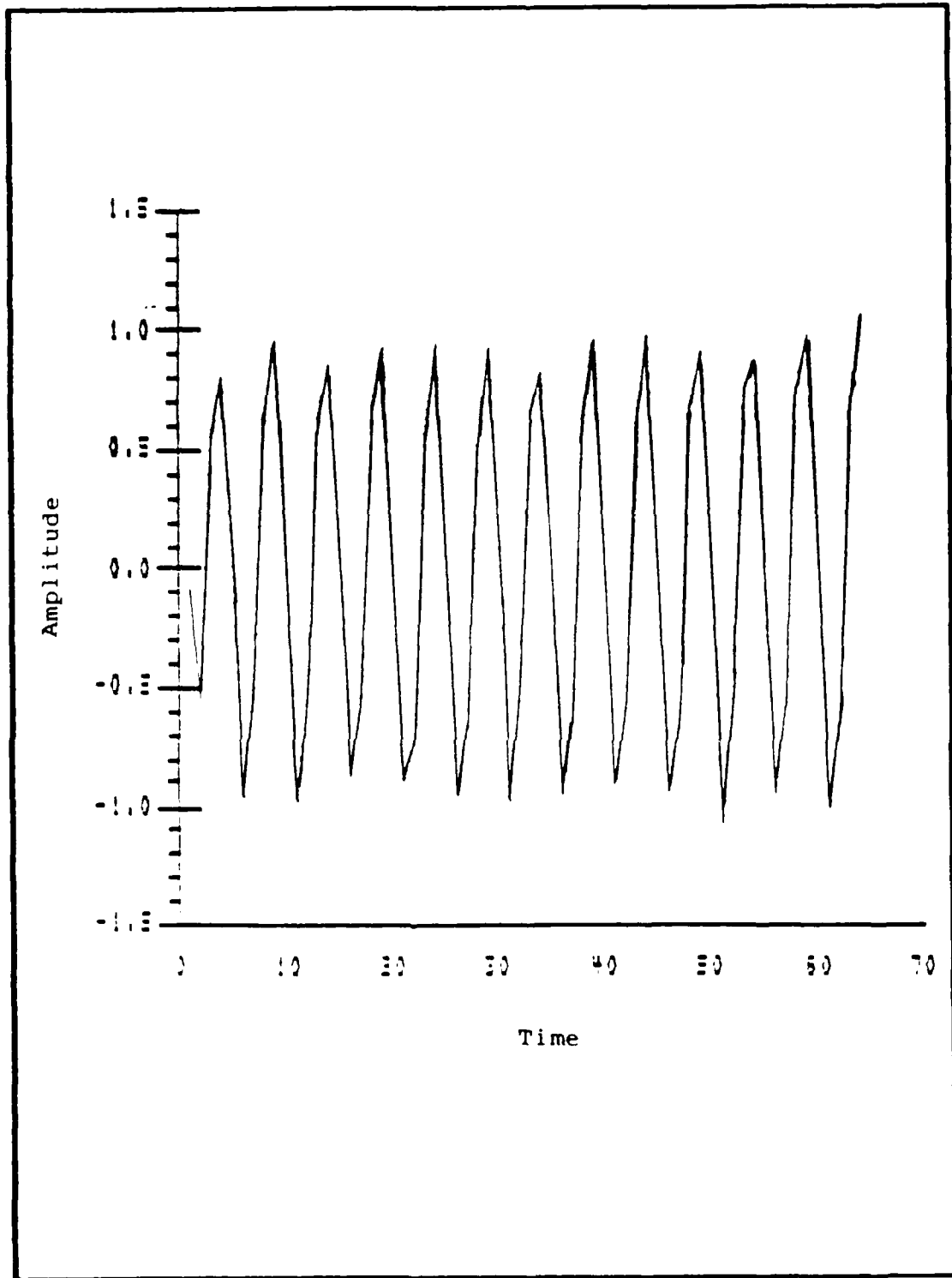


Figure 4.3. Sixty-Four Samples of a Single Sinusoid in WGN, SNR = 20 dB

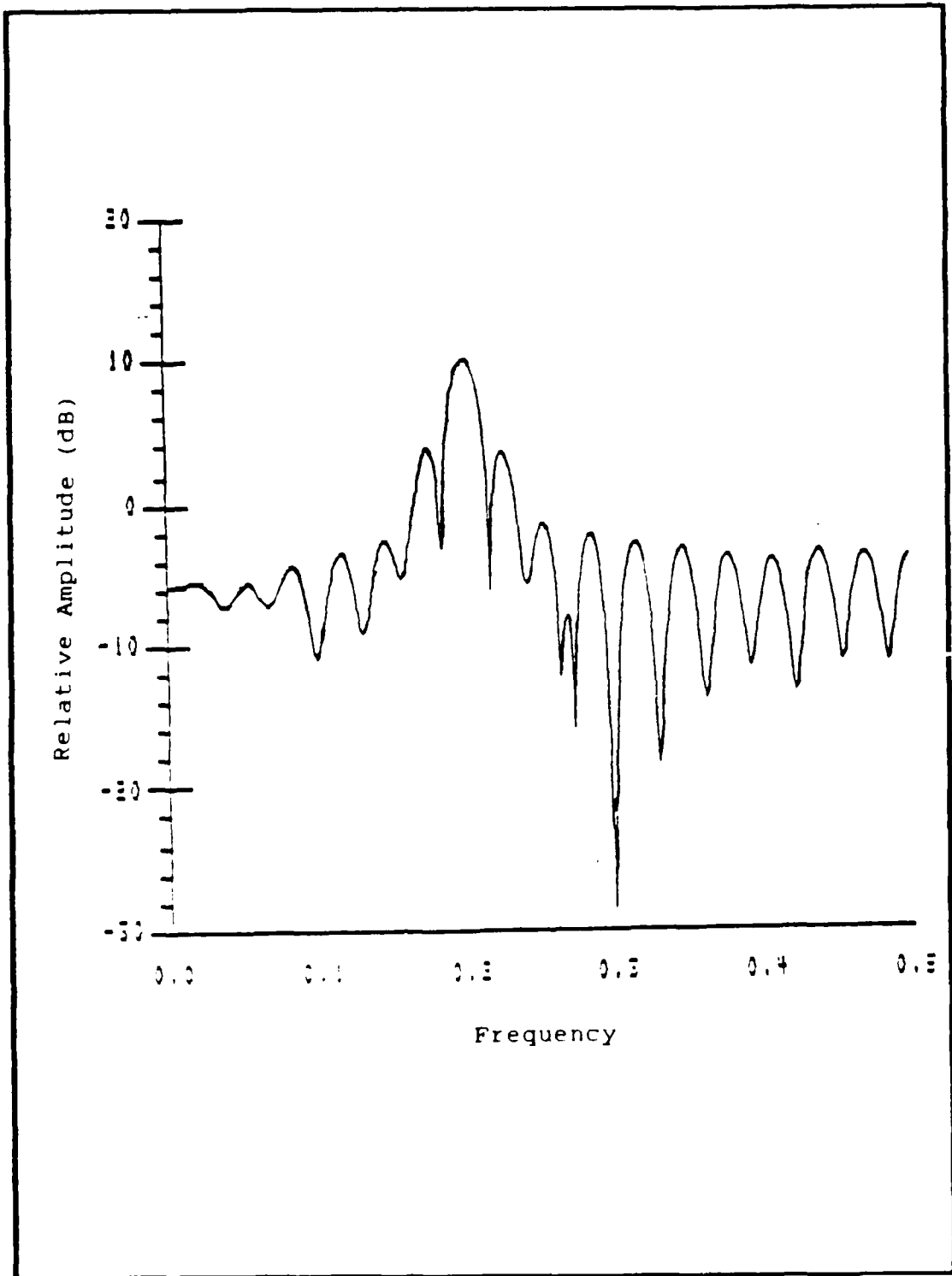


Figure 4.4a. BT Estimator of the Single Sinusoid in WGN, SNR = 10 dB

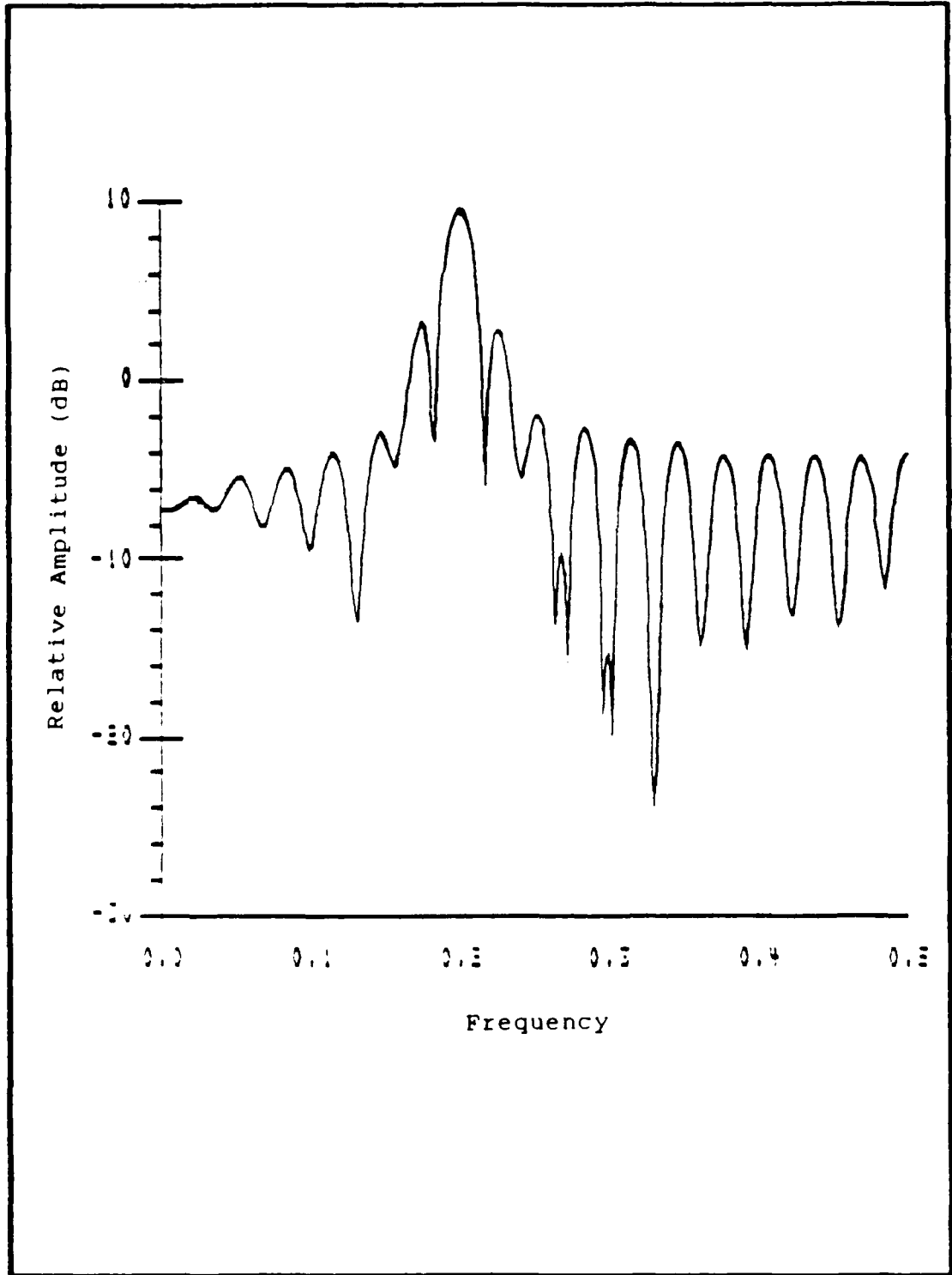


Figure 4.4b. BT Estimator of the Single Sinusoid in WGN, SNR = 15 dB

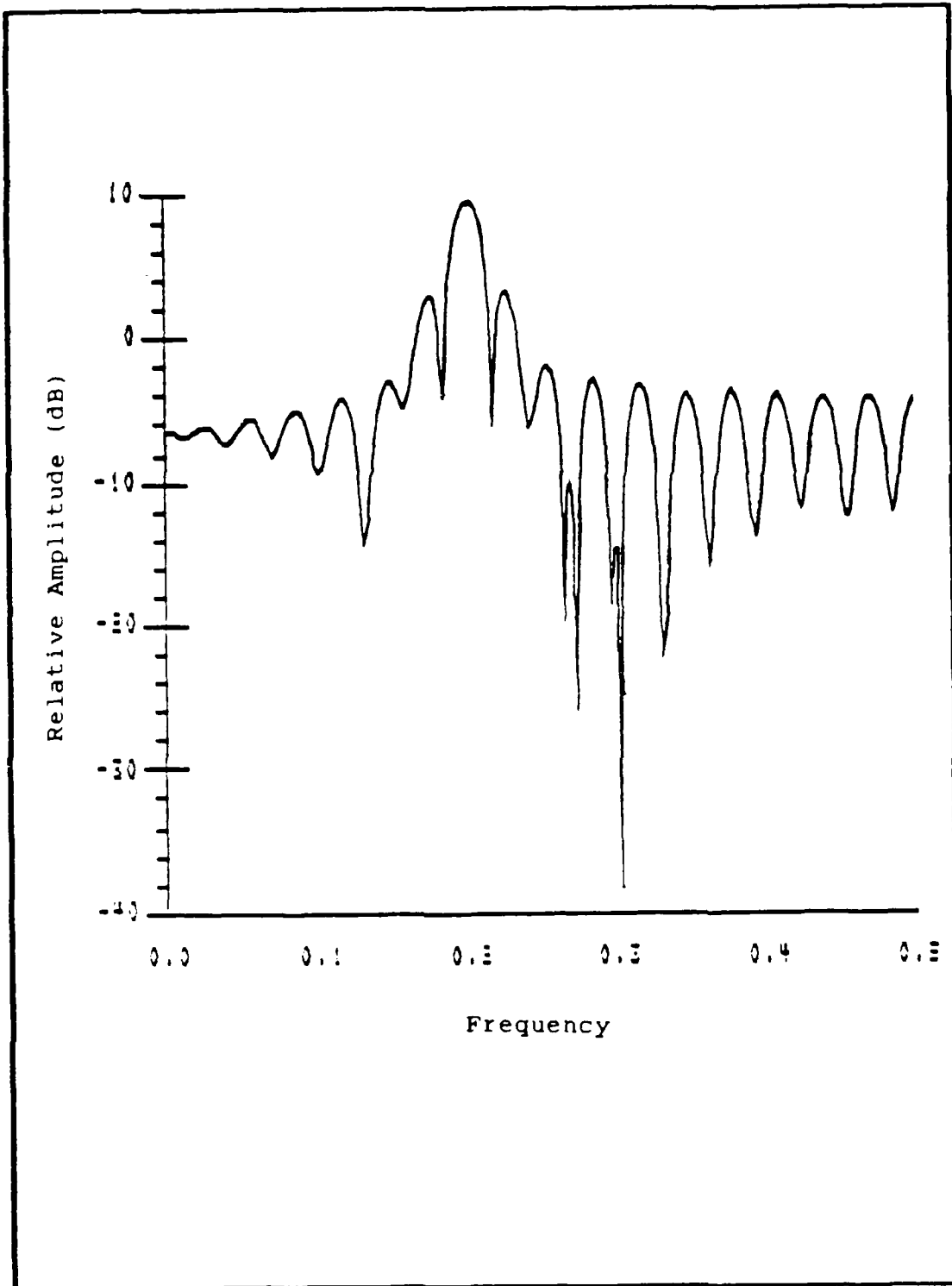


Figure 4.4c. BT Estimator of the Single Sinusoid in WGN, SNR = 20 dB

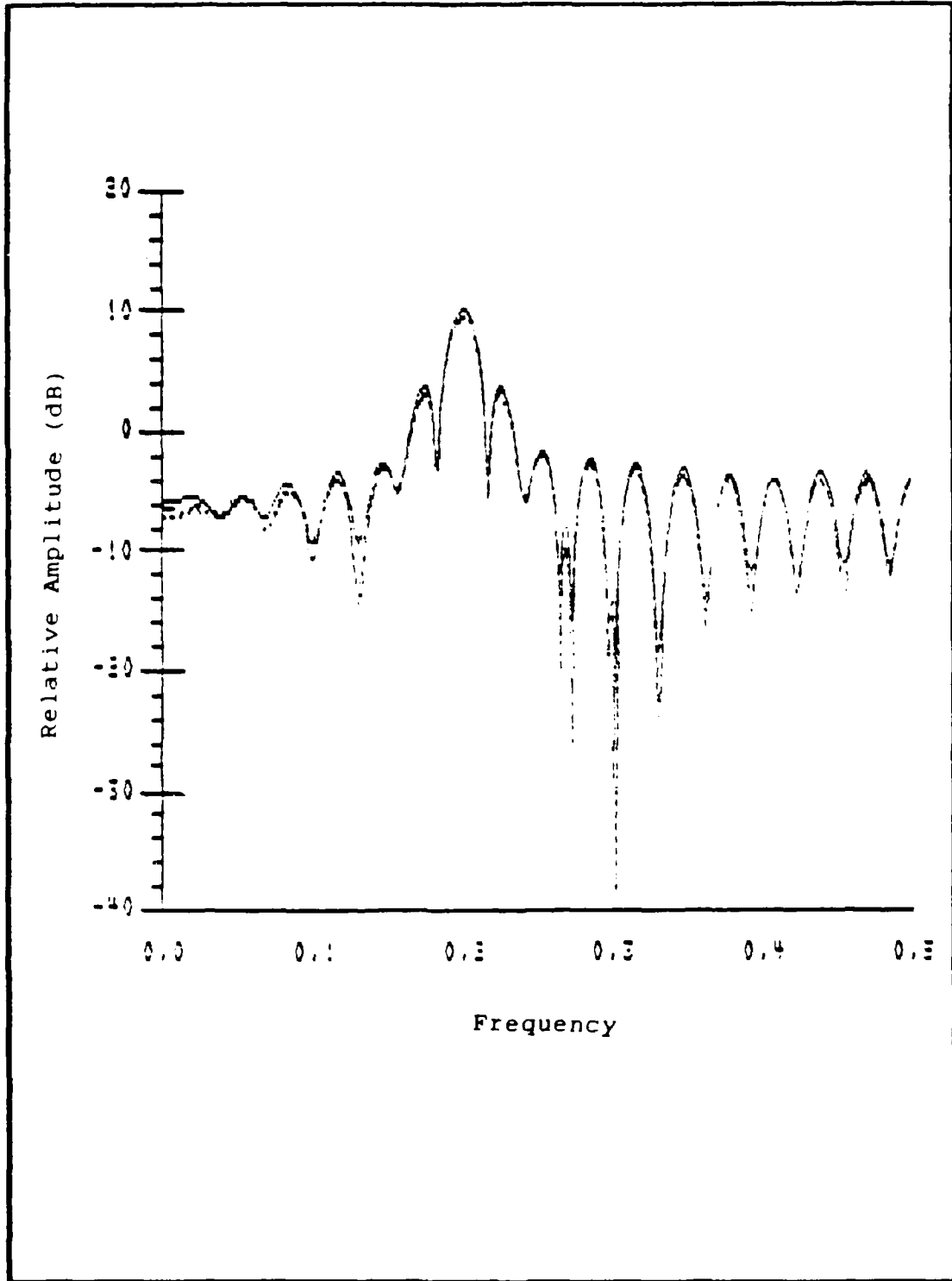


Figure 4.5. Superposition of the BT Estimator for SNR's 10, 15, and 20 dB

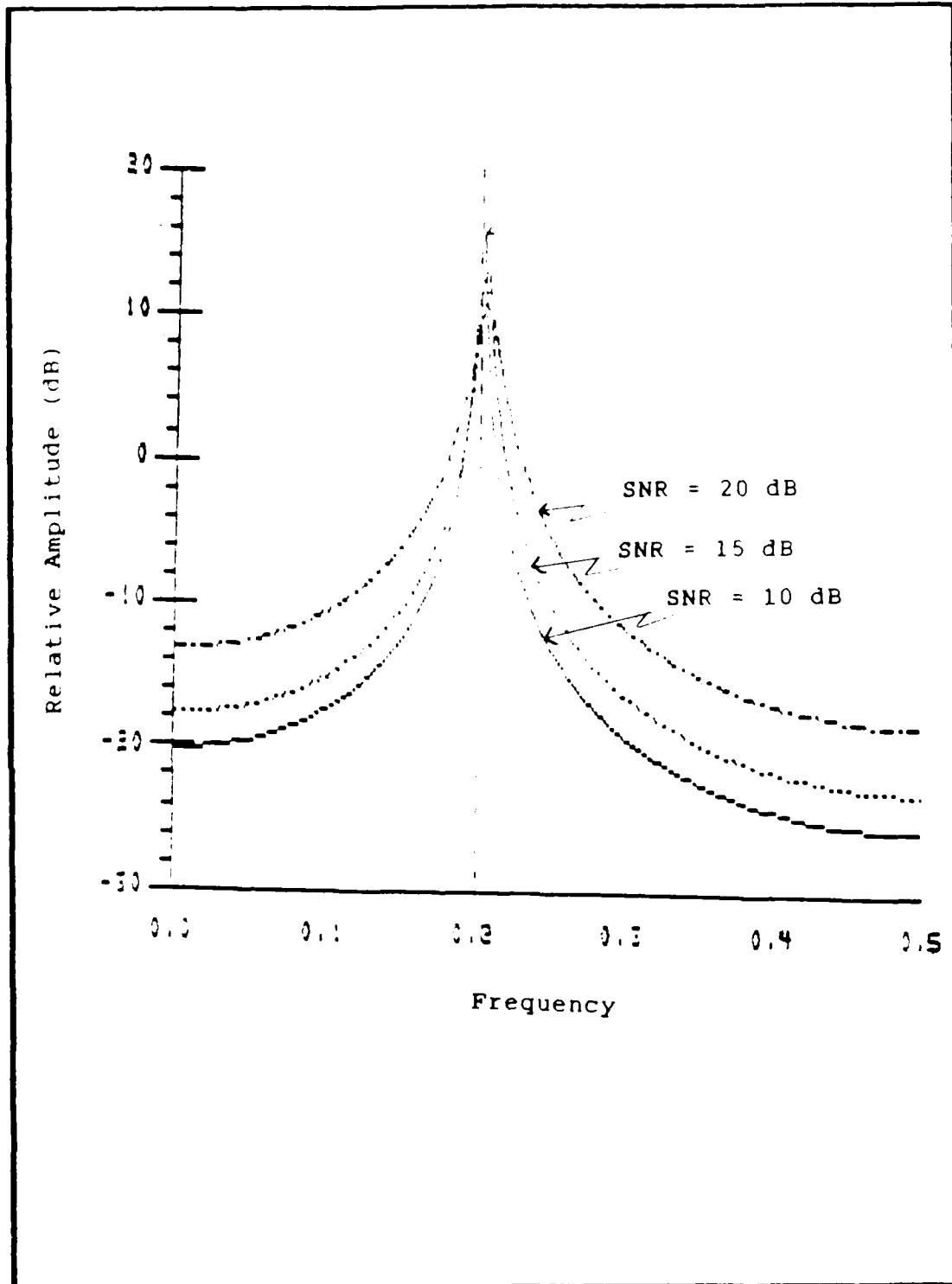


Figure 4.6. Superposition of the Burg Estimator for SNR's 10, 15, and 20 dB with $P = 2$

formidable task. In fact, very little is known quantitatively about noisy AR-processes (4:184-187). However, it is qualitatively instructive to consider specific cases. As will be shown in the following examples, the model order number P can sometimes be increased to mitigate the effects of noise for a given SNR. A word of caution, however, is in order here. As discussed in the previous chapter if the model order number P is too large, spurious peaks in the spectral estimate will appear. This is simply explained by considering Eq (3.36), repeated here for convenience

$$\tilde{P}_{AR}(f) = \frac{\tilde{\sigma}_p^2}{\left| 1 + \sum_{k=1}^P \tilde{a}_p(k) \exp(-j2\pi fk) \right|^2} \quad (4.2)$$

Note that if P is too large, then extra poles are produced. These extra poles, commonly referred to as noise poles, have a tendency to situate themselves too close to the unit circle in the z -plane, resulting in unwanted (or spurious) peaks.

Problem Two

This problem and the remaining two problems consider data records with a minimum SNR of 15 dB. The Avionics Lab indicated that 15 dB is typically the lowest SNR of interest for their applications.

The problem addressed here is a data record consisting

of two unequal amplitude sinusoids embedded in WGN. This data record is given by

$$x(n) = 0.2\sin[2\pi(0.2)n] + \sin[2\pi(0.25)n] + g(n) \quad (4.3)$$

Figure 4.7 shows this input process for a SNR of 15 dB relative to the weaker sinusoid. The BT PSD estimator is presented in Figure 4.8. Notice that the main lobe of the weaker signal is not present. Obviously, the BT PSD estimator is not capable of distinguishing both sinusoids. This is a common dilemma for all conventional schemes of spectral estimation, particularly for data records consisting of weak and strong sinusoids. This is explained by considering Eq (3.9), repeated here for convenience

$$\tilde{P}_{BT}(f) = \sum_{k=-M}^M w(k) \tilde{R}_x(k) \exp(-j2\pi fk) \quad (4.4)$$

The BT PSD estimator involves a linear operation on a weighted ACS derived from a given data record. Thus, the spectrum of the sum of two sinusoids (uncorrelated) is simply the sum of their respective spectra. The amplitude of the spectra is directly proportional to the power in the sinusoids. Therefore, the amplitude of the spectra corresponding to the strong sinusoid is greater than that corresponding to the weaker sinusoid. In fact, so much so that the main lobe amplitude of the weaker sinusoid is buried (or masked) by the sidelobe amplitudes of the strong sinusoid. It is important, however, to point out that the

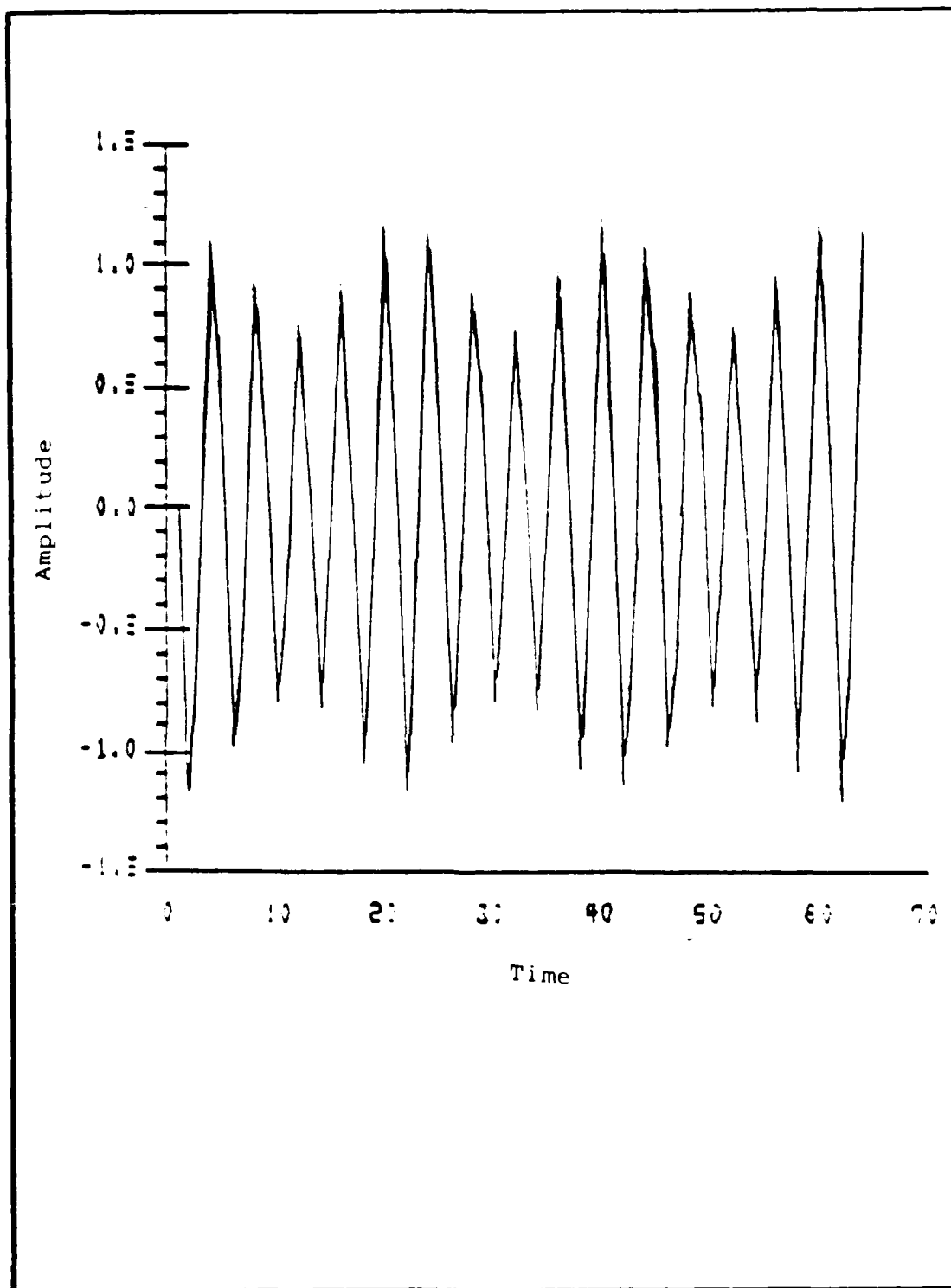


Figure 4.7. Sixty-Four Samples of Two Sinusoids in WGN, SNR = 15 dB

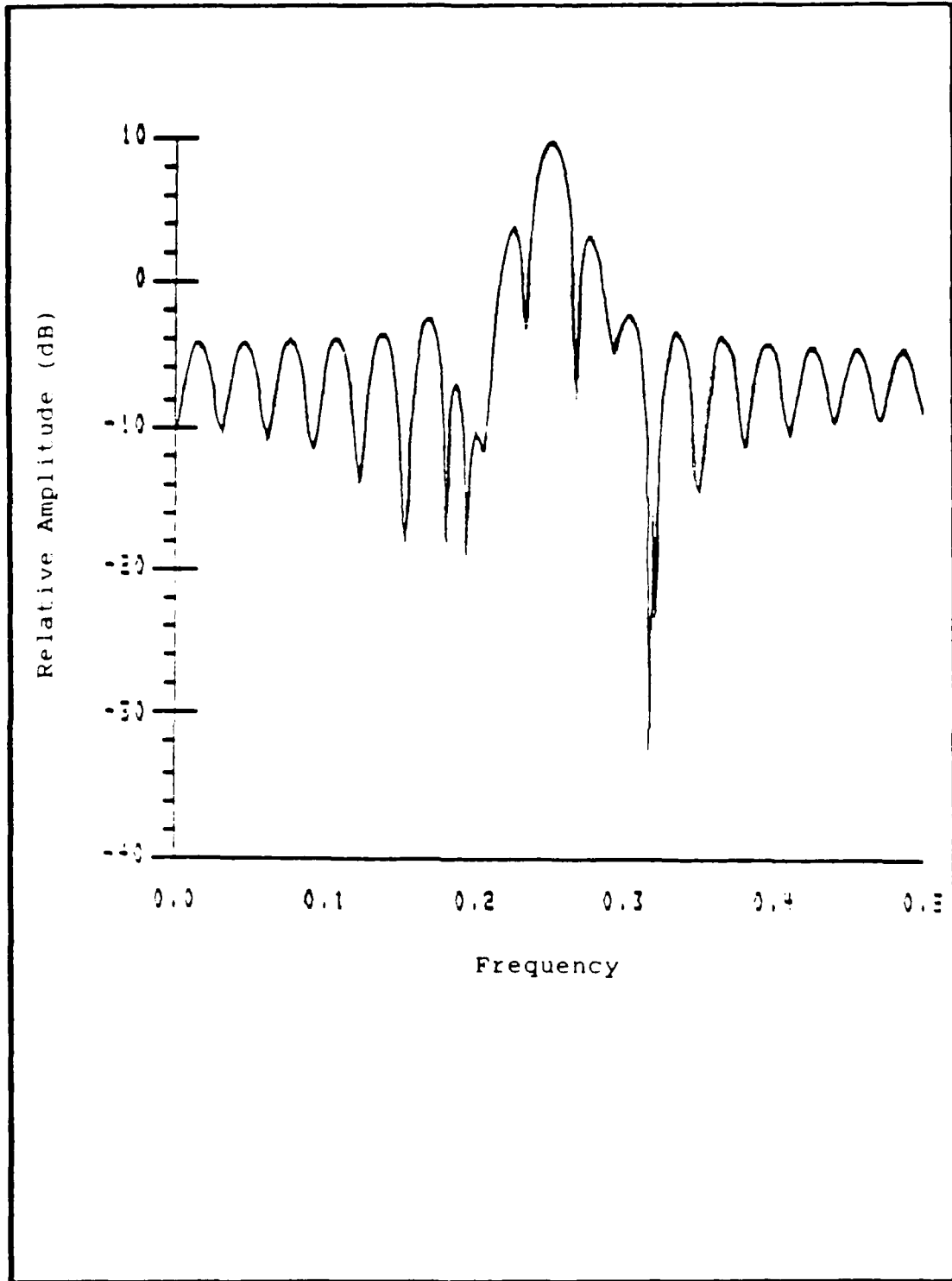


Figure 4.8. BT Estimator of Two Single Sinusoid in WGN, SNR = 15 dB

inability of the estimator to detect both sinusoids is not due to poor frequency resolution. That is, the two sinusoids are spaced sufficiently in frequency to be resolved by this estimator. Again, to reiterate the problem is that the main lobe of the weaker signal is canceled by the sidelobes of the strong signal. If the problem considered two equal amplitude sinusoids, then both sinusoids would have been resolved. Recall, that the resolution of the BT PSD estimator is govern largely by the lag window chosen. Of course, a lag window with a faster roll-off rate could have been chosen possibly to retrieve the weaker sinusoid. But as stated earlier, of the available lag windows provided by ISPX, the hamming window provides the best compromised between frequency resolution and leakage. Problem four considers an example in which sinusoids are so closely spaced in frequency, that it is impossible to resolve them using the BT method regardless of power.

The Burg PSD estimator is shown in Figure 4.9. As stated earlier, the model order P can be increased in order to mitigate the effects of noise for a given SNR. Observe that for a model order number of four, the appropriate order for no noise, the results of the Burg PSD estimator are no better than the results of the BT PSD estimator. Only the strong signal is detected. For model order numbers of six and ten, the Burg PSD estimator is capable of detecting both the strong

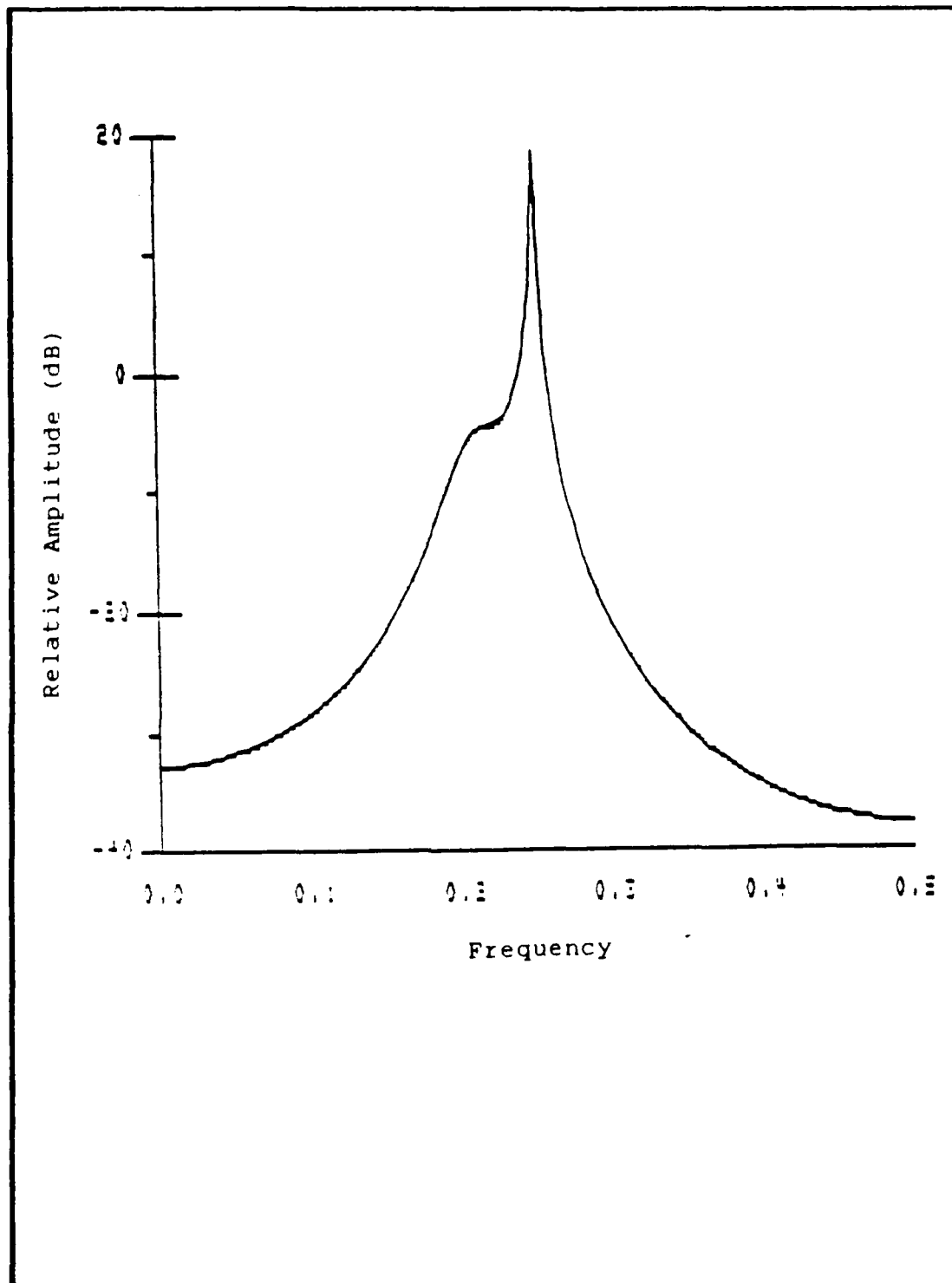


Figure 4.9a. Burg Estimator of Two Single Sinusoid in WGN, SNR = 15 dB with $P = 4$

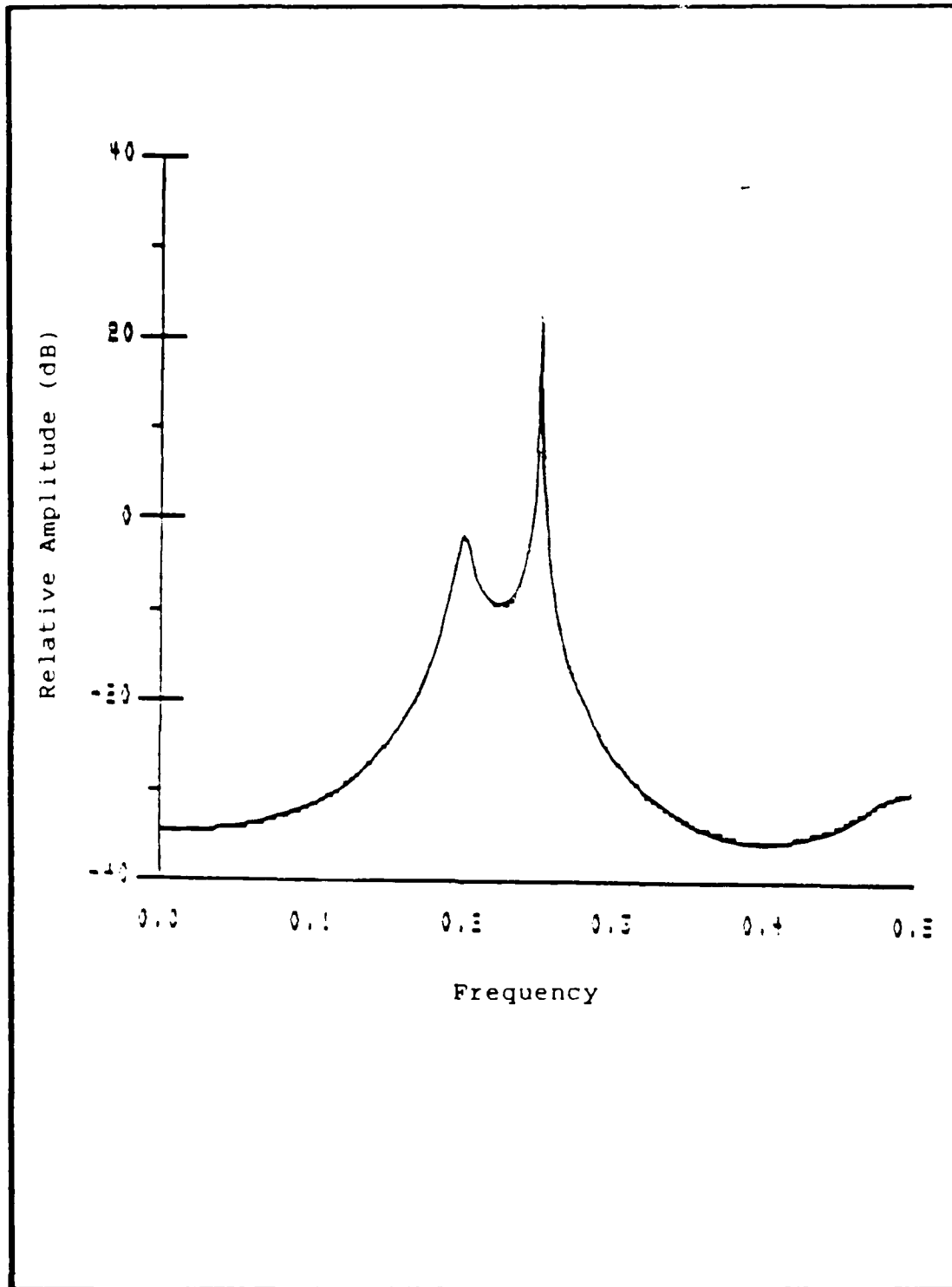


Figure 4.9b. Burg Estimator of Two Single Sinusoid in WGN, SNR = 15 dB with $P = 6$

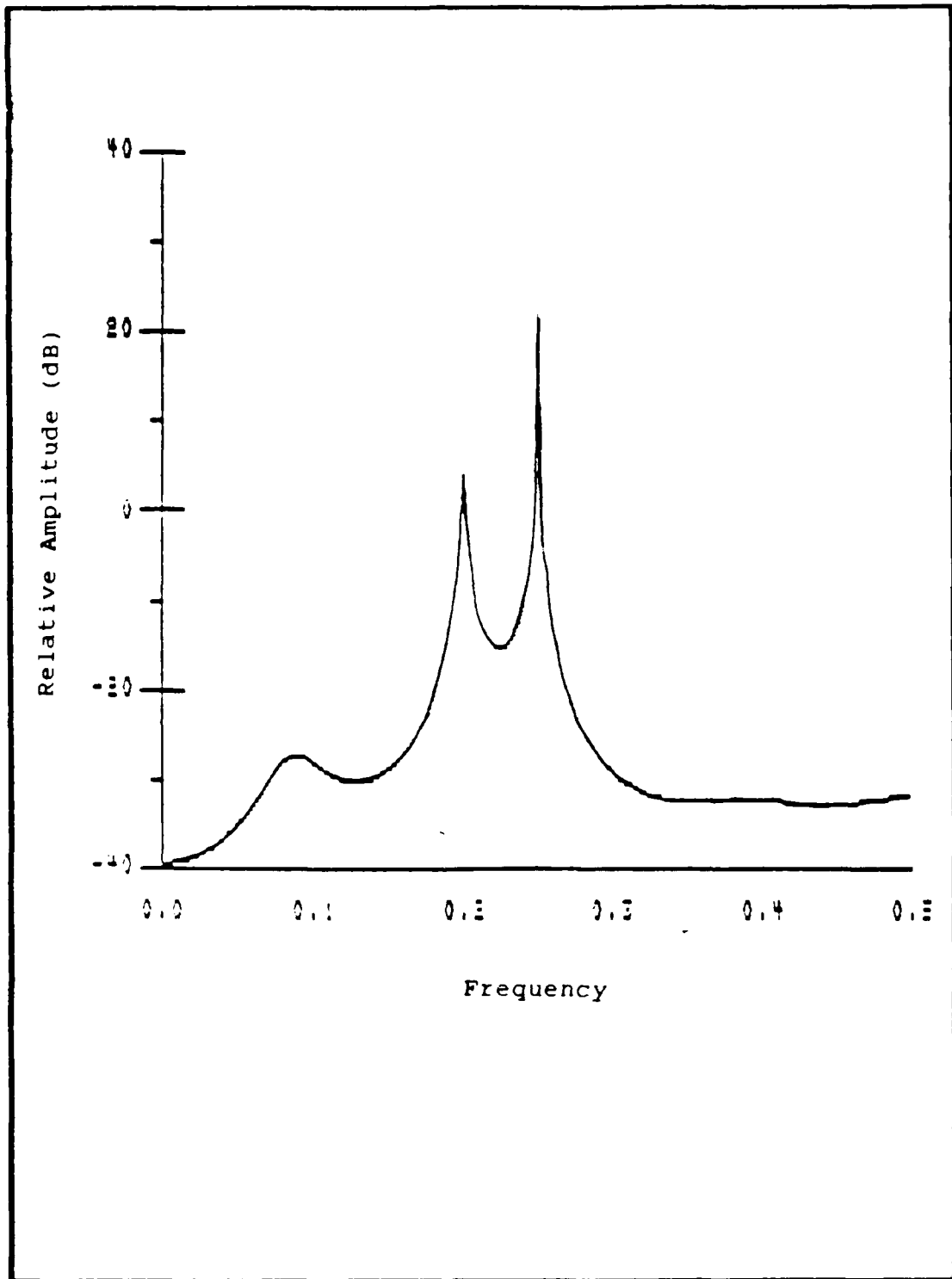


Figure 4.9c. Burg Estimator of Two Single Sinusoid in WGN, SNR = 15 dB with $P = 10$

and weaker sinusoids. Note the resolution of the estimator is slightly improved for the model order number ten. However, a spurious peak is just starting to appear. As explained in the previous section, spurious peaks are the result of noise poles. This phenomenon can also be explained from a statistical point of view by considering Eq (3.38b), repeated here for convenience,

$$\text{Var} \left\{ \tilde{P}_{AR}(f) \right\} \cong \frac{2P}{N} P_{AR}^2(f) \quad (4.5)$$

It is observed that as model order P increases for a given data record length N , the variance increases. Thus, P can be considered analogous to the length of the lag window M for the BT PSD estimator, see Eqs (3.12) and (3.13).

Problem Three

A data record consisting of one or more delayed sinusoids is another interesting and often common occurrence. For simplicity, a modified version of the previous example is considered. That is, the strong signal is delayed by sixteen time units. Thus, the data record is given by

$$x(n) = 0.2\sin[2\pi(0.2)n] + \sin[2\pi(0.25)(n-16)] + g(n) \quad (4.6)$$

This process is shown in Figure 4.10. Again, the BT PSD estimator is unable to distinguish both sinusoids as illustrated in Figure 4.11. A comparison of Figures 4.8 and 4.11 indicates that the shift appears to have no apparent effect on the frequency resolution. This should not be too

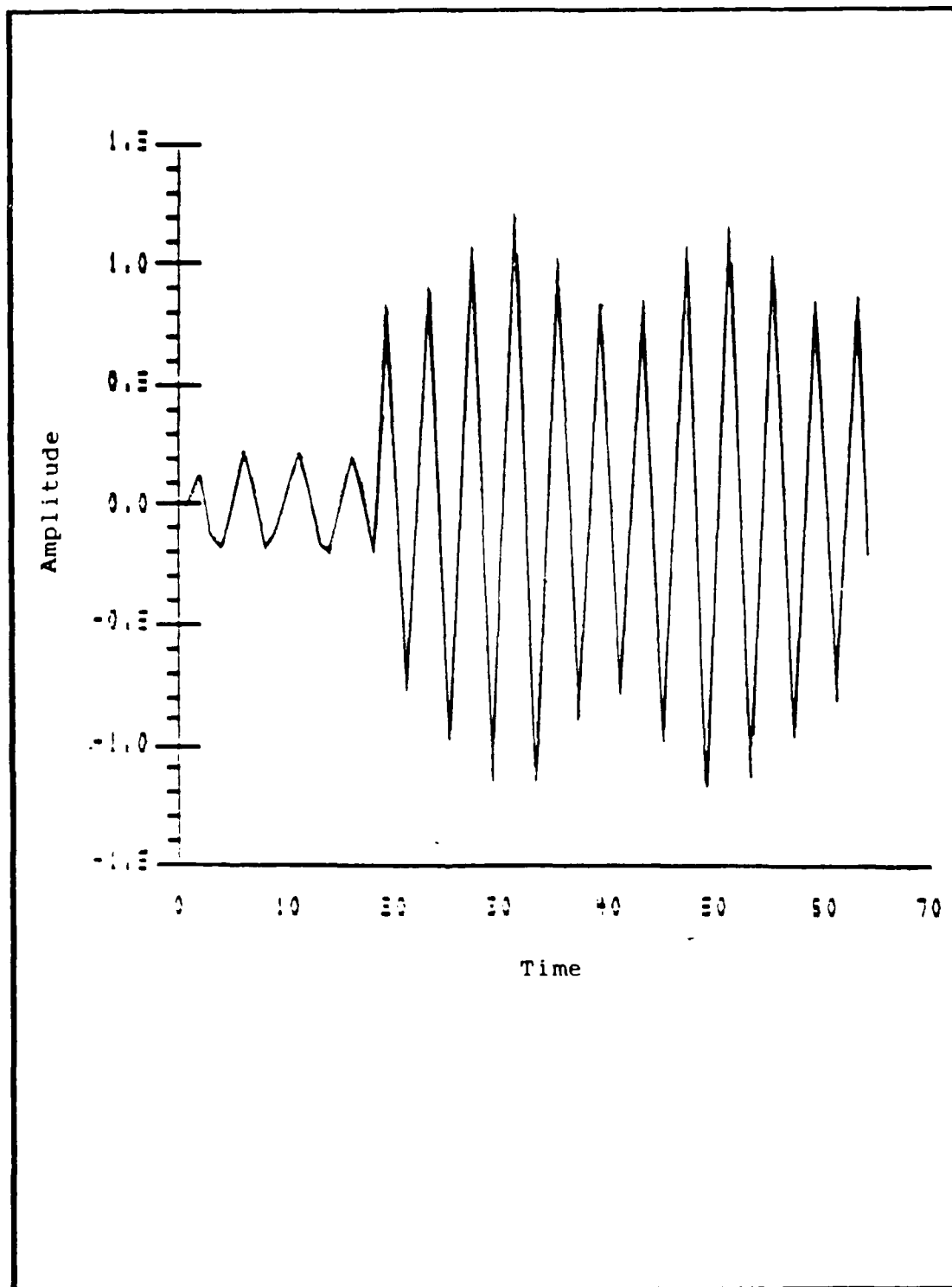


Figure 4.10. Sixty-Four Samples of Two Sinusoids in WGN, SNR = 15 dB

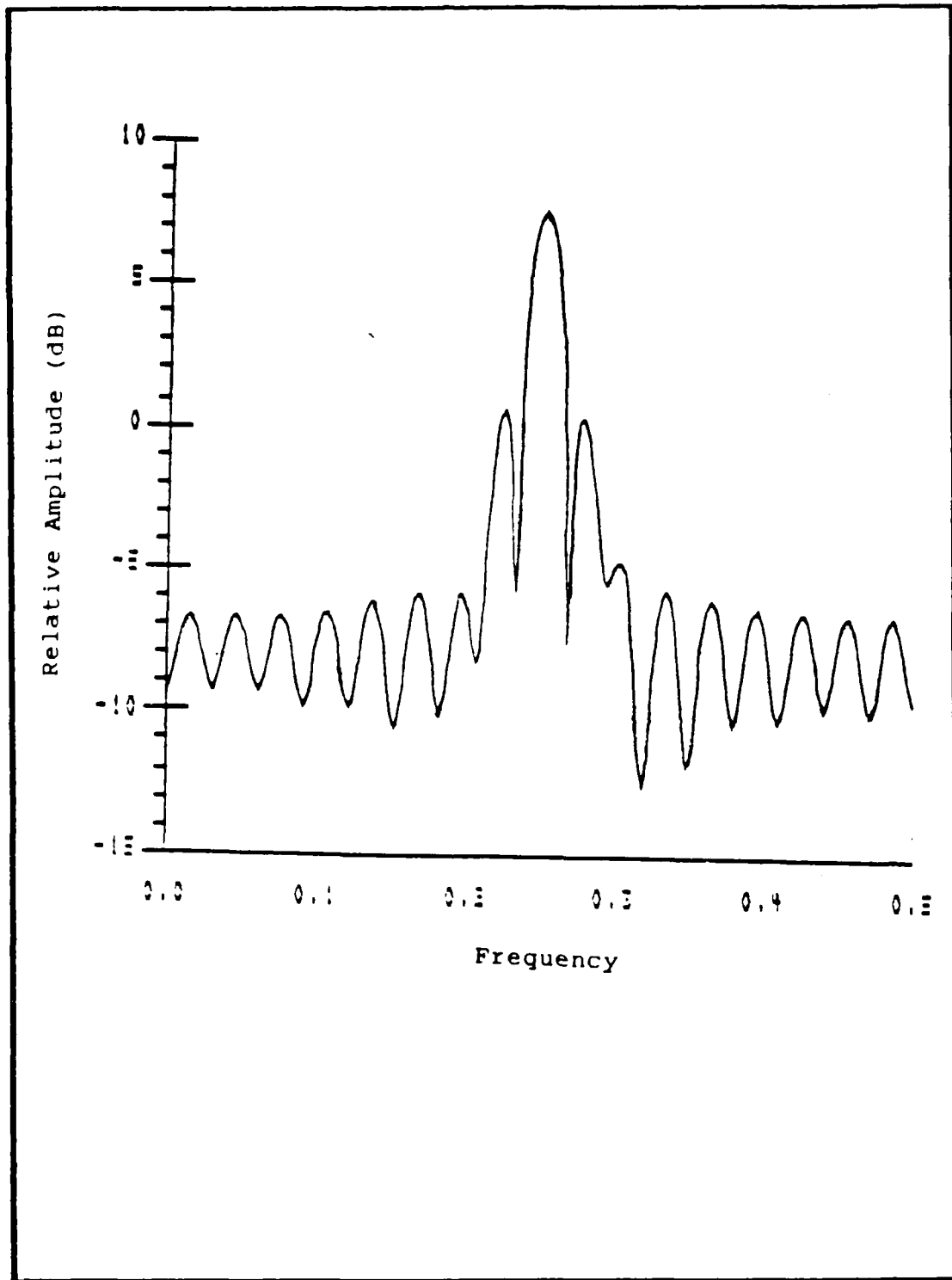


Figure 4.11. BT Estimator of Two Single Sinusoid in WGN, SNR = 15 dB

surprising considering that the BT PSD estimator is a FFT based operator.

The results of the Burg PSD estimator are shown in Figure 4.12. Comparing these results with those of Figure 4.9 indicate that the time shift causes the required model order number to increase. A model order number $P = 20$ is required to resolve both sinusoids. In the previous example, the two sinusoidal peaks first appeared at $P = 6$. The reason for this increased model order number is due the overall lower SNR.

Problem Four

The final problem considers a data record consisting of four closely spaced sinusoids. This data record is given by

$$x(n) = 0.2\sin[2\pi(0.2)n] + 0.7\sin[2\pi(0.22)n] \\ + \sin[2\pi(0.24)] + 0.5\sin[2\pi(0.26)] + g(n) \quad (4.7)$$

Figure 4.13 illustrates this process. The BT PSD is given in Figure 4.14. Observe that the sinusoids are too closely spaced to be resolved by this estimator. The main lobe shown is a result of the destructive and constructive interference of the four sinusoids and in itself does not represent any one of the sinusoids. Figure 4.15 presents the Burg PSD estimator for $P = 24$. Note that all four sinusoids are resolved with no inaccuracies cause by the spurious peaks. That is, the highest spurious peak is about 24dB below the lowest desirable peak. This gives rise to

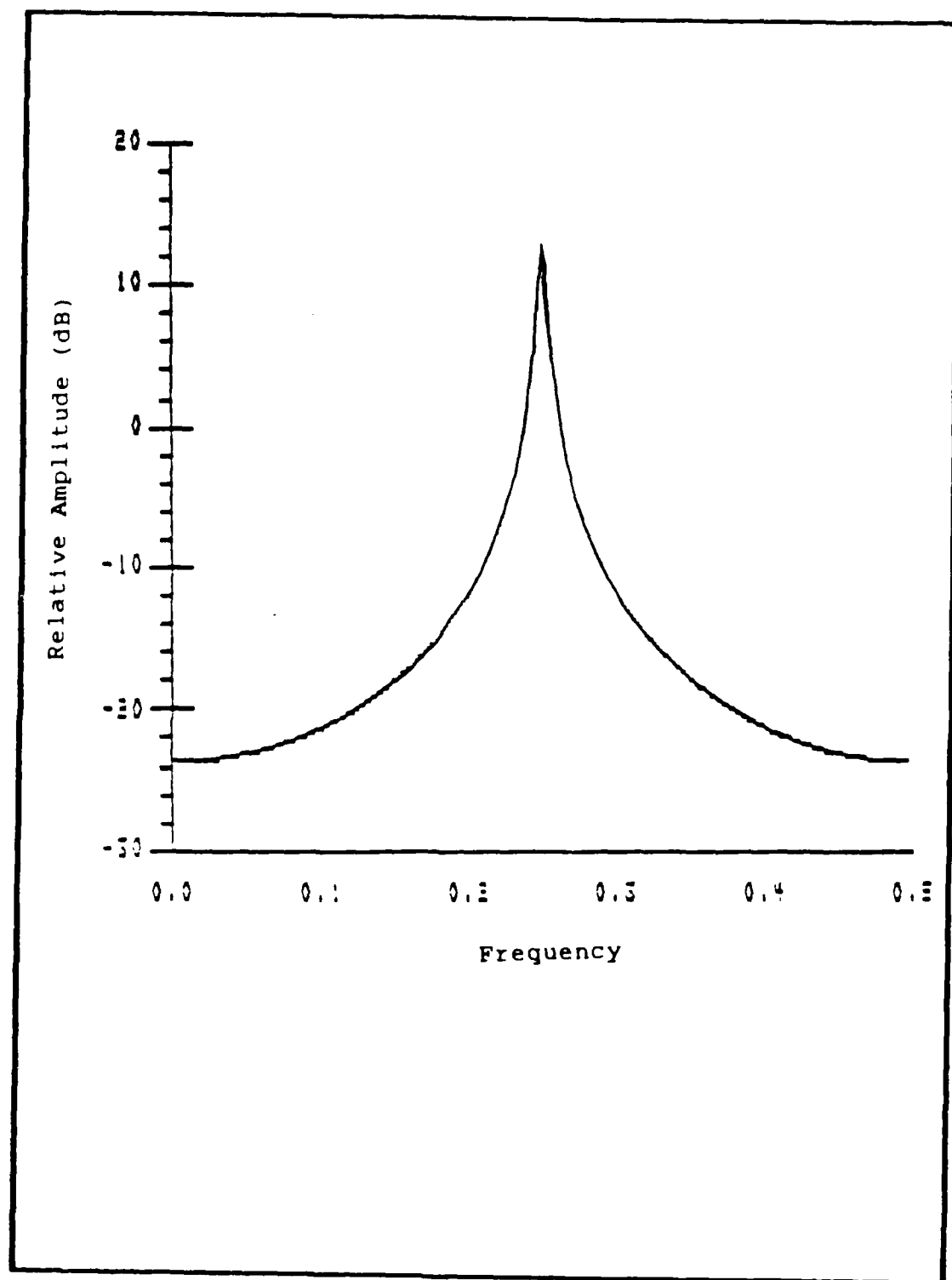


Figure 4.12a. Burg Estimator of Two Single Sinusoid in WGN, SNR = 15 dB with $P = 4$

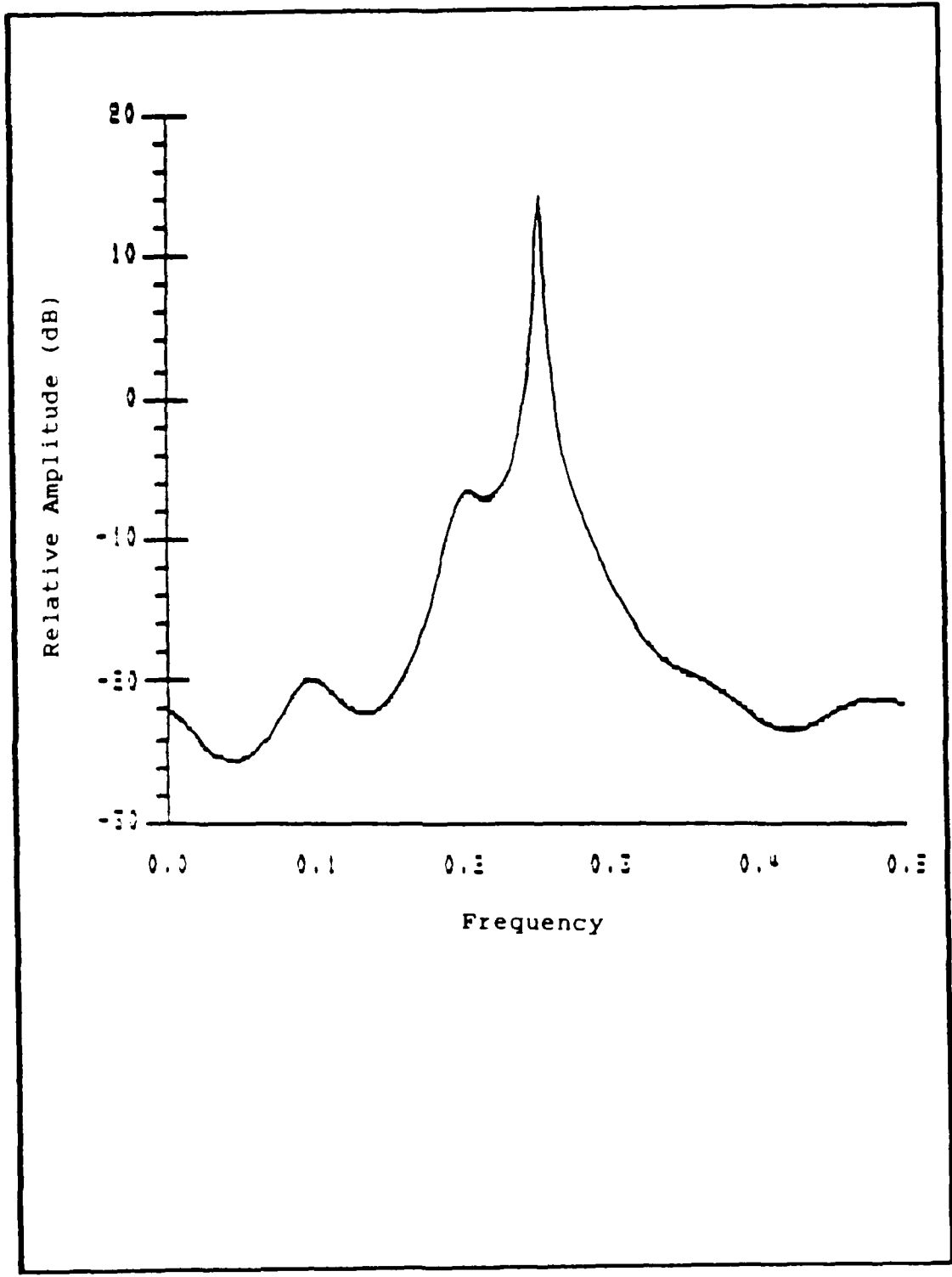


Figure 4.12b. Burg Estimator of Two Single Sinusoid in WGN, SNR = 15 dB with P = 14

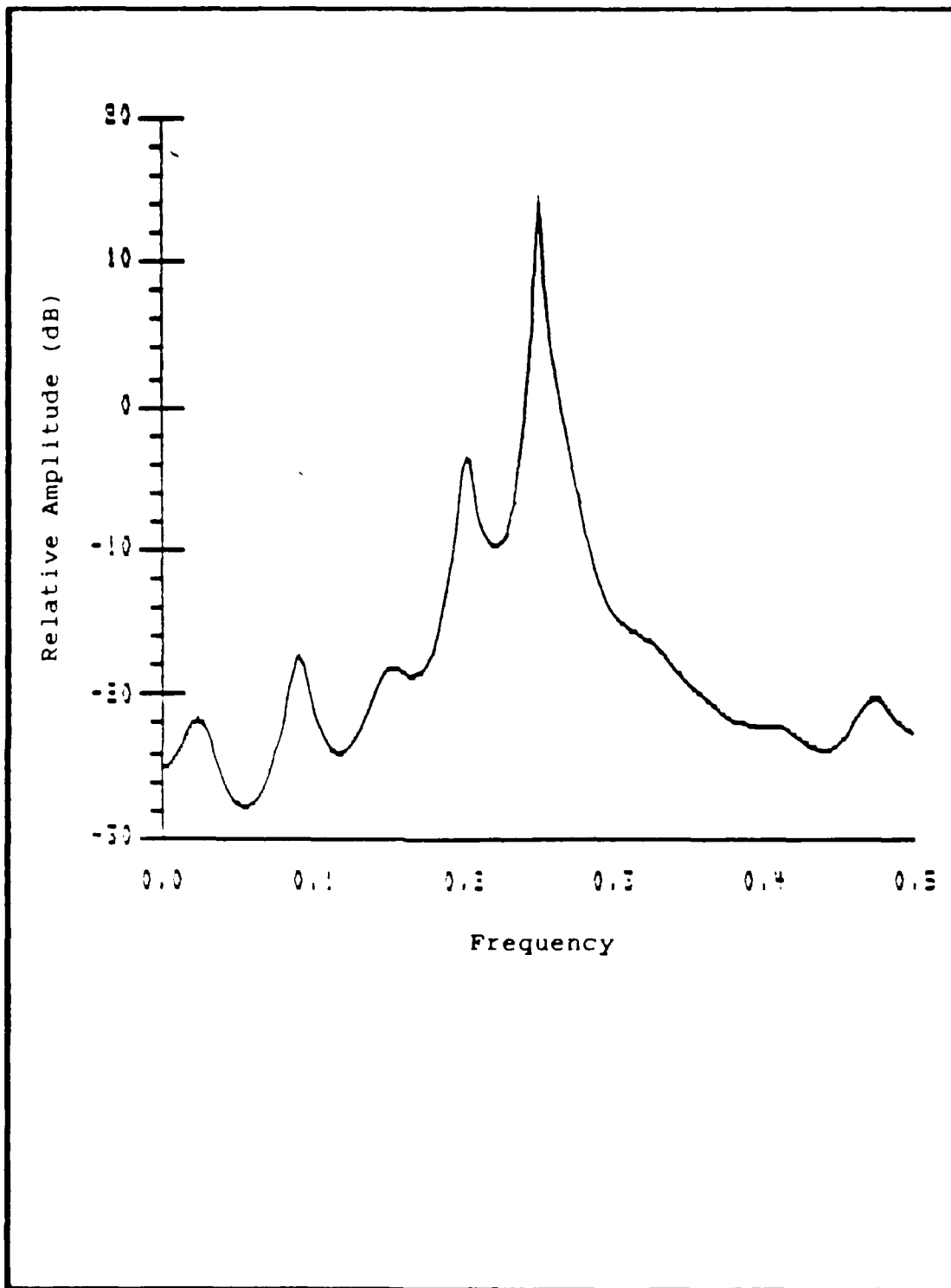


Figure 4.12c. Burg Estimator of Two Single Sinusoid in WGN, SNR = 15 dB with $P = 20$

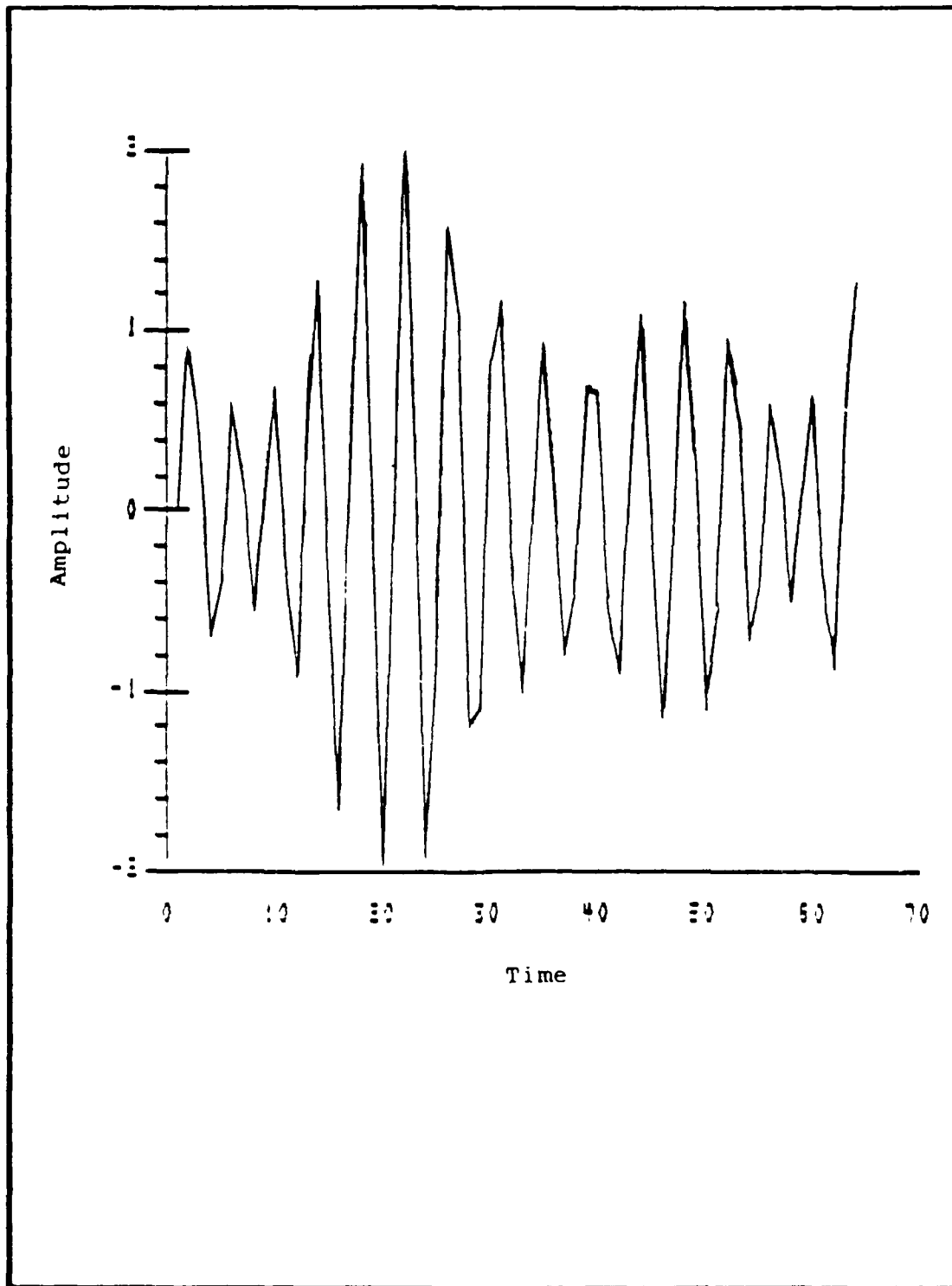


Figure 4.13. Sixty-Four Samples of Four Sinusoids in WGN, SNR = 15 dB

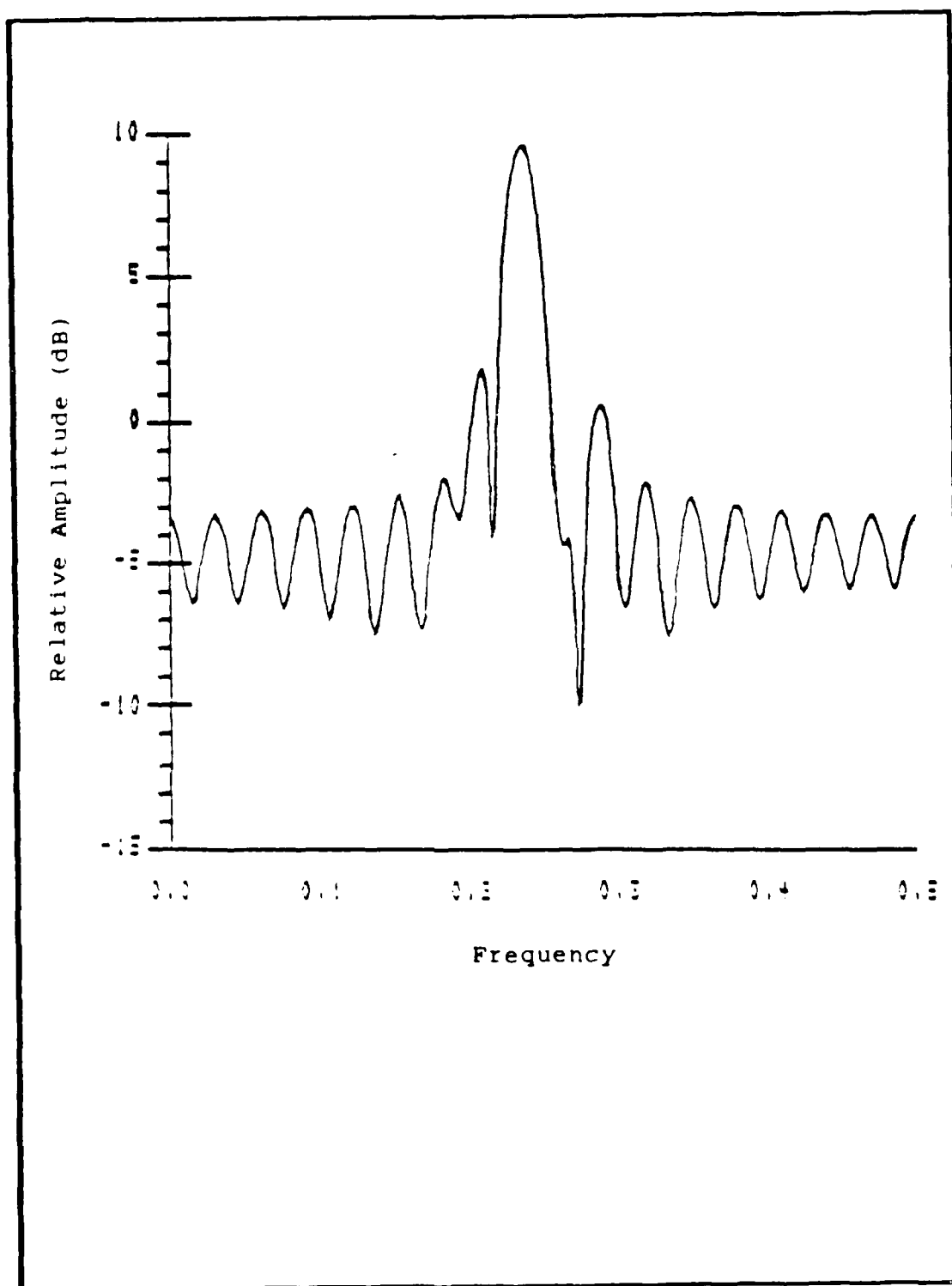


Figure 4.14. BT Estimator of Four Single Sinusoid in WGN, SNR = 15 dB

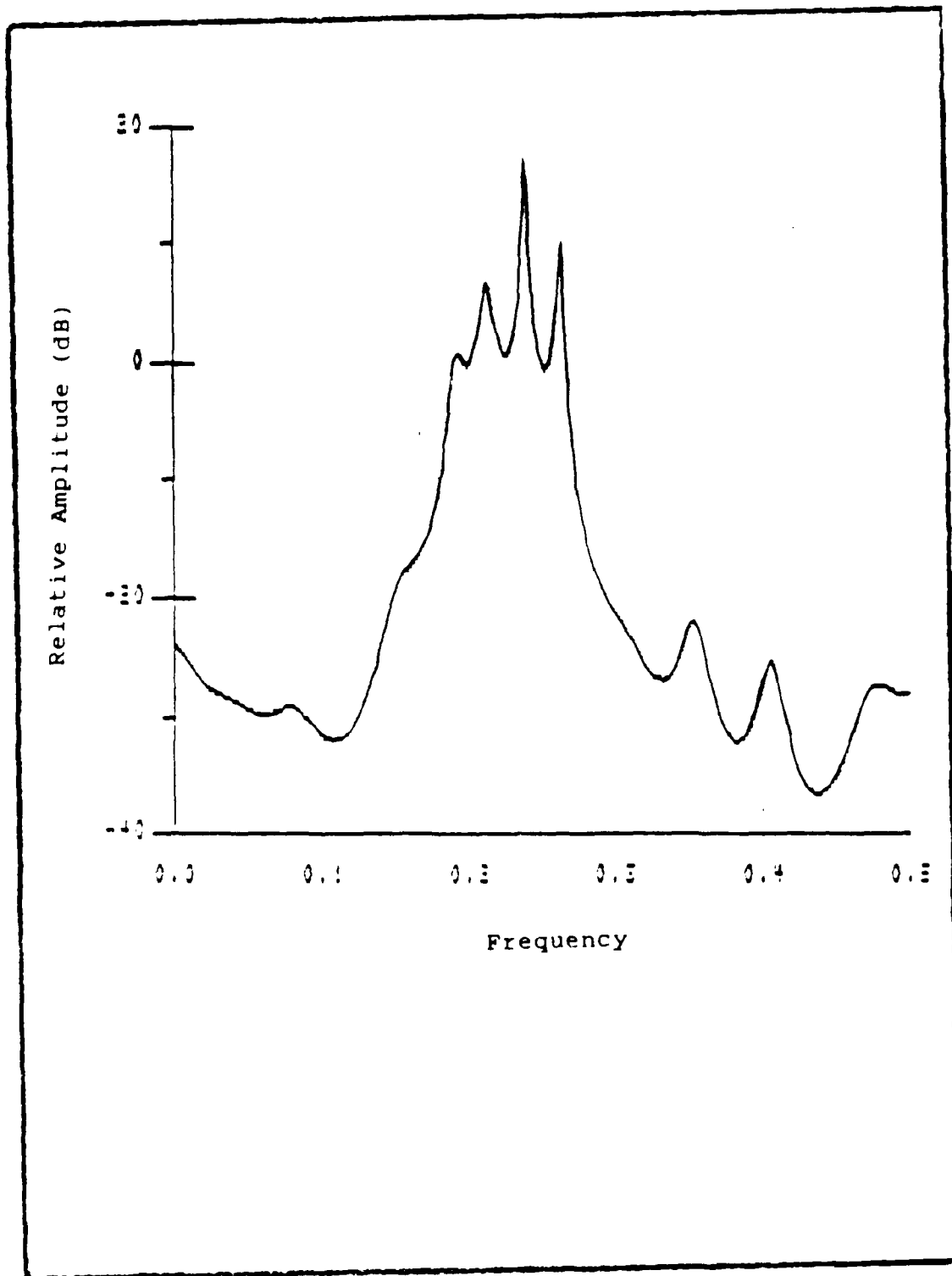


Figure 4.15. Burg Estimator of Four Single Sinusoid in WGN, SNR = 15 dB with $P = 24$

developing a threshold detecting scheme for determining peaks corresponding to actual frequencies - the focus of the next section.

Threshold Detection Routine

The above four problems are by no means an exhaustive list of all possible signal types. However, the data collected certainly suggest that the Burg method of spectral estimation is far superior to the BT method for short data records. This, of course, assumes that the input SNR is much greater than unity. Under the assumption that a sufficient input SNR (typically ≥ 15 dB) is available, the method of choice is obviously the Burg method. Thus, the threshold detection routine developed is based on applying the Burg method to short data records.

The foregoing analysis assumes a priori knowledge of the input data records. This assumption is necessary in order to investigate the merits of both spectral estimators. In practice, however, a priori knowledge is generally not known about the input data records. In this case, it is often very difficult to determine precisely the peaks corresponding to actual frequencies and the peaks resulting from inaccuracies of the spectral estimator. For example, given the PSD plot of Figure 4.12c without having any knowledge of the input data record, it might easily be interpreted as resulting from a data record consisting of six sinusoids. Recall, Figure 4.12c is actually the result

of a data record consisting of two sinusoids at fractional frequencies of 0.2 and 0.25. The other peaks are spurious peaks resulting from the inaccuracies or statistics of the Burg estimator. The obvious dilemma is that of differentiating between actual peaks and spurious peaks. One possible approach might be that of threshold detection.

The problem proposed by the Avionics Lab is to devise a routine that is capable of automatically detecting a maximum of five actual peaks and their corresponding frequencies. That is, if a data record consists of m sinusoids (unknown to the observer), then is it possible to detect up to five actual peaks and their frequencies.

In order to come up with an "adaptive" threshold value, several test cases are investigated (see Appendix B). The test cases presented in Appendix B represent only a few of the cases actually considered. However, they serve to summarize the implied results of the many cases investigated. The test cases include data records, with 64 data samples, consisting of one to five independent sinusoids. The upper limit five is a software constraint (see Chapter II). The amplitude (or power) of each sinusoid is varied. It is observed, that if the amplitudes of the sinusoids vary by two orders of magnitude or more (e.g. a data record consisting of three sinusoids with respective amplitudes of 0.1, 2.0 and 30), then retrieving the lower amplitude sinusoid is virtually impossible (see Figure B.7).

However, if the amplitudes of the sinusoids vary by no more than one order of magnitude, then "all" sinusoids may possibly be retrieved (see Figures B.1 through B.6). The test cases suggest that a suitable adaptive threshold is 28 dB below the highest peak in the spectrum. The word adaptive is used rather loosely in that a threshold of 30 dB below the highest peak does not adapt for all cases. This method of determining the threshold is purely empirical, resulting from determining an average value below the highest peak for all test cases considered.

The ideal model order number P required to detect five sinusoids is ten. However, as previously pointed out the corruption of noise causes this number to increase. The test cases suggest that a model order number of $P = 24$, using the threshold value previously stated, allows the estimator to correctly resolve actual peaks in most cases for data records consisting of up to five sinusoids. It is pointed out, however, that a minimum SNR of 15 dB is used in each case considered. Varying this parameter will change the required value of P . Also the software limitation of a maximum of five sinusoids in a data record certainly does not represent all possible data record types. In practice it may be necessary to change the value of P if it is believed that the actual data record consist of many sinusoids (i.e., $m \gg 5$). Obviously, there are several parameters that effect the value of P ; thus, it is not

possible to come up with a value suitable for all possible scenarios.

The "smart" routine that determines the actual peaks and their corresponding frequencies, incorporating the above criteria, is also presented in Appendix B. For purposes of illustration, consider the PSD plot of Figure 4.16. Figure 4.16 is actually the Burg PSD of Problem Three for $P = 24$ - note the many spurious peaks. The results of applying the "smart" routine are as follows:

$$f_1 = 0.1992$$

and

$$f_2 = 0.2460$$

The reason for the discrepancy between the computed frequencies and the actual frequencies is due to way in which the Burg PSD is computed. That is, the Burg PSD is computed based on 256 discrete data points over the frequency range 0 to 0.5. Thus, the computed frequencies are actually multiples of $0.5/256$ (or $1/512$) and represent close approximations.

The following chapter presents conclusions and recommendations of the above analysis.

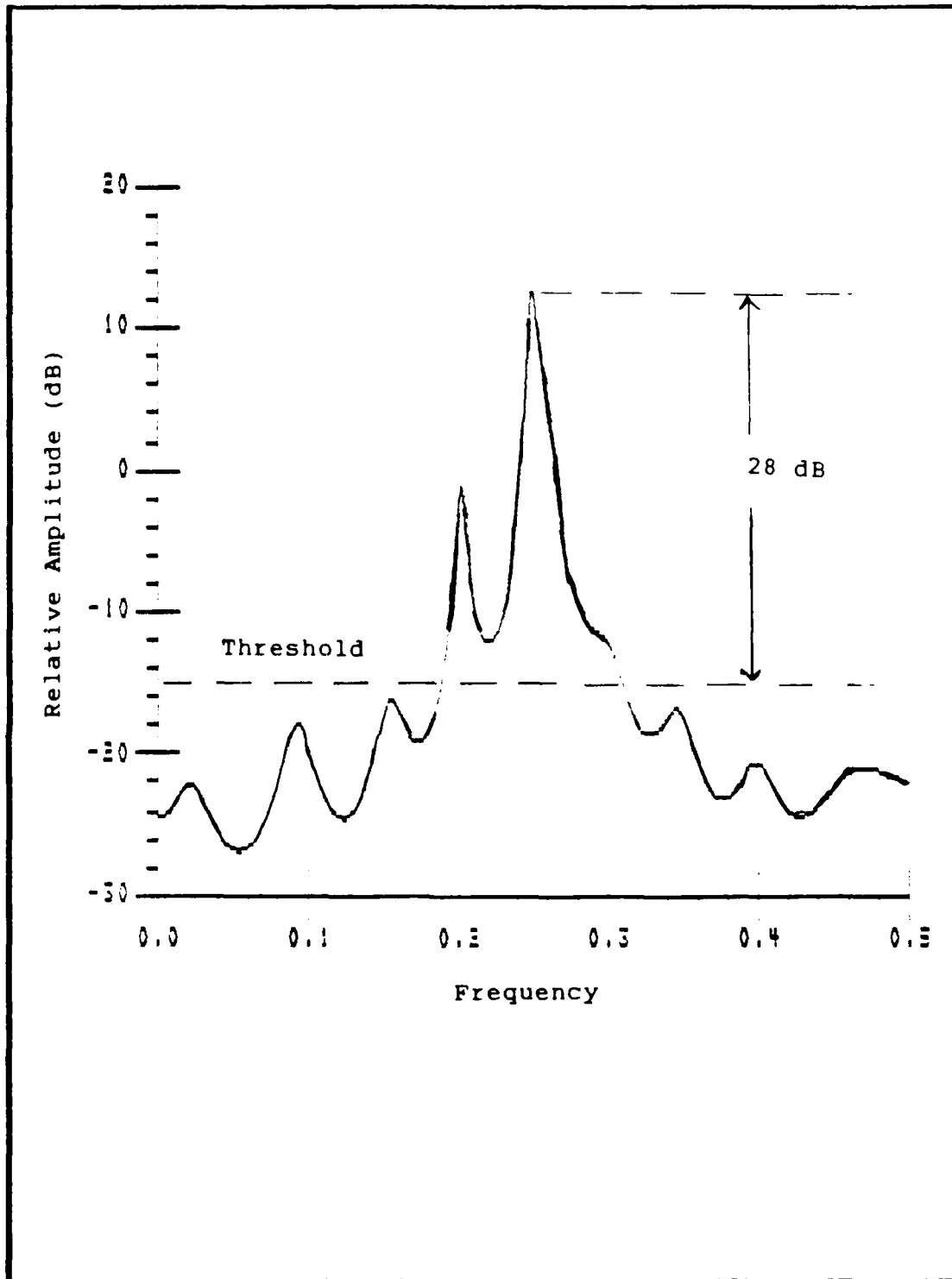


Figure 4.16. Burg Estimator of Two Single Sinusoid in WGN, SNR = 15 dB with $P = 24$

V. Conclusions and Recommendations

Conclusions

This study has investigated the performance of two popular but distinctly different methods of spectral estimation from an EW receiver point of view. In an EW environment the duration of the received pulse is usually relatively short, resulting in only a few data samples available for processing. Thus, the method used for spectral estimation has to be capable of providing reasonable results for short data records. Several "real world" data records, each consisting of 64 data samples, were analyzed using both the BT and Burg methods of spectral estimation. The Burg method was found to yield far superior results in terms of frequency resolution. However, its performance was determined to be a function of the input SNR. It was noted that for low input SNR (i.e., $\text{SNR} \leq 10$ dB) the results of the Burg method degraded substantially. Another parameter affecting the resolution capability was the model order number P . Increasing the value of P has a tendency of increasing the frequency resolution, as well as introducing spurious peaks into the spectrum. Therefore, the value P has to be selected carefully. The test cases that were analyzed suggest a $P \approx 24$ for detecting actual peaks of data records consisting of up to five independent sinusoids. A minimum SNR of 15 dB was used in each test

case. Evaluation of the test cases suggested that an appropriate scheme for differentiating between actual peaks and spurious peaks was that of threshold detection.

Recommendations

This study is not intended to present an all encompassing approach of spectral estimation for short data records. The two techniques presented in this study represent only a some fraction of the many methods proposed and currently being evaluated by several researchers (9:1383). Several appropriate recommendations are as follows:

1. Investigate some of the other methods of spectral estimations. For example, the method proposed by Pisarenko (42:347-366) which provides a very accurate discrete spectrum for data records consisting of deterministic harmonics in WGN.
2. Increase the maximum allowable sinusoids in a data record currently provided by ISPX. This will allow for developing a more comprehensive data base; thus, allowing for more conclusive data.
3. Apply the two methods discussed in this study to other types of data. For example, the Burg might have great promise if applied to two dimensional imaging data.
4. Investigate and possibly incorporate some of the schemes that have evolved of the past decade for

determining the correct model order number P into the ISPX software package.

Appendix A: Subroutines Used for Spectral Estimation

Several algorithms are used in the analysis sections of this paper. This appendix provides a brief explanation of each routine with a FORTRAN listing. All FORTRAN listings appear exactly as they appear in the ISPX software package. The listings were not generated by the author. They were used merely as a "tool" for analyzing several data records.

Subroutine Blackman-Tukey

```
subroutine blacktukey(x,n,mode,wind,m,nexp,pbt)

c   This program computes the Blackman-Tukey spectral
c   estimator as given by (3.9). Either the biased or
c   unbiased autocorrelation estimator may be used as well
c   as a lag window.
c   The spectral estimate is evaluated at the frequencies
c    $F = -1/2 + (I-1)/L$  for  $I = 1, 2, \dots, L$ . The number of
c   frequencies is given by  $L = 2**NEXP$ .
c
c   Input Parameters:
c
c   x       -Complex array of dimension Nx1 of data points.
c   n       -Number of data points.
c   mode    -Set equal to zero for unbiased autocorrelation
c           estimator; otherwise, biased estimator used.
c   wind    -Real array of dimension 2M+1 of lag window
c           weights; wind(1),...,wind(m+1),...,wind(2M+1)
c           correspond to  $w[-M], \dots, w[0], \dots, w[M]$ .
c   m       -Largest lag desired.
c   nexp    -Power of two which determines number of
c           frequency samples desired,  $L = 2**NEXP$ ; must be
c           chosen so that L is  $\geq 2*M+2$ .
c
c   Output Parameters:
c
c   pbt     -Real array of dimension  $L = 2**NEXP \times 1$  of samples
c           of the Blackman-Tukey spectral estimate, where
c           pbt(i) corresponds to the spectral estimate at
c           frequency  $F = -1/2 + (i-1)/L$ .
c
c   External Subroutines:
c   PREFFT, FFT
c
```

```

c      Notes:
c
c      The calling program must dimension the array
c      x,wind,pbt.
c      The array w,r,rcorr,p must be dimensioned >= the
c      variable dimension shown, or equal to 2**NEXP. Also,
c      the array RCORR should be dimensioned >= 2M+1.
c
c      complex x(1), w(512), r(512), recorr(129)
c      dimension window(1), p(512), pbt(1)
c      pi=4.*atan(1.)
c      compute the autocorrelation estimates from the data.
c      m1=m+1
c      call correlation(n,m1,mode,x,x,rcorr)
c      Window the M+1 autocorrelation estimates and insert
c      them into the last M+1 locations of rcorr. Then, fill
c      first m points of rcorr array with the complex
c      conjugates of the last m points (shift the
c      autocorrelation
c      sequence to the right by m samples so that FFT may be
c      used).
c      r(m1)=wind(m1)*rcorr(1)
c      do 10 i=1,m
c      r(m1+i)=wind(m1+i)*rcorr(i+1)
10    r(m1-i)=wind(m1-i)*conjg(rcorr(i+1))
c      Zero pad the array of windowed autocorrelation samples
c      to obtain an array of dimension equal to L.
c      l=2**nexp
c      do 20 i=2*m+2,l=256
20    r(i)=(0.,0.)
c      Compute FFT of the autocorrelation sequence.
c      invrs=-1
c      npad=1
c      call prefft(1,npad,invrs,nexp,w)
c      norm=0
c      call fft(1,npad,nexp,norm,w,r)
c      Compensate for shifting the autocorrelation sequence to
c      the right by m samples.
c      do 30 i=1,l
c      f=(i-1.)/l
c      arg=2.*pi*f*m
30    p(i)=real(r(i)*cexp(cmplx(0.,arg)))
c      Transpose halves of FFT output so that first PSD sample
c      is at a frequency of -1/2.
c      do 40 I=1,l/2
c      pbt(i+1/2)=p(i)
40    pbt(i)=p(i+1/2)
c      return
c      end

```

Subroutine Burg

```
subroutine brug(x,n,ip,a,sig2)

c   This program implements the Burg method for estimation
c   of the AR parameters (3.21)-(3.27).
c
c   Input Parameters:
c
c   x       -Complex array of dimension Nx1 of data points.
c   n       -Number of data points.
c   ip      -AR model order desired.
c
c   Output Parameters:
c
c   a       -Complex array of dimension IPx1 of AR filter
c           parameter estimates arranged as A(1) to A(IP).
c   sig2    -White noise variance estimate.
c
c   Notes:
c
c   The calling program must dimension the X,A arrays.
c   The arrays EFK,EFK1,EBK,EBK1,AA,RHO must be dimensioned
c   >= (n,n,n,n,ipxip,ip respectively).
c
c   complex x(1),a(1),efk(512),ebk(512),efk1(512),
c   ebk1(512),aa(128,128),: sumn,sumd
c   dimension rho(128)
c   Compute the estimate of the autocorrelation at lag zero
c   (3.21).
c   rho0=0
c   do 10 i=1,n
10  rho0=rho0+cabs(x(i))**2/n
c   Initialize the forward and backward prediction
c   errors(7.39).
c   do 20 i=2,n
c   efk1(i)=x(i)
20  ebk1(i-1)=x(i-1)
c   Begin recursion.
c   do 80 k=1,ip
c   Compute the reflection coefficient estimate (3.27).
c   sumn=(0.,0.)
c   sumd=(0.,0.)
c   do 30 i=k+1,n
c   sumn=sumn+efk1(i)*conjg(ebk1(i-1))
30  sumd=sumd+cabs(efk1(i))**2+cabs(ebk1(i-1))**2
c   aa(k,k)=-2.*sumn/sumd
c   Update the prediction error power (7.40).
c   if(k.eq.1)rho(k)=(1.-cabs(aa(k,k))**2)*rho0
c   if(k.gt.1)rho(k)=(1.-cabs(aa(k,k))**2)*rho(k-1)
c   if(ip.eq.1) go to 90
c   if(k.eq.1) go to 50
c   Update the prediction error filter coefficients (3.27).
```

```

do 40 j=1,k-1
40 aa(j,k)=aa(j,k-1)+aa(k,k)*conjg(aa(k-j,k-1))
c Update the prediction error filter coefficients (3.24).
50 do 60 i=k+2,n
efk(i)=efkl(i)+aa(k,k)*ebkl(i-1)
60 ebk(i-1)=ebkl(i-2)+conjg(aa(k,k)*efkl(i-1))
do 70 i=k+2,n
efkl(i)=efk(i)
70 ebkl(i-1)=ebk(i-1)
80 continue
c Find final values of the prediction error power, which
c is the white noise variance estimate, and the
c prediction coefficients, which are the AR filter
c parameter estimates.
90 sig2=rho(ip)
do 100 i=1,ip
100 a(i)=aa(i,ip)
return
end

```

Subroutine PreFFT

```

subroutine prefft(n,npad,invrs,nexp,w)

c This program sets up the complex exponential table
c needed to compute the fast Fourier transform of an
c array of complex datasamples using a
c decimation-in-frequency algorithm. Pruning is
c performed if zero padding is requested. The output
c table contained in the array is input to the program
c FFT which computes the fast Fourier transform of the
c data
c
c Input Parameters:
c n -number of data samples
c npad -Set to 1 for no zero padding (N-point
c transform), 2 for double padding (2N-point
c transform), 4 for quadruple padding (4N-point
c transform).
c invrs -Set to -1 for forward transform, 1 for inverse
c transform.
c
c Output Parameters:
c nexp -Indicates power of two exponent such that
c n=2**nexp. Set to -1 to indicate error
c condition if n is not a power of two in which
c case program terminates prematurely.
c w -Complex array of dimension n*npadxl containing
c exponential table.
c

```

```

c      Notes:
c
c      The calling program must dimension the complex array w
c      greater than or equal to n*npad.
c
      complex w(1),u
      nexp=1
5      nt=2**nexp
      if (nt.ge.n) go to 10
      nexp=nexp+1
      go to 5
10     if(nt.eg.n) go to 15
      nexp=-1
      return
15     nt=n*npad
      ang=8.*atan(1.)/nt
      u=cplx(cos(ang),invrs*sin(ang))
      w(1)=(1.,0.)
      do 20 i=2,nt
20     w(i)=w(i-1)*u
      return
      end

```

Subroutine FFT

```

      subroutine fft(n,npad,nexp,norm,w,x)

c      Input parameters:
c
c      n,npad,nexp,w      -See parameter list for subroutine
c      "PREFFT"
c      norm      -Set to 0 for forward transform, else the sum is
c                divided by n for inverse transform.
c      x          -Complex array of dimension nxl of data samples.
c
c      Output parameters:
c
c      x          -Complex array of dimension n*npadxl of
c                transform values.
c
c      Notes:
c
c      The calling program must dimension arrays x,w.
c
      complex x(1),w(1),t,u
      if(nexp.eq.-1)return
      go to (30,20,10,10)npad
10     n2=n*2
      nt=n2*2
      x(n2+1)=x(1)
      do 12 k=2,n
12     x(n2+k)=x(k)*w(k)

```

```

x(n+1)=x(1)
nx=n2+1
x(n+nx)=x(nx)
jj=3
do 14 k=2,n
x(n+k)=x(k)*w(jj)
nx=2n+k
x(n+nx)=x(nx)*w(jj)
14  jj=jj+2
mm=4
go to 35
20  x(n+1)=x(1)
do 22 k=2,n
22  x(n+k)=x(k)*w(k)
mm=2
nt=n*2
go to 35
30  nt=n
mm=1
35  ll=n
do 70 k=1,nexp
nn=ll/2
jj=mm+1
do 40 i=1,nt,ll
kk=i+nn
t=x(i)+x(kk)
x(kk)=x(i)-x(kk)
40  x(i)=t
if(nn.eq.1) go to 70
do 60 j=2,nn
u=w(jj)
do 50 i=j,nt,ll
kk=i+nn
t=x(i)+x(kk)
x(kk)=(x(i)-x(kk))*u
50  x(i)=t
60  jj=jj+mm
ll=nn
mm=mm*2
70  continue
nv2=nt/2
nml=nt-1
j=1
do 90 i=1,nml
if(i.ge.j) go to 80
t=x(j)
x(j)=x(i)
x(i)=t
80  k=nv2
85  if(k.ge.j) go to 90
j=j-k
k=k/2
go to 85

```

AD-A190 616

SPECTRAL ANALYSIS OF SHORT DATA RECORDS(U) AIR FORCE
INST OF TECH WRIGHT-PATTERSON AFB OH SCHOOL OF
ENGINEERING T E CARTER DEC 87 AFIT/GE/ENG/8DD-9

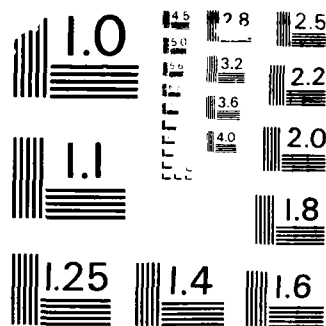
2/2

UNCLASSIFIED

F/G 17/4

NL





MICROCOPY RESOLUTION TEST CHART
NATIONAL BUREAU OF STANDARDS - 1963-A

```
90  j=j+k
    if(norm.eq.0) return
    do 100 i=1,nt
100  x(i)=x(i)/n
    return
    end
```

Appendix B: Theshold Detection Routine

This appendix contains the threshold detection routine called "Peak Detector". The peaks are computed by determining negative slope changes in a given PSD plot. In order to differentiate between actual peaks and spurious peaks an "adaptive" threshold value was empirically determined as discussed in Chapter IV. Also several test cases are presented

Routine Peak Detector

```
Integer I,K,count
Character fname*20
Complex z(512)
Real Fn,Magn,FnNxt,MagNxt,Slope,SlopeNxt,LMagNxt,
thold,test,ABSFN,Pt0,Pt1,MaxPt

C
C The user specifies the appropriate filename.
C
C Print*, 'Enter a filename.'
C Read'(a)', fname
C
C
C Open (unit=1,file-fname,status='old')
C
C Initialization
C
C count = 0
C Pt0 = 0.0
C Slope = 0.0
C Fn = 0.0
C Magn = 0.0
C
C The value of maximum peak is computed.
C
C Do 20 K = 1,257
C   Read(1,*) z(k)
C   Pt1 = real(z(k))
C   MaxPt = AMAX1(Pt1,Pt0)
C   Pt0 = MaxPt
C   LMaxPt = 10.0*ALOG10(MaxPt)
```

```

20      continue
c
c      The pointer is re-initialized
c
c      REWIND (unit=1)
c
c      The peaks are determined.
c
c      Do 10 I = 1,257
c          FnNxt = Fn
c          MagNxt = Magn
c          SlopeNxt = Slope
c          Read(1,*) Z(I)
c          Magn = real(z(I))
c          Fn = -0.5 + (I-1)/512.0
c          ABSFn = ABS(Fn)
c      If (I.EQ.1) Go To 10
c          Slope = (Magn - MagNxt)/(Fn - FnNxt)
c          If (SlopeNxt.GT.0.0) then
c              test = SlopeNxt + Slope
c              If (test.LE.SlopeNxt) then
c                  LMagNxt = 10.0*ALOG10(MagNxt)
c          The adaptive threshold value is set.
c              thold = LMagPt - 28.0
c              If (LMagNxt.GE.thold) then
c                  count = count + 1
c          The actual peaks and their corresponding
c          frequencies are printed
c              Print* ABSFn, LMagNxt, count
c          ENDIF
c      ENDIF
c      ENDIF
10      continue
c
c      CLOSE (unit=1)
c
c      Stop
c      End

```

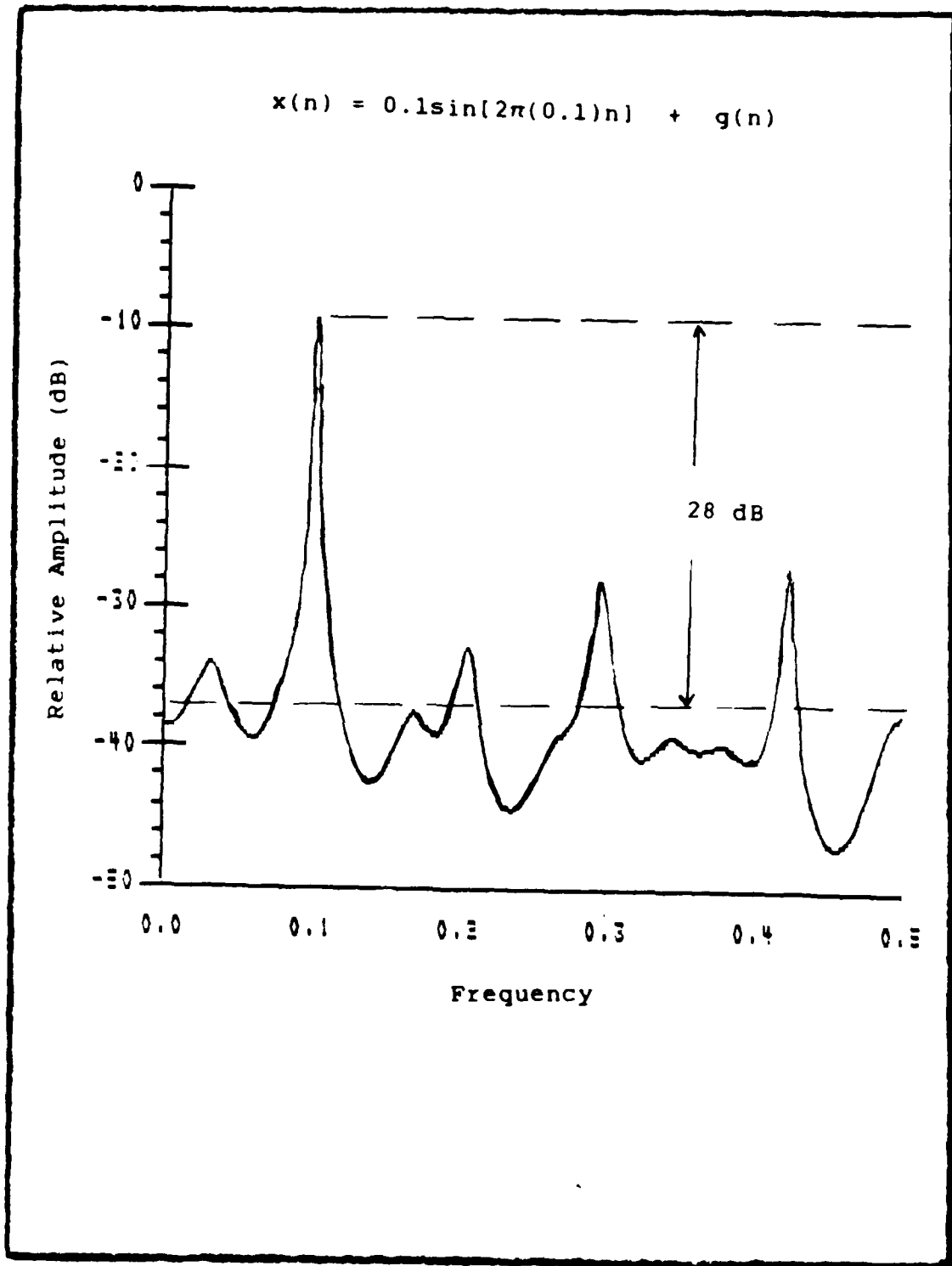


Figure B.1. Burg Estimator of a Single Sinusoid in WGN, SNR = 15 dB with P = 24

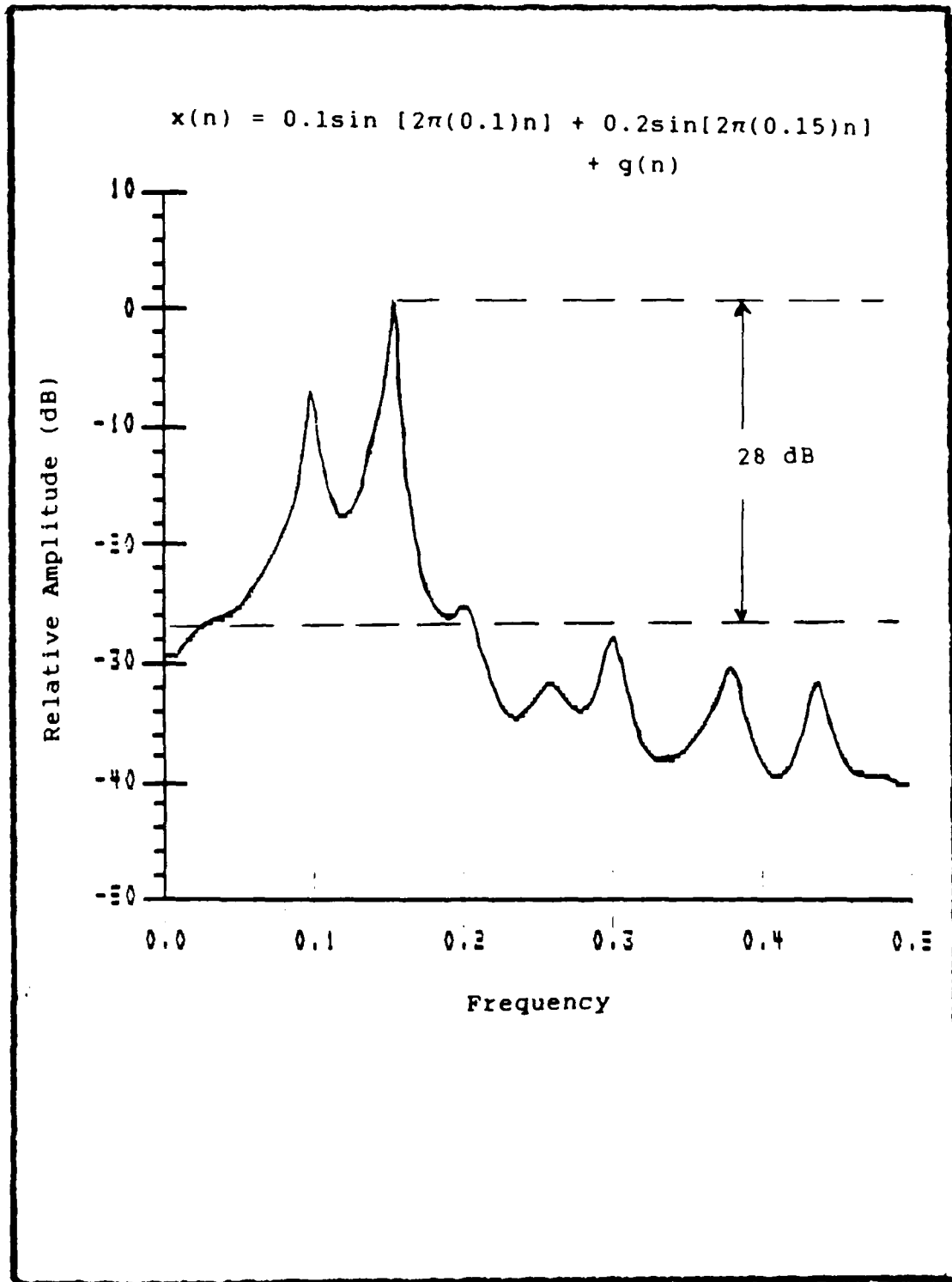


Figure B.2. Burg Estimator of Two Single Sinusoid in WGN, SNR = 15 dB with P = 24

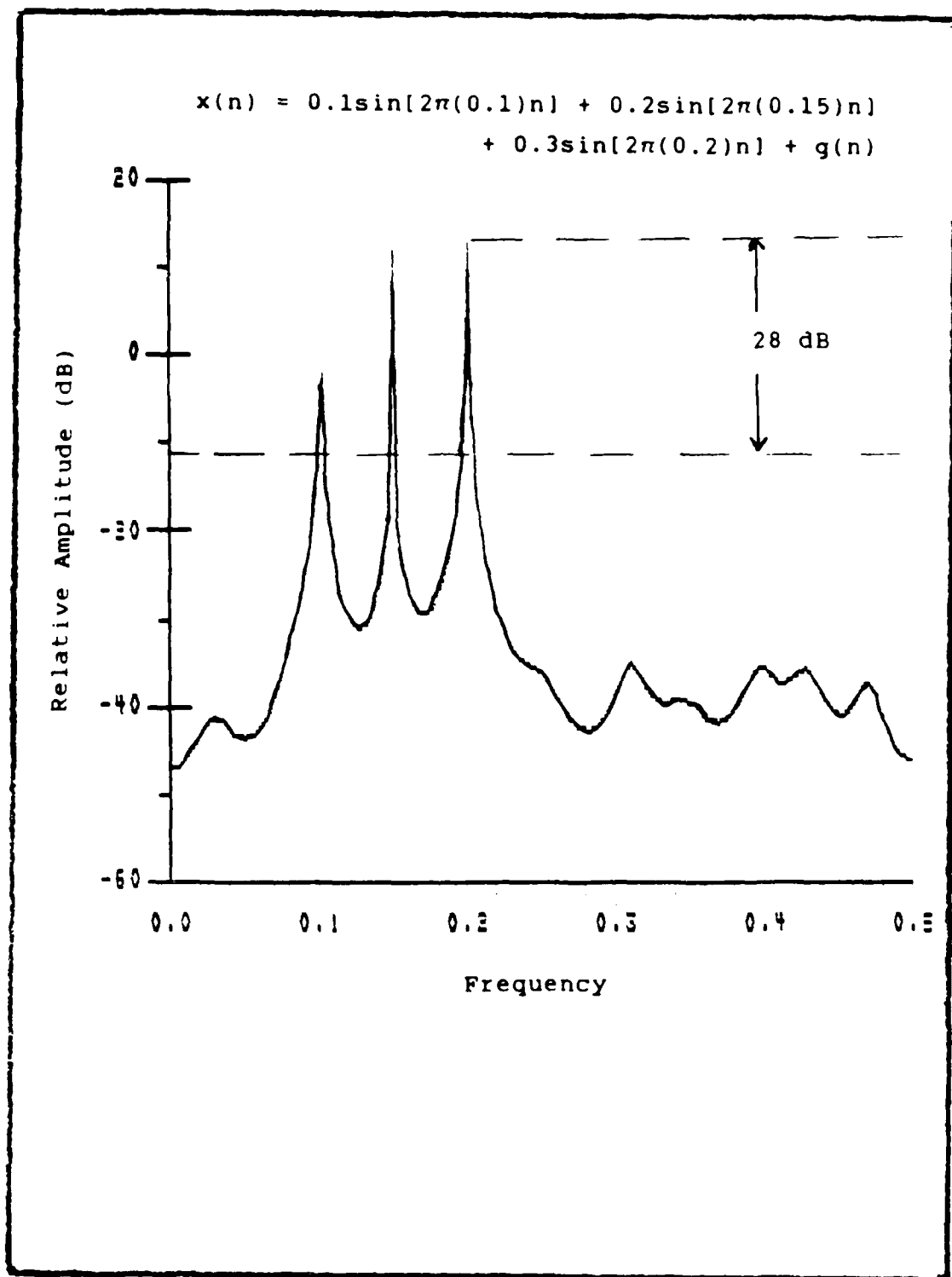


Figure B.3. Burg Estimator of Three Single Sinusoid in WGN, SNR = 15 dB with $P = 24$

$$x(n) = 0.1\sin[2\pi(0.1)n] + 0.2\sin[2\pi(0.15)n] + 0.3\sin[2\pi(0.2)n] + 0.4\sin[2\pi(0.25)n] + g(n)$$

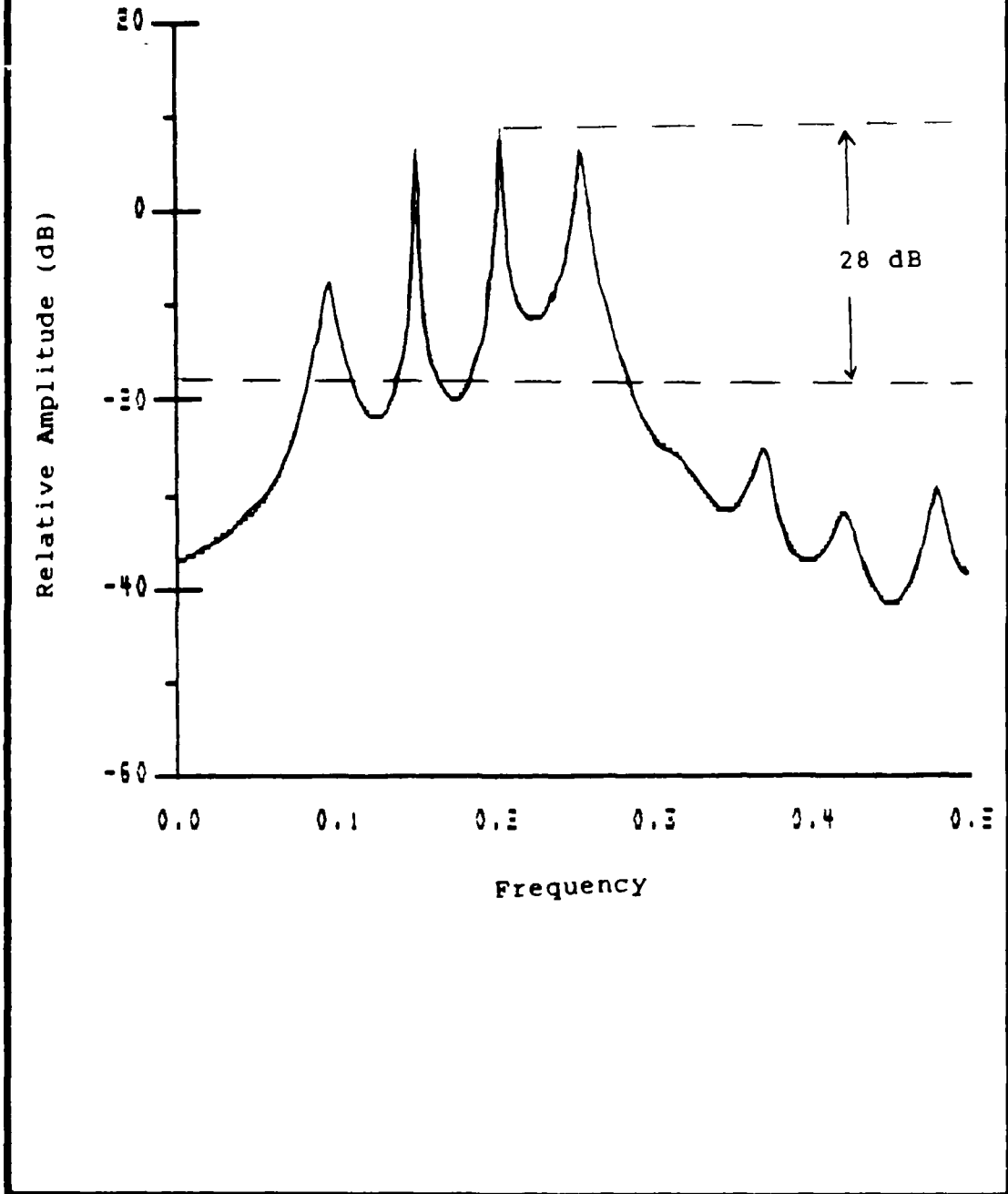


Figure B.4. Burg Estimator of Four Single Sinusoid in WGN, SNR = 15 dB with P = 24

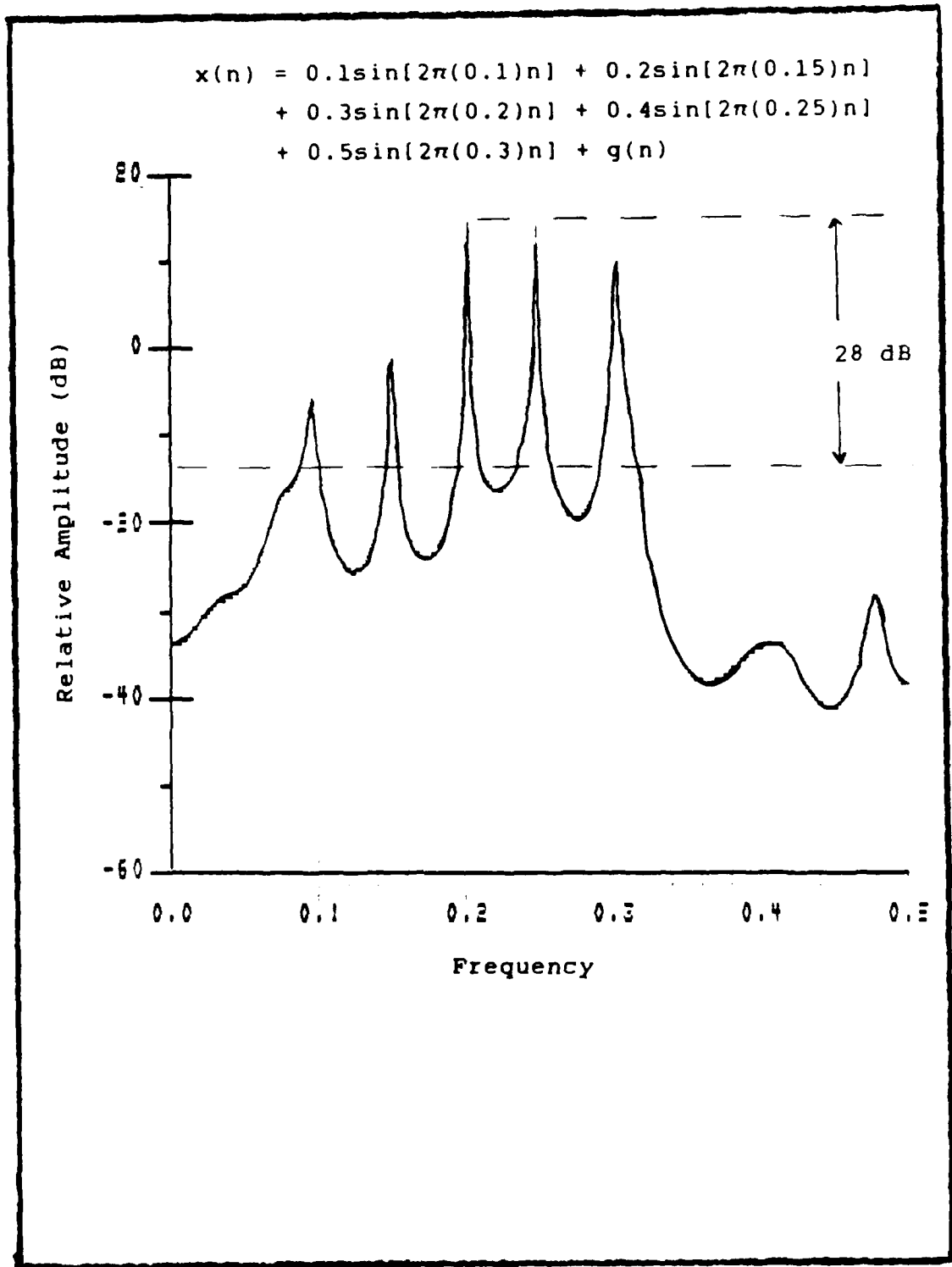


Figure B.5. Burg Estimator of Five Single Sinusoid in WGN, SNR = 15 dB with $P = 24$

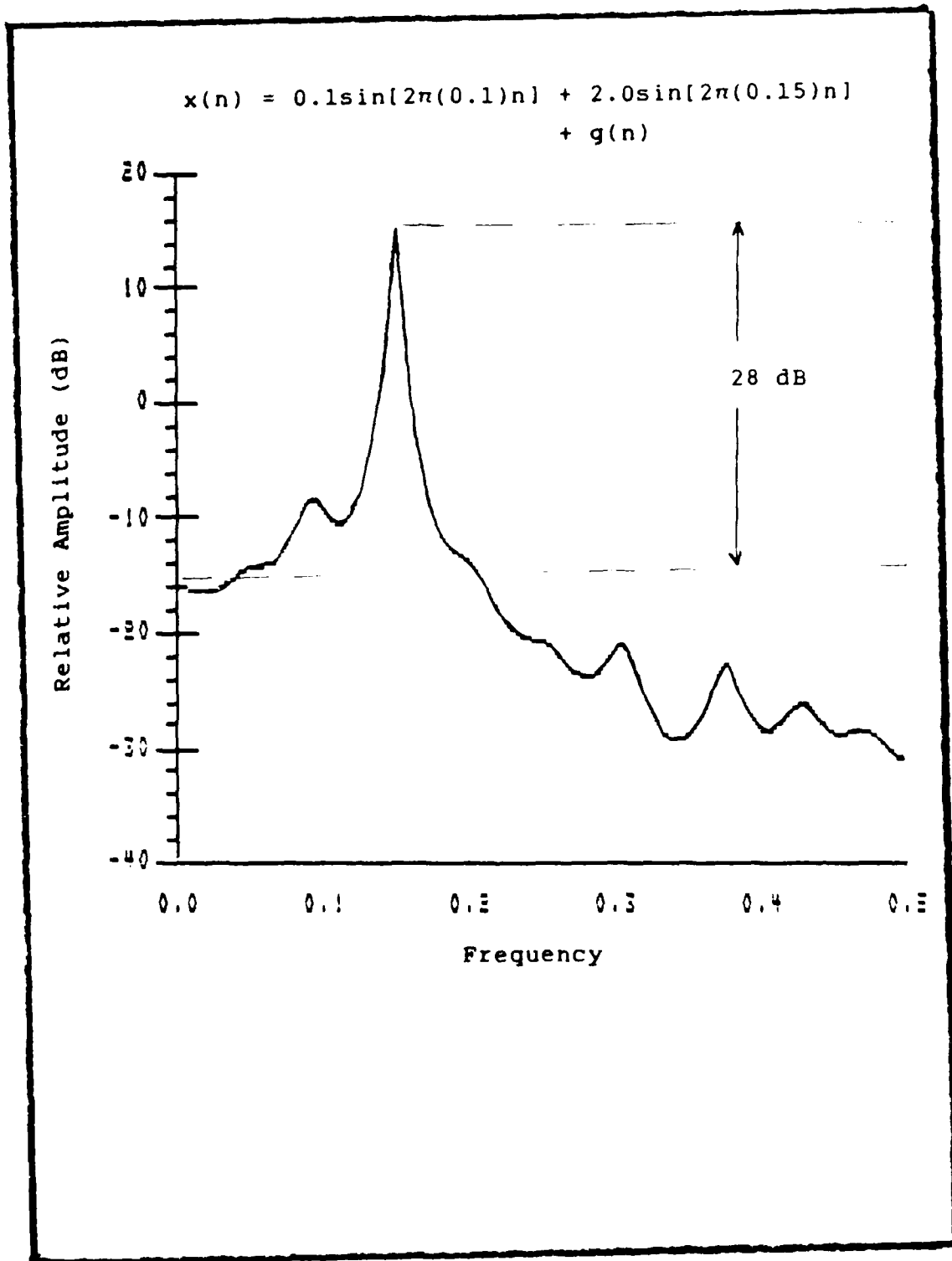


Figure B.6. Burg Estimator of Two Single Sinusoid in WGN, SNR = 15 dB with P = 24

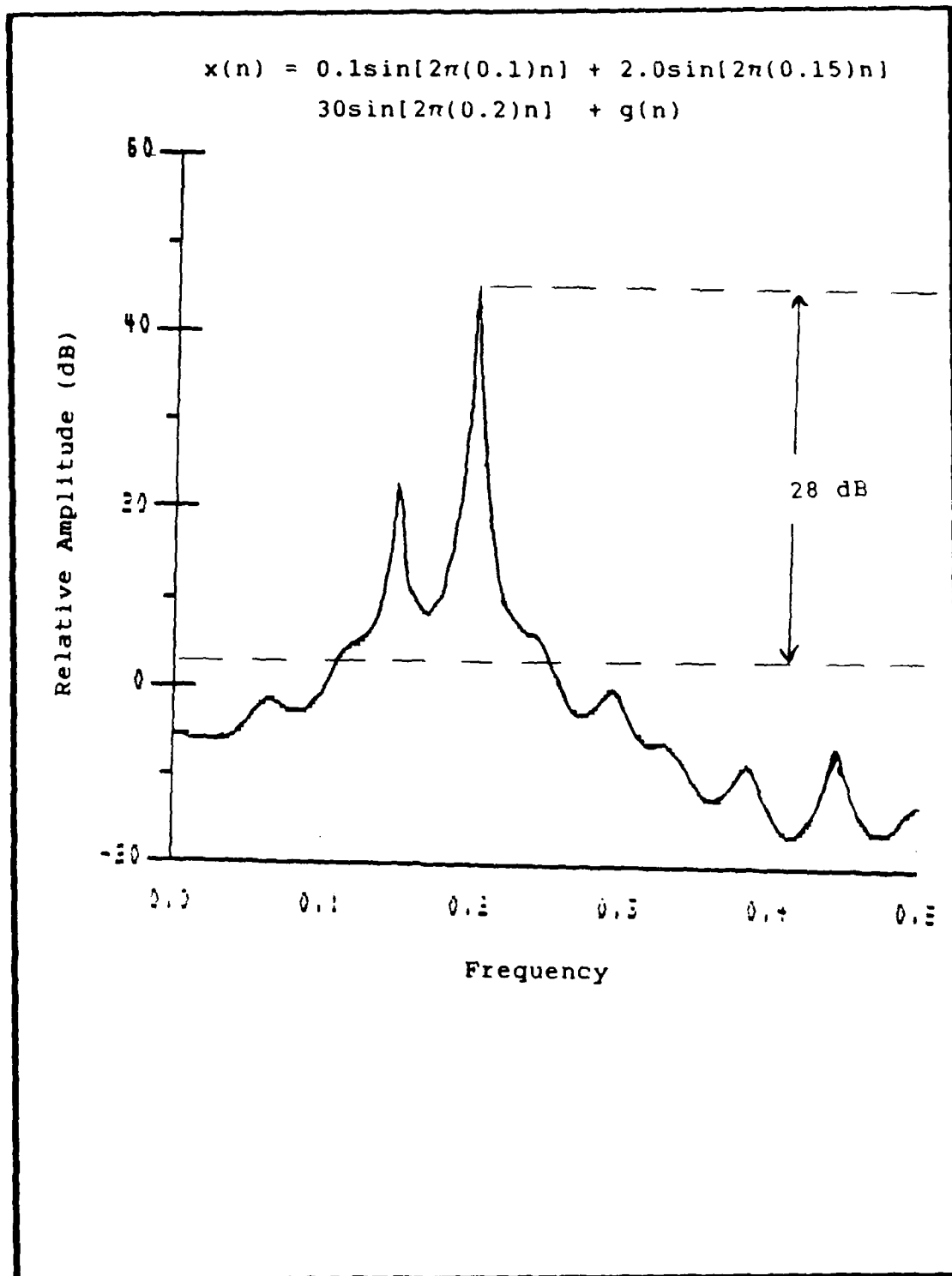


Figure B.7. Burg Estimator of Three Single Sinusoid in WGN, SNR = 15 dB with $P = 24$

Bibliography

1. Achilles, Gunter D. "Spectral Estimation," Signal Processing II: 447-454 (September 1983).
2. Air Force Wright Aeronautical Laboratories, Air Force System Command. Contract F49620-85C-0013 with University of Oklahoma. Wright-Patterson AFB OH, 28 July 1986.
3. Akaike, H. "A New Look at the Statistical Model Identification," IEEE Transaction on Automatic Control, 19: 716-723 (December 1974).
4. Bishop, Thomas N. and Tad J. Ulrych. "Maximum Entropy Analysis and Autoregressive Decomposition," Geophysics and Space Physics Review, 13: 183-200 (February 1975).
5. Blackman, R. B. and J. W. Tukey. "The Measurement of Power Spectra from the Point of View of Communications Engineering," Bell System Technical Journal, 37: 185-282 (August 1957).
6. Chen, Chi H. Digital Waveform Processing and Recognition. Boca Raton, Florida: CRC Press, 1982.
7. Cooper, George R. and Mostafa Kaveh. "An Empirical Investigation of the Properties of the Autoregressive Spectral Estimator," IEEE Transaction on Information Theory, 22: 313-323 (May 1976).
8. Dubroff, Richard. "The Effective Autocorrelation Function of Maximum Entropy Spectra," IEEE Proceedings, 63: 1622-1623 (November 1975).
9. Gagliardi, Robert M. Introduction to Communications Engineering. New York: Wiley, 1978.
10. Gardner, William A. Introduction to Random Processes. New York: MacMillan Publishing Company, 1986.
11. Harris, F. J. "On the Use of Windows for Harmonic Analysis with the Discrete Fourier Transformation," IEEE Proceedings, 66: 51-83 (March 1978).
12. Haykin, Simon. Array Signal Processing. Englewood Cliffs, New Jersey: Prentice-Hall, 1985.

13. Haykin, Simon. Communication Systems (Second Edition). New York: Wiley, 1983.
14. Haykin, Simon. Communication Systems. New York: Wiley, 1978.
15. Jenkins, Gwilym M. and Donald G. Watts. Spectral Analysis and its Applications. San Francisco: Holden-Day, 1968.
16. Kashap, R. L. "Inconsistency of the AIC Rule for Estimating the Order of Autoregressive Models," IEEE Transaction on Automatic Control, 25: 996-998 (March 1980).
17. Kay, Steven M. Modern Spectral Estimation. New Jersey: Prentice-Hall, 1987.
18. Kay, Steven M. and Stanley Lawrence Marple. "Spectrum Analysis-A Modern Perspective," IEEE Proceedings, 69: 1380-1419 (November 1981).
19. Kunt, Murat. Digital Signal Processing. Norwood, Massachusetts: Artech House, 1986.
20. Makhoul, John. "Linear Prediction: A Tutorial Review," IEEE Proceedings, 63: 561-580 (April 1975).
21. Marple, Lawrence S. Digital Spectral Analysis. Englewood Cliffs, New Jersey: Prentice-Hall, 1987.
22. Nadal, Marino and Sam Daniel. Advanced MTI Processor Baseline Demonstration for Improved Detection Performance, April 1982 - November 1982. Contract F30602-82C-0047. Tempe, Arizona: Motorola Inc., July 1982 (AD-B077837).
23. Orfanidis, Sophocles. Optimum Signal Processing. New York: MacMillan Publishing Company, 1985.
24. Papoulis, Athanasios. Probability, Random Variables, and Stochastic Processes. New York: McGraw-Hill, 1984.
25. Parzen, Emanuel. "Some Recent Advances in Time Series Modeling," IEEE Transaction on Automatic Control, 19: 723-730 (December 1974).
26. Peebles, Peyton Z. Communication System Principles. London: Addison-Wesley, 1976.

27. Schwartz, Mischa. Information Transmission, Modulation and Noise. New York: McGraw-Hill, 1980.
28. Skolnik, Merrill L. Introduction to Radar Systems. New York: McGraw-Hill, 1980.
29. Sterns, Samuel D. Digital Signal Analysis. Rochelle Park, New Jersey: Hayden Book Company, 1975.
30. Terry, Paul B. Spectral Analysis of Short Record Time Series Data. MS thesis, AFIT/GE/EE/79-38. School of Engineering, Air Force Institute of Technology, Wright-Patterson AFB OH, December 1979 (AD-A080156).
31. Tong, P. S. "Quantization Requirements in Digital MTI," IEEE Transaction on Aerospace and Electronics, 13: 512-521 (September 1977).
32. Van Trees, H. L. Detection, Estimation, and Modulation Theory. New York: Wiley, 1968.
33. Wiley, Richard G. Electronic Intelligence: The Analysis of Radar Signals. Dedham, Massachusetts: Artech House, 1982.

VITA

Lieutenant Thorlough E. Carter Jr. was born on 22 November 1961 in Washington, District of Columbia. He graduated from Calvin Coolidge High School in 1979 and received the degree of Bachelor of Science in Electrical Engineering from Howard University in May 1984. He served as a radar engineering analyst at the Foreign Technology Division, Wright-Patterson AFB, from August 1984 to May 1986. His responsibility was that of determining the characteristics, capabilities, and vulnerabilities of foreign over-the-horizon radar systems. In May 1986, he entered the School of Engineering, Air Force Institute of Technology, to pursue the degree of Master of Science in Electrical Engineering.

Permanent Address: 7005 21st Avenue

Hysttville, Maryland 20783

REPORT DOCUMENTATION PAGE

1a REPORT SECURITY CLASSIFICATION UNCLASSIFIED		1b RESTRICTIVE MARKINGS	
2a SECURITY CLASSIFICATION AUTHORITY		3. DISTRIBUTION / AVAILABILITY OF REPORT Approved for public release; distribution unlimited	
2b DECLASSIFICATION / DOWNGRADING SCHEDULE		4. PERFORMING ORGANIZATION REPORT NUMBER(S) AFIT/GE/ENG/87D-9	
4. PERFORMING ORGANIZATION REPORT NUMBER(S) AFIT/GE/ENG/87D-9		5. MONITORING ORGANIZATION REPORT NUMBER(S)	
6a. NAME OF PERFORMING ORGANIZATION School of Engineering	6b OFFICE SYMBOL (if applicable) AFIT/ENG	7a. NAME OF MONITORING ORGANIZATION	
6c. ADDRESS (City, State, and ZIP Code) Air Force Institute of Technology Wright-Patterson AFB, Ohio 45433		7b. ADDRESS (City, State, and ZIP Code)	
8a. NAME OF FUNDING / SPONSORING ORGANIZATION Avionics Lab	8b OFFICE SYMBOL (if applicable) AFWAL/AAWP	9. PROCUREMENT INSTRUMENT IDENTIFICATION NUMBER	
8c. ADDRESS (City, State, and ZIP Code) Wright-Patterson AFB, Ohio 45433		10. SOURCE OF FUNDING NUMBERS	
		PROGRAM ELEMENT NO	PROJECT NO
		TASK NO	WORK UNIT ACCESSION NO
11. TITLE (Include Security Classification) Spectral Analysis of Short Data Records			
12. PERSONAL AUTHOR(S) Carter, Thorlough E. Jr., B.S.E.E., 1Lt, USAF			
13a. TYPE OF REPORT MS Thesis	13b. TIME COVERED FROM _____ TO _____	14. DATE OF REPORT (Year, Month, Day) 1987 December	15. PAGE COUNT 109
16. SUPPLEMENTARY NOTATION			
17. COSATI CODES		18. SUBJECT TERMS (Continue on reverse if necessary and identify by block number)	
FIELD	GROUP	SUB-GROUP	
20	05	Spectrum Analysis	
19. ABSTRACT (Continue on reverse if necessary and identify by block number) (see reverse)			
20. DISTRIBUTION / AVAILABILITY OF ABSTRACT <input checked="" type="checkbox"/> UNCLASSIFIED/UNLIMITED <input type="checkbox"/> SAME AS RPT <input type="checkbox"/> DTIC USERS		21. ABSTRACT SECURITY CLASSIFICATION UNCLASSIFIED	
22a. NAME OF RESPONSIBLE INDIVIDUAL Glenn Prescott, Major, USAF		22b. TELEPHONE (Include Area Code) 513-255-2024	22c. OFFICE SYMBOL AFIT/ENG

Johnathan 14 MAR 88

The purpose of this study was to examine the Blackman-Tukey (BT) and Burg methods of spectral estimation for typical electronic warfare received signals. Such signals are generally short in duration, resulting in short data records. The BT method is a conventional spectral estimation scheme and is based on computing the discrete Fourier transform of the autocorrelation sequence (ASC) derived from the data record. An inherent problem of this approach is that of data windowing. Data windowing may result in poor frequency resolution, particularly for short data records.

The Burg method of spectral estimation, a modern approach, is capable of providing relatively good frequency resolution for short data records. However, this method requires sufficient input signal-to-noise ratio (SNR). The idea here is to extend the ACS by extrapolation (or prediction) rather than windowing the data.

The Burg method was found to yield far superior performance for data records consisting of 64 data samples. Note, however, that a minimum SNR of 15 dB was assumed. Using this method a "smart" routine was developed that automatically determines the actual frequency components of the data record.

END
DATE
FILMED
DTIC
4/88